NUREG/CR–6327
MCS 950302

Models for Embrittlement Recovery Due to Annealing of Reactor Pressure Vessel Steels

Prepared by
E. D. Eason, J. E. Wright, E. E. Nelson/MCS
G. R. Odette, E. V. Mader/Univ CA

Modeling and Computing Services

Department of Chemical and Nuclear Engineering
University of California

Prepared for
U.S. Nuclear Regulatory Commission

AVAILABILITY NOTICE

Availability of Reference Materials Cited in NRC Publications

Most documents cited in NRC publications will be available from one of the following sources:

1. The NRC Public Document Room, 2120 L Street, NW., Lower Level, Washington, DC 20555-0001

2. The Superintendent of Documents, U.S. Government Printing Office, P. O. Box 37082, Washington, DC 20402-9328

3. The National Technical Information Service, Springfield, VA 22161-0002

Although the listing that follows represents the majority of documents cited in NRC publications, it is not intended to be exhaustive.

Referenced documents available for inspection and copying for a fee from the NRC Public Document Room include NRC correspondence and internal NRC memoranda; NRC bulletins, circulars, information notices, inspection and investigation notices; licensee event reports; vendor reports and correspondence; Commission papers; and applicant and licensee documents and correspondence.

The following documents in the NUREG series are available for purchase from the Government Printing Office: formal NRC staff and contractor reports, NRC-sponsored conference proceedings, international agreement reports, grantee reports, and NRC booklets and brochures. Also available are regulatory guides, NRC regulations in the *Code of Federal Regulations,* and *Nuclear Regulatory Commission Issuances*.

Documents available from the National Technical Information Service include NUREG-series reports and technical reports prepared by other Federal agencies and reports prepared by the Atomic Energy Commission, forerunner agency to the Nuclear Regulatory Commission.

Documents available from public and special technical libraries include all open literature items, such as books, journal articles, and transactions. *Federal Register* notices, Federal and State legislation, and congressional reports can usually be obtained from these libraries.

Documents such as theses, dissertations, foreign reports and translations, and non-NRC conference proceedings are available for purchase from the organization sponsoring the publication cited.

Single copies of NRC draft reports are available free, to the extent of supply, upon written request to the Office of Administration, Distribution and Mail Services Section, U.S. Nuclear Regulatory Commission, Washington, DC 20555-0001.

Copies of industry codes and standards used in a substantive manner in the NRC regulatory process are maintained at the NRC Library, Two White Flint North, 11545 Rockville Pike, Rockville, MD 20852-2738, for use by the public. Codes and standards are usually copyrighted and may be purchased from the originating organization or, if they are American National Standards, from the American National Standards Institute, 1430 Broadway, New York, NY 10018-3308.

DISCLAIMER NOTICE

NUREG/CR-6327
MCS 950302

Models for Embrittlement Recovery Due to Annealing of Reactor Pressure Vessel Steels

Manuscript Completed: April 1995
Date Published: May 1995

Prepared by
E. D. Eason, J. E. Wright, E. E. Nelson, Modeling and Computing Services
G. R. Odette, E. V. Mader, University of California

Modeling and Computing Services
6400 Lookout Road, Suite 105
Boulder, CO 80301

University of California
Santa Barbara, CA 93106

Prepared for
Division of Engineering Technology
Office of Nuclear Regulatory Research
U.S. Nuclear Regulatory Commission
Washington, DC 20555-0001
NRC Job Code L1107

ABSTRACT

The reactor pressure vessel (RPV) surrounding the core of a commercial nuclear power plant is subject to embrittlement due to exposure to high energy neutrons. The effects of irradiation embrittlement can be reduced by thermal annealing at temperatures higher than the normal operating conditions. However, a means of quantitatively assessing the effectiveness of annealing for embrittlement recovery is needed. The objective of this work was to analyze the pertinent data on this issue and develop quantitative models for estimating the recovery in 30 ft-lb (41 J) Charpy transition temperature and Charpy upper shelf energy due to annealing. Data were gathered from the Test Reactor Embrittlement Data Base and from various annealing reports. An analysis data base was developed, reviewed for completeness and accuracy, and documented as part of this work. Independent variables considered in the analysis included material chemistries, annealing time and temperature, irradiation time and temperature, fluence, and flux. To identify important variables and functional forms for predicting embrittlement recovery, advanced statistical techniques, including pattern recognition and transformation analysis, were applied together with current understanding of the mechanisms governing embrittlement and recovery. Models were calibrated using multivariable surface-fitting techniques. The quality of fit was evaluated by considering both the Charpy annealing data used for fitting and a surrogate hardness data base. Several iterations of model calibration, evaluation with respect to mechanistic and statistical considerations, and comparison with the trends in hardness data produced correlation models for estimating Charpy upper shelf energy and transition temperature after irradiation and annealing.

This work provides a clear demonstration that 1) microhardness recovery is generally a very good surrogate for shift recovery, and 2) there is a high level of consistency between the observed annealing trends and fundamental models of embrittlement and recovery processes. These results justified a quantitative treatment of the effect of flux based on Charpy data irradiated in test reactors and microhardness data from surveillance samples irradiated in power reactors. Low flux irradiations were shown to significantly reduce the amount of annealing recovery at and below 750°F but to have little effect at higher temperatures. Hence, the new model removes some conservatism in previous formulations, which imposed significant penalties on recovery for low flux irradiations at all annealing temperatures. The nonlinear annealing time and temperature dependence in the current model may also expand the time-temperature window for effective annealing treatments, compared to previous correlations.

TABLE OF CONTENTS

TABLE OF CONTENTS (cont.)

LIST OF FIGURES

LIST OF TABLES

Table **Page**

ACKNOWLEDGMENTS

The authors appreciate the advice and encouragement received from A. Taboada and A. L. Hiser, current and former project managers, respectively, at the U.S. Nuclear Regulatory Commission. The advice and support from other NRC staff is also appreciated, including E. Hackett and M. Mayfield. The staff at Oak Ridge National Laboratory have provided data and advice which is well appreciated, including R. Nanstad, S. Iskander, F. Kam, and J-A. Wang. Special thanks are due to R. Hawthorne of Materials Engineering Associates for his review and documentation of the annealing database and recalculation of the older fluences. This work was performed under U.S. NRC contract 04-92-048.

1 INTRODUCTION

1.1 Background

The reactor pressure vessel (RPV) surrounding the core in a commercial nuclear power plant is subject to embrittlement due to exposure to neutrons from the core. This embrittlement can be so severe that plant operations must cease pending detailed studies and/or remedial measures. One U.S. power plant (Yankee Rowe) has been affected by this problem, and others are expected to become affected as they age.

The effects of radiation embrittlement can be reduced by thermal annealing at temperatures higher than the normal operating conditions. Although such an annealing process has not been applied to any commercial plants in the United States, one U. S. Army reactor (Potapovs, 1968), the BR3 plant in Belgium (Fabry, 1994), and several plants in the former USSR have been successfully annealed.

A quantitative evaluation of embrittlement recovery due to annealing is required to determine continued operation limits for aging commercial plants. The objective of this work is to analyze the pertinent data on this issue and develop quantitative models for estimating the recovery in 30 ft-lb (41 J) Charpy transition temperature (TT) and Charpy upper shelf energy (USE) due to annealing.

1.2 Previous Annealing Models

Models for estimating the degree of recovery due to post irradiation annealing have been developed previously. Powers proposed in 1968 that the percentage recovery in the irradiated transition temperature shift could be related to a time-temperature superposition parameter P, where

$$P = T \ln(10^{21} t) \tag{1-1}$$

In Equation 1-1, temperature T is in degrees K, and time t is in seconds. The parameter P is evaluated both after irradiation and after annealing. The change in P,

$$\Delta P = P_{anneal} - P_{irrad} \tag{1-2}$$

is approximately proportional to the percentage recovery. This approach works to some extent, but better results are obtained by the method of Macdonald (1985).

Macdonald refined the approach of Powers (1968) by defining an Annealing Effect Parameter,

$$AEP = C \Delta P (\Delta TT_i)^n \tag{1-3}$$

where C is a constant, ΔP is as defined by Equation 1-2, and ΔTT_i is the shift in transition temperature due to irradiation. The exponent n was found to be approximately -0.5. A reasonable correlation was obtained for estimating the residual transition temperature shift after annealing as

$$\Delta TT_{ia} = a_1 + a_2 \, erf(AEP) \tag{1-4}$$

where a_1 and a_2 are empirical fitting constants. Both Powers' and Macdonald's models use the same time-temperature superposition factor P.

The fitting form used by Macdonald (1985) appears to have been determined somewhat arbitrarily. The text implies that the exponent n was chosen by eye, and the value of the constant C in Equation 1-3 was chosen to allow the use of the assumed functional form *erf(AEP)*.

Another preliminary model is presented in the recent draft annealing Regulatory Guide DG-1027 (Oct 1994). The form of the equation is

$$\begin{aligned} fTT_{recov} = {} & 0.287 T_a + 0.00406 (T_a + 460) \ln t_a - \\ & 0.090 \, Cu^{0.844} (T_a + 460) - 0.00706 (T_i + 460) \ln t_i - \\ & 0.0182 T_i + 0.981 \, \Delta TT_i^{0.617} - 90 \end{aligned} \tag{1-5}$$

where

- fTT_{recov} = fractional recovery due to annealing
- T_a = annealing temperature, °F
- t_a = annealing time, s
- T_i = irradiation temperature, °F
- t_i = irradiation time, s
- ΔTT_i = transition temperature shift due to irradiation, °F
- Cu = copper content, wt%

This formulation has an explicit treatment of irradiation time which significantly reduces the amount of recovery at low flux for all annealing temperatures. As shown below, low flux irradiations significantly reduce the amount of recovery for $T_a \leq 750$°F but have little effect at higher temperatures. Another weakness of this model is that it is based on irradiation time in high flux test reactors, which reflects both flux and fluence effects. It is not clear how to use irradiation time for power reactors in this model.

In the current work, pattern recognition, transformation analysis techniques, residual studies and the current understanding of the mechanisms involved in the annealing process were used to guide the selection of the most sensitive variables and correlating parameters and to determine the optimal form for fitting the data. The resulting models were fitted by nonlinear least squares. The use of advanced tools, the larger database now available, and insight from the surrogate hardness data produced improved models for quantitative evaluation of the effects of annealing.

1.3 Current Mechanistic Understanding

The current understanding of embrittlement mechanisms provides a useful framework for assessing correlations for annealing recovery of transition temperature shift (TTS) and drop in Charpy upper shelf energy (ΔUSE). In manganese-molybdenum steels, transition temperature shifts to higher values and upper shelf energy drops as yield stress and hardening increase. The yield stress increases, or hardening, are related to ultra-fine-scale microstructural features introduced by irradiation (Odette, et al., ASTM STP 870, ASTM STP 909, ASTM STP 1125, ASTM STP 1175, EPRI Report NP-6114; Fisher and Buswell, 1987; Kampmann, et. al., 1992; Mader, Odette, and Lucas, 1993; Odette, AEA TR, in press; Odette, MRS Symposium, in press).

The general categories of hardening features include:

1) unstable matrix defects (UMD), which are thermally (and possibly mechanically) unstable,
2) stable matrix defects (SMD), and
3) copper-rich precipitates (CRP).

These general categories may contain multiple features with a range of characteristics. The relative numbers and volume fractions of these features depend on the combination of metallurgical and irradiation variables, including first order effects of copper content (Cu), nickel content (Ni), fluence (ϕt), irradiation temperature (T_i), and flux (ϕ). Second order variables may include, for example, phosphorous and manganese contents (P and Mn), heat treatment, product form, and neutron spectrum. To some extent, the detailed character of a feature (e.g., composition of the CRP) depends on the same variables. Interactions among the variables are common. One example involves the interplay between ϕ, ϕt, T_i, and Cu (Odette, ASTM STP 1175):

- high ϕt with low T_i results in a larger population of UMD, since the UMD anneal in-situ during irradiation
- the increased number of UMD act as sinks and reduce the radiation-enhanced diffusion efficiency
- in turn, the reduced efficiency retards CRP evolution

The consequence is that high flux may retard hardening at low fluence and/or low temperature for high copper steels but have the opposite effect at high fluence and/or high temperature, particularly for low copper steels.

Ignoring possible interactions, the radiation-induced features also undergo individual evolutions during post-irradiation annealing, depending on the annealing temperature (T_a) and time (t_a) (Mader, et al., ASTM STP 1125; Mader, Odette, and Lucas, 1993). The residual embrittlement following post-irradiation annealing depends on the balance and character of the residual features.

Existing mechanistic models for annealing are based in part on "theory" but are primarily formulated empirically from results of controlled, single-variable experiments including both microstructural observations and an extensive hardness data base on annealing. While there may not always be a one-to-one correspondence between changes in hardness and Charpy transition temperature shifts, the hardness data base provides useful surrogate information that was used to help formulate the correlation functions for mechanisms-based modeling and for quantitative, independent tests of the shift-based models.

The current mechanistic models can be used to describe the approximate effect of T_a (and t_a) on the various features (Mader, Odette, and Lucas, 1993; Odette, et. al., 1994):

- T_a = 650°F (343°C) -- The primary recovery is due to UMD dissolution; at long annealing times, partial recovery of part of the SMD population and perhaps minor changes in the CRP composition are also important. Thus, it may be convenient to lump the UMD and SMD in long-term annealing models.
- T_a = 750°F (399°C) -- The UMD and almost all the SMD recover, primarily by dissolution. The CRP also undergo limited dissolution (reductions in their manganese and nickel contents) and coarsening.
- T_a = 850°F (454°C) -- The SMD recover essentially completely, and the CRP undergo further dissolution; dissolution includes resolutioning of Cu and extensive coarsening. The effective (non-equilibrium) copper solubility is greatly increased over equilibrium values, due both to the body-centered cubic (bcc) crystal structure and small size/high interface energy of the

CRP. At long annealing times (t_a > 50 h), the CRP number densities are reduced by factors of 10 to 20. Recovery of the hardening is strongly enhanced by the reduced CRP number density -- the coarsened CRP are much less effective in pinning dislocations among a population of pre-existing strong barriers. The residual hardening due to the CRP is dependent on the copper content, but it is relatively insensitive to the ϕ, ϕt (beyond a minimum value), and T_i. The effect of Ni and P on residual hardening would also be expected to be modest for long-time anneals.

The concepts outlined above can be used to understand the interactions between the irradiation, metallurgical, and annealing variables. For example, the fractional shift recovery due to annealing would be expected to diminish with increasing irradiation temperature due to the corresponding decrease in matrix defect hardening at all annealing temperatures. The irradiation temperature dependence would be expected to decrease with increasing copper content (smaller fraction of hardening from matrix defects) and higher annealing temperature (more complete recovery of CRP). The kinetic effects of flux would be expected to have a similar trend. Specifically, lower fluxes (like higher temperatures) would produce less matrix defect damage and, hence, less recovery at lower annealing temperatures. However, beyond some critical fluence, the effect of flux on the CRP would be minimal.

1.4 Objectives and Scope of Work

This work is Task 4 of a larger project to develop improved irradiation embrittlement correlations using advanced data analysis techniques, results from mechanistic research, and the large body of embrittlement data that has become available in recent years in the Power Reactor Embrittlement Data Base (PR-EDB, NUREG/CR-4816) and the Test Reactor Embrittlement Data Base (TR-EDB, NUREG/CR-6076) compiled at Oak Ridge National Laboratory. The objective of this part of the contract is to provide empirical methods to estimate annealing recovery of irradiation-induced embrittlement, specifically, the effect of annealing on the transition temperature shift (TTS) and drop in Charpy upper shelf energy (ΔUSE).

The first sub-task of the annealing task was the development of a working data base for use with analysis codes. TTS and ΔUSE data were extracted from various reports and the TR-EDB, together with associated independent variables such as composition, irradiation, and annealing details.

The second sub-task of the annealing task was the analysis. Pattern recognition and transformation analyses were used in conjunction with mechanistically-motivated analyses of annealing data to define the variables and functional forms to characterize annealing recovery. The variables considered in the analysis included irradiation and annealing time and temperature, the irradiation-induced shift, the post-annealed residual shift, fluence, flux, chemical composition, material type (i.e., weld, base metal), and combinations of these variables in the form of various correlation parameters.

The final subtask was calibration and evaluation of correlation models. Results of pattern recognition and transformation analysis were used iteratively with physical and mechanistic considerations, evaluation of selected subsets of Charpy data, and evaluation of trends in the surrogate hardness data base to develop the final correlation models. Least squares techniques were used, in each case minimizing the sum of the squares of the residuals between calculated and actual values of the quantity being modeled. Extensive residual analysis was performed on the resulting model using various subsets of both the shift data and the surrogate data base. Combined with statistical considerations, residual analysis helps to define a meaningful range of annealing variables consistent with reliable application of the correlations.

2 DATA BASE DEVELOPMENT

2.1 Charpy Data Base

Charpy data were gathered from the TR-EDB and from various annealing reports, documented in Appendix A and a compendium of data by R. Hawthorne, (1994). Since many of the annealing data were originally generated by R. Hawthorne while at Naval Research Laboratory and Materials Engineering Associates, Mr. Hawthorne reviewed the data from his experiments and cross-checked the computer data base with his original laboratory notes as a part of this work. His review resulted in clarifications regarding discrepancies between reports and the TR-EDB, some corrections, a few new data points and elimination of some duplicate entries, and suggestions to omit a few unreliable data points. In addition, many of the fluences in the reports and the TR-EDB were fission spectrum fluences; in most cases, Mr. Hawthorne provided calculated spectrum fluence values to replace the older numbers. Complete documentation of irradiation conditions and test data are given elsewhere (Hawthorne, 1994).

2.2 Independent Variables

The independent variables in the data base include chemistries, irradiation time and temperature, annealing time and temperature, fluence, flux, pre-irradiated transition temperature (TT) and upper shelf energy (USE), and changes in TT and USE due to irradiation. All the independent variables considered in the analysis are shown in Table 2-1. Note that candidate dependent variables described below were sometimes considered as independent variables in runs where they were not the dependent variable.

Particularly important variables include the change from unirradiated to irradiated TT and USE, annealing parameters such as T_a and t_a, irradiation parameters such as T_i, ϕt, ϕ, and t_i, and chemical composition (particularly Cu, Ni, and P). Combinations of variables were also considered, such as the difference T_a-T_i and combinations of chemical components such as Cu*Ni. The combinations of variables considered in the early pattern recognition stages of analysis are shown in Table 2-2.

2.3 Dependent Variables

Several algebraically-related measures of annealing recovery were investigated for both TTS and ΔUSE. The generic types of dependent variables considered were:

- final quantity (TT or USE) after irradiation and annealing (USE_{ia} or TT_{ia})
- fraction of the irradiated shift or drop recovered by annealing ($fUSE_{recov}$ or fTT_{recov})
- absolute residual shift or drop after annealing (ΔUSE_{resid} or ΔTT_{resid})
- residual fraction of the irradiated shift remaining after annealing (fTT_{resid})
- absolute reduction in TT or increase in USE due to annealing (ΔTT_a or ΔUSE_a)

Depending on the application, one form may be preferred over another. From a model calibration point of view, some forms produce much better correlations than others. Consequently, a study was performed to pick the best dependent variable for model calibration purposes, as described in the Results section. Formulas for calculating the candidate dependent variables are shown in Table 2-3. Since the candidate dependent variables are related algebraically, the final model may be expressed in whatever form is most desirable from the standpoint of the end user.

2.4 Computed Data Base Entries

The source documents for the annealing data base contain results presented in different formats. For example, one document might give TT_u, ΔTT_i, and ΔTT_a, whereas another might give TT_u, TT_{ia}, and ΔTT_{resid}. In order to "fill" the data base table, some quantities not presented directly were computed from the quantities listed. These computed quantities are shown in Table 2-4. Where more than one method can be used to compute a quantity, the methods are listed in the order of priority used to create the annealing data base, with the favored method first.

2.5 Characterization of Charpy Annealing Data Base

The entire Charpy annealing database contains 187 data points. The data base is attached as Appendix A. As in most data bases composed of data from various experiments, there are many cases of missing data in the annealing data base; some independent variables are missing, and in many cases recovery of only one quantity -- TTS or ΔUSE -- is available. Missing values are indicated by "-999" in the Charpy annealing data base shown in Appendix A.

An ideal analysis data base would contain data that are well distributed over the full ranges of interest of all variables considered. However, real data bases compiled from several studies often have gaps and uneven distributions of data, random errors, and biases. These weaknesses of combined data bases can lead to misleading or inaccurate results that may not be apparent in statistical fitting parameters. Hence, a careful assessment of the "character" of the data base is important in assessing the limits of the correlations and reliability of conclusions drawn from the analysis, as well as indicating where additional data are needed. The distribution of the data in the Charpy annealing data base is summarized below.

- irradiation temperature (T_i) -- Most of the data are "clumped" around T_i of about 550°F, as shown in Figure 2-1a. There are only two higher values of T_i. There is a moderately large set of data at about 440 to 450°F (10 points) and a smaller set (5 points) at 500°F. However, the low T_i data are restricted to a low annealing temperature of 650°F. There is no subset of data on the same heat of steel irradiated at comparable conditions over a range of temperatures.

- fluence (ϕt) -- The data base contains data over a range of ϕt from 0.32 to 5.9×10^{19} n/cm^2. Figure 2-1b shows the distribution of the number of data points for various ϕt intervals. Most of the data fall in the interval 0.5 to 3.5×10^{19} n/cm^2. There are 12 subsets of data with different ϕt for the same heat, T_i, and annealing conditions.

- flux (ϕ) -- The range of flux calculated from the data base is from about 2 to 16×10^{12} n/cm^2-s (E>1MeV) as shown in Figure 2-1c. Independent flux measurements were not reported for many experiments in the Charpy annealing data base, so flux is calculated by dividing fluence by irradiation time.

- phosphorus content (P) -- The data base contains data over a range of P (0.002 to 0.028 wt%), distributed as shown in Figure 2-1d. Phosphorus varies along with a large number of other metallurgical, irradiation, and annealing variables. There are five data subsets that have a systematic variation in P for similar heats or welds that were irradiated and annealed under the same or similar conditions.

- annealing temperature (T_a) -- The distribution of T_a is shown in Figure 2-1e. Most data are at T_a = 650 and 750°F. There are only 20 data points at T_a = 850°F. As noted below, there are somewhat different distributions of Cu and Ni at the various T_a.

- annealing time (t_a) -- Annealing times in the data base range from 1.5 to 1944 h, with the majority at 168 h, as shown in Figure 2-1f. The data base contains a number of data subsets for the same heat or weld annealed for various times: nine at 750°F; three at 800 and 850°F; and two at 650°F, including three steels with multiple T_a of 750, 800, and 850°F. The Cu in this data subset ranges from 0.16 to 0.41 wt%.

- copper (Cu) and nickel (Ni) contents -- There is a reasonable range in Cu in the data base at several annealing temperatures for steels with intermediate nickel content (0.5 to 0.8 wt%). However, there are relatively few data with Cu < 0.15 wt%, especially for the higher annealing temperatures ($T_a \geq$ 750°F). Cu versus Ni data are shown for T_a = 625, 650, 700, 750, 800 and 850°F in Figure 2-2. The variation in Cu is much more limited for low Ni (0 to 0.5 wt%) steels. Further, there are only two high Ni (>0.8 wt%) data points for anneals at 650 and 750°F and none at higher T_a. Both of these high Ni points are for low Cu steels (< 0.1 wt%). The complete lack of high Ni (≥ 1 wt%), intermediate Cu (0.2 to 0.3 wt%) points represents a large and practically significant hole in the annealing data base. There are two subsets of data for heats with controlled variations in Ni that were irradiated and annealed under the same conditions. There are two other data subsets for welds that are similar except for Ni.

2.6 Hardness Data Base and Other Surrogate Data

Over the last several years, a group at the University of California at Santa Barbara (UCSB) has been developing a large microhardness annealing data base as part of an NRC-sponsored research program. This microhardness data base covers a wide range of T_a (550 to 844°F) and t_a (0 to 600 h) for various irradiation conditions (flux, fluence, and temperature) and alloy compositions (primarily variations in Cu and Ni). In most cases, the results derive from fully controlled experiments: the same heat irradiated over a range of specified conditions and split melt heats irradiated at the same conditions. The microhardness measurements were made using a semi-automated method involving sequenced patterns of a large number of indents. Measurements of the as-irradiated condition and the effect of different annealing treatments on the annealed condition were made on the same sample. This may lead to unusually good accuracy and precision estimated to be about ± 5 DPH. A detailed report of this work is under preparation. These data were used to help develop and test the correlation functions.

Various subsets of the UCSB hardness data base were used to help independently evaluate the reliability of the

Table 2-1. Independent Variables Considered in Annealing Analysis

Variable	Units
Irradiation temperature, T_i	°F
Irradiation time, t_i	hours
Annealing temperature, T_a	°F
Annealing time, t_a	hours
Transition temperature before irradiation, TT_u	°F
Transition temperature after irradiation, TT_i	°F
Shift in transition temperature due to irradiation, ΔTT_i	°F
Upper shelf energy before irradiation, USE_u	ft-lb
Upper shelf energy after irradiation, USE_i	ft-lb
Drop in upper shelf energy due to irradiation, ΔUSE_i	ft-lb
Copper content, Cu	weight %
Nickel content, Ni	weight %
Phosphorus content, P	weight %
Sulfur content, S	weight %
Silicon content, Si	weight %
Chromium content, Cr	weight %
Manganese content, Mn	weight %
Molybdenum content, Mo	weight %

Table 2-2. Combinations of Variables Treated as Additional Independent Variables

$T_a \ln t_a$	$Cu(T_a \ln t_a)$	$Cu^*T_i \ln t_i$	Cr/T_a	Ni^*T_a
$T_i \ln t_i$	Cu^*Ni	Ni/T_a	Mn/T_a	P^*T_a
Cu^*T_a	Ni/Cu	P/T_a	Mo/T_a	S^*T_a
Cu/T_a	$Cu^*\phi t$	S/T_a	TT_u/T_a	Mo^*T_a
$Cu(T_aT_i)$	$Cu^*\Delta TT_i$	Si/T_a	US_u/T_a	$\Delta TT_i^*T_a$
$Cu/\phi t$,	$T_a^*T_i$	$\Delta US_i^*T_a$		

Table 2-3. Dependent Variable Definitions†

Dependent Variable	Formula for Calculation
USE_{ia}	USE after irradiation and annealing
$fUSE_{recov}$ - fractional increase in USE	$\frac{USE_{ia} - USE_i}{USE_u - USE_i}$
ΔUSE_{resid} - residual drop in USE	$USE_u - USE_{ia}$
ΔUSE_a - increase in USE due to annealing	$USE_{ia} - USE_i$
TT_{ia}	TT after irradiation and annealing
fTT_{recov} - fractional recovery in TT	$\frac{TT_i - TT_{ia}}{TT_i - TT_u}$
ΔTT_{resid} - residual increase in TT	$TT_{ia} - TT_u$
ΔTT_a - decrease in TT due to annealing	$TT_i - TT_{ia}$
fTT_{resid} - residual fraction embrittlement after irradiation and annealing	$fTT_{resid} = 1 - fTT_{recov}$

† Subscripts u, i, and ia refer to unirradiated, irradiated, and irradiated and annealed, respectively.

Table 2-4. Computed Data Base Entries

Quantity	Formulas Used to Compute Quantity, If Not Given Directly
TT_i	$TT_i = TT_u + \Delta TT_i$
ΔTT_i	$\Delta TT_i = TT_i - TT_u$ $\Delta TT_i = \Delta TT_a + \Delta TT_{resid}$
TT_{ia}	$TT_{ia} = TT_i - \Delta TT_a$ $TT_{ia} = TT_u + \Delta TT_i - \Delta TT_a$ $TT_{ia} = TT_u + \Delta TT_{resid}$
ΔTT_a	$\Delta TT_a = TT_i - TT_{ia}$ $\Delta TT_a = \Delta TT_i - \Delta TT_{resid}$
ΔTT_{resid}	$\Delta TT_{resid} = TT_{ia} - TT_u$ $\Delta TT_{resid} = \Delta TT_i - \Delta TT_a$
USE_i	$USE_i = USE_u - \Delta USE_i$
ΔUSE_i	$\Delta USE_i = USE_u - USE_i$ $\Delta USE_i = \Delta USE_a + \Delta USE_{resid}$
USE_{ia}	$USE_{ia} = USE_i + \Delta USE_a$ $USE_{ia} = USE_u - \Delta USE_i + \Delta USE_a$ $USE_{ia} = USE_u - \Delta USE_{resid}$
ΔUSE_a	$\Delta USE_a = USE_{ia} - USE_i$ $\Delta USE_a = \Delta USE_i - \Delta USE_{resid}$
ΔUSE_{resid}	$\Delta USE_{resid} = USE_u - USE_{ia}$ $\Delta USE_{resid} = \Delta USE_i - \Delta USE_a$

(a)

T_{ann}	T_i (°F)					
	450	500	550	600	650	700
850			19			1
800		1	8	1		
750		2	50			
700			8			
650	10	4	39			
625	8					

(b)

T_{ann}	ϕt ($x10^{19}/cm^2$)					
	0.5 -1	1	3	5	7	>9
850	7	13				
800	6	1	3			
750	14	30	8			
700	3	4	1			
650	9	24	17	3		
625	1	7				

(c)

T_{ann}	ϕ ($x10^{12}/cm^2$-s)					
	<3	3	5	7	9	>11
850	6	4		6	4	
800	6	2			2	
750	9	3		19	21	
700	3	3		2		
650	6	2	16	17	11	1
625			2	2	1	3

(d)

T_{ann}	Phosphorus (wt%)					
	0.000	0.005	0.010	0.015	0.020	0.025
850	2	9	5	4		
800		6		3	1	
750	13	10	4	14	5	2
700		6		1	1	
650	1	16	8	12	13	
625					8	

(e)

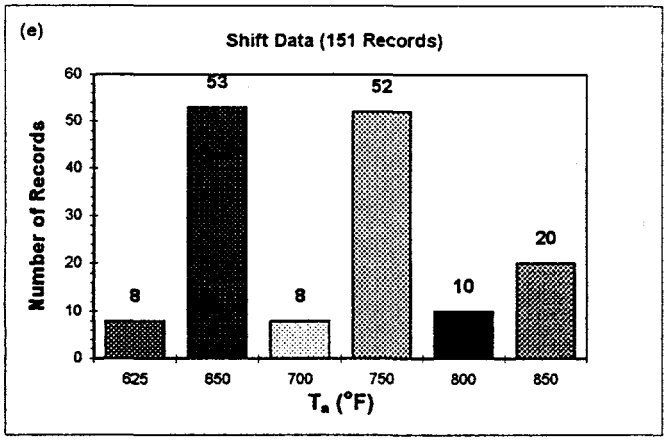

(f)

T_{ann}	t_{ann} (hrs)					
	<22	22	44	88	168	>335
850	3	1			16	
800	1	3	1		5	
750	3	7	1		40	1
700					8	
650			2		44	7
625			2		2	4

Figure 2-1 Distribution of Charpy Annealing Data

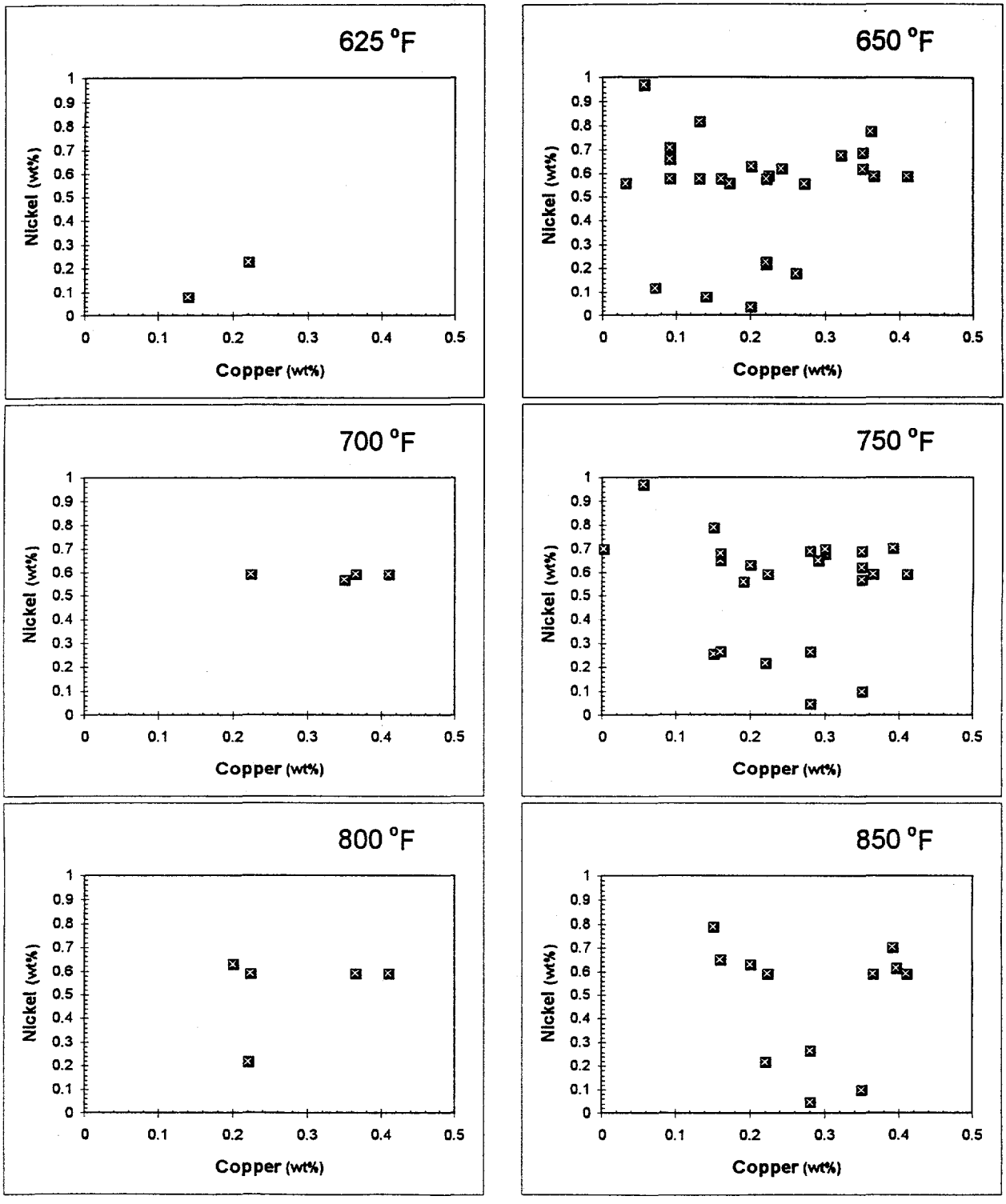

Figure 2-2 Distribution of Charpy Data by Cu and Ni

TTS correlation. The primary assessments were carried out using a total of 384 samples with long time anneals (>50 h). These specimens were irradiated at temperatures between 500 and 620°F for fluences greater than $5x10^{18}$ n/cm^2, at fluxes between 0.3 and $6x10^{12}$ n/cm^2-s. Other evaluations were carried out using 250 additional data points from shorter annealing times (between 1 and 50 h) and 12 data points from very high flux irradiations (about $50x10^{12}$ n/cm^2-s). The UCSB data base was supplemented with additional hardness data from the literature, including 27 annealing recovery measurements at low flux from Westinghouse surveillance specimens irradiated in power reactors reported by Westinghouse (Mager and Lott, 1989). As described in the Results section, 17 of these points had available flux values and were combined with the Charpy TTS data at higher flux to develop a flux-dependent model of fractional recovery. Finally, three data points for recovery of high Ni-intermediate Cu welds (Leitz et al., 1994) were also included in the microhardness data base to supplement the meager information in the Charpy data base for such compositions. The distributions of the microhardness data base variables are shown in Figures 2-3 and 2-4.

In addition to the surrogate microhardness data base, Charpy shift data in very recent literature or prepublication reports were used to test the correlation against Charpy data not used in fitting. This supplemental shift data base incorporated 18 data points on recovery of Mn-Mo type steels, including three high nickel-intermediate copper welds, and seven points for VVER Cr-Mo steels, for a total of 25 points.

(a)

T_{ann}	T_i (°F) 500	518	536	572	590	>608
842	4	4	17	44	1	4
797		4	8	44		4
752	5	2	13	26	1	2
707		4	8	44		4
662	1		6		1	
650		24	67	57		15

(b)

T_{ann}	ϕt ($\times 10^{19}$/cm^2) 0.5 - 1	1	2	3	4	>6
842	42	20	8	1	1	2
797	36	20	4			
752	29	10	6	1	1	2
707	36	20	4			
662	3		2	1	1	1
650	63	97	3			

(c)

T_{ann}	ϕ ($\times 10^{12}$/cm^2-s) <0.1	0.1	0.2	0.4	1.0	>3
842	2	5	4	6	1	56
797			4			56
752	2	5	2	7	1	32
707			4			56
662	2	3		2	1	
650			21	36		106

(d)

T_{ann}	Phosphorus (wt%) 0.000	0.005	0.010	0.015	0.020	0.025
842		56	9			
797		52	8			
752		35	5			
707		52	8			
662		1	1			
650		130	33			

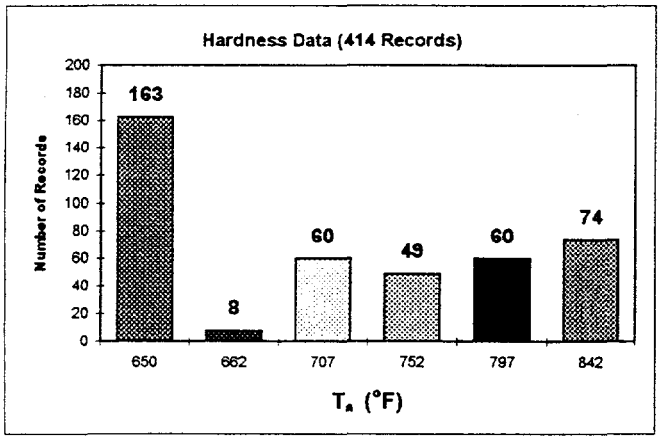

(f)

T_{ann}	t_{ann} (hrs) 50	150	168	300	336	600
842	15	19	10	15		15
797	15	15		15		15
752	17	5	10	17		
707	15	15		15		15
662		1	7			
650	58	47		17	41	

Figure 2-3 Distribution of Hardness Annealing Data

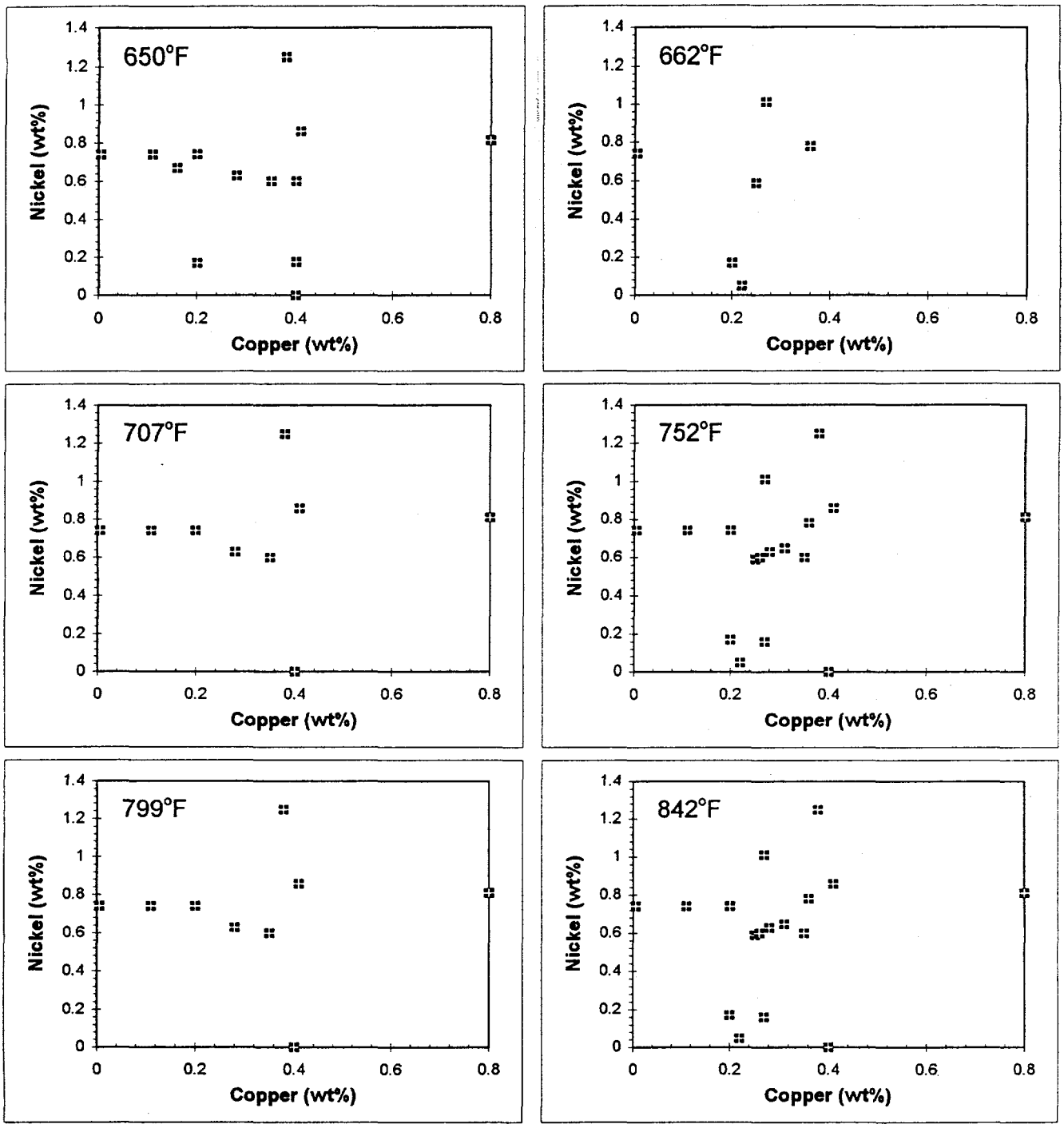

Figure 2-4 Distribution of Hardness Data by Cu and Ni

3 ANALYSIS METHODOLOGY

The data base development, pattern recognition, statistically- and physically-motivated model development, and calibration of final models is an iterative process. One reason is that outliers, regions of poor fit, and other anomalies are discovered throughout the analysis, right up to the point where final normalized plots are produced. Each time an anomaly is discovered, it requires correcting the data base or modifying the fitting form and recalculating all affected results. An additional aspect of the iterative process used in this project was the interaction between statistically-based and physically-motivated analyses. Insights from mechanistic studies were investigated in the statistical analyses, and vice versa.

3.1 Pattern Recognition and Correlations Among Independent Variables

The overall approach taken in the statistical analysis part of this project was the same as that used in several previous characterizations of materials behavior (Eason and Nelson, 1994; NUREG/CR-5356; NUREG/CR-5729). The data were reviewed for completeness and format, and then the analysis data base was assembled in the matrix form required by the advanced statistical tools.

All available variables and many combinations of variables were considered in the initial pattern recognition phase to ensure the best possible chance of identifying the secondary variables or combinations of variables and their optimal functional forms for the final correlations. Both the Transformation Analysis Code (TAC) and classification and regression analysis software (CART) were applied, first to identify key variables and then to determine optimal functional forms. TAC and CART results were used in conjunction with results of previous research on embrittlement mechanisms to provide guidance as to which variables, combinations of variables, or subsets of data might warrant closer investigation.

The TACMVS computer code was used to identify correlations among the supposedly-independent variables in the data base; such hidden correlations can be misleading in the type of analysis carried out here.

3.2 Physically-Motivated Analysis of Data Subsets and Comparison with Hardness Data

The evaluation of shift data subsets was carried out in two ways. In the first approach, groups of data sets involving differences in only one variable were assessed to try to discern systematic trends that might be hidden in the overall data base. For example, one such group contained materials of the same (or similar) heats or welds with a range in fluence but similar flux and irradiation temperature conditions. In some cases, this assessment was carried out for the absolute or fractional recovery; in other cases, the residuals (predicted minus measured values) from a proposed correlation model were evaluated. Particular emphasis was placed on the variables that had shown effects in some experiments but were not identified as significant in the pattern recognition step: Ni, fluence, P for TTS recovery, and Cu for USE recovery. The second approach involved looking for trends based on broader groupings of the data: two Ni, P, fluence, and annealing time groups, four Cu groups, and five annealing temperature groups.

The validity of the preliminary recovery correlations were tested by applying them directly to the hardness data base, based on the residual fraction in the Charpy transition temperature shift, fTT_{resid}, as

$$\Delta H_{ia} = fTT_{resid}\,\Delta H_i \qquad (3\text{-}1)$$

where ΔH is the change in hardness (DPH) from the unirradiated condition, and the subscripts are as in Table 2-3. The measures of validity included

1) the overall standard error in the predicted hardness

2) residual trends in the hardness as a function of the independent (and generally controlled) variables: Cu, Ni, P, irradiation temperature, flux, and fluence, and

3) the predicted dependence of the fractional recovery on irradiation temperature and Cu content.

These analyses proved to be very useful in helping to improve the preliminary correlation models by providing a physical basis for the correlation functions and variable sets, avoiding unphysical predictions such as negative shifts, and mitigating "local" data inconsistencies. Further, as discussed below, the consistency of the trends in the hardness data base with those in the Charpy data base lends considerable confidence to the robustness of the resulting annealing recovery models.

3.3 Model Calibration

The basic tool for correlation model calibration was the non-linear least squares code SURFIT. This code has been used continually by the Principal Investigator since he

developed it in 1976; it has proven to be extremely robust and convenient for calibrating non-linear models. It allows complete flexibility in the specification of the function to be fitted. Note that nonlinear least squares is a minimization-based procedure, for which it is always necessary to solve a problem at least twice using different starting estimates to assure that a minimum has been found and to explore the sensitivity of the minimum to changes in the variables.

All available data were used for each model calibration. For some data records in the analysis data base (see Appendix A), not all independent variables or possible dependent variables were available from the information given in reports or laboratory records. If the independent variables are different from one model to another, the number of data points used may also be slightly different, since a point is included in the calibration only if all variables required by the model being calibrated are present.

The quality of each candidate model was evaluated by looking at the standard error of estimate of the measured data about the model line, a plot of the measured versus predicted dependent variable, and plots of all the independent variables versus the predicted dependent variable, normalized relative to the variables not plotted. The standard error of estimate is computed by

$$S_e = \sqrt{\frac{\sum_{i=1}^{npts} \left(Y_{predicted} - Y_{actual}\right)^2}{npts - nparam}} \qquad (3\text{-}2)$$

where Y is either USE or TT, as appropriate, *npts* is the number of data points used, and *nparam* is the number of fitting parameters. In addition, residual analysis and checks against the surrogate (hardness) data were performed, as previously discussed.

Preliminary correlation models were developed for recovery of TTS and ΔUSE using SURFIT. These models were then reviewed and revised based on the current understanding of the mechanisms involved in embrittlement and annealing recovery. In addition, physically-based models were developed and calibrated using a non-linear fitting program in the Microsoft EXCEL® Solver mathematical library. This code uses least squares fitting with an optional, additional requirement that the bias (i.e., the sum of the residuals) is forced to zero. The similar results from these different modeling perspectives, using different fitting techniques, gives additional confidence in the fitted models.

The models derived from pattern recognition and statistical analysis and those derived from mechanistic considerations were compared and iteratively refined. Terms suggested by mechanistic considerations were tried in the statistical model and vice versa, with two teams of researchers independently calibrating but frequently comparing results. The models converged by this approach to single models for estimating USE and TTS recovery for engineering purposes. The resulting models incorporate both statistical and mechanistic considerations. A physically-based model that was useful for comparison and validation purposes is also presented.

4 RESULTS

4.1 Upper Shelf Energy Recovery

4.1.1 Selection of Dependent Variable

During the current study, several types of dependent variables were investigated, as discussed in Section 2.3. The candidate dependent variables considered for USE are shown in Table 2-3. Results of computer codes TACMVS and CART were used to select the dependent variables yielding the best correlations. Results of TACMVS are in the form of correlation coefficients, indicating how well each dependent variable can be *predicted* as the effects of additional independent variables are considered. CART provides ranking information indicating the relative importance of the independent variables considered. Results of both codes were used to determine which of the dependent variables are predicted best by the five most sensitive independent variables.

TACMVS and CART analyses were run with each of the candidate dependent variables and all of the independent variables. Due to limitations on the number of variables that can be considered by the analysis codes at once, the list of independent variables was broken into two groups: one containing basic variables plus the T_a combinations and one containing the basic variables plus the Cu combinations (see Table 2-2). Results are shown in Tables 4-1 and 4-2.

Cumulative correlation coefficients from the transformation analyses are shown in the "TAC R^2" columns. The cumulative R^2 represents the degree of correlation (relative to 1), with the current and previous variables considered. For example, in the second column of Table 4-1 one finds $R^2 = 0.95$ next to T_a in the first column. That means that the R^2 value for a TACMVS run including USE_i, USE_u, and T_a would be 0.95, so 95% of the variation in the dependent variable USE_{ia} is accounted for by the first three variables. Adding P to the list of variables increases R^2 to 0.96 -- not a significant change, generally. The first variable (USE_i in the first column) is the strongest individual variable for the particular run.

Relative importance rankings according to the regression analyses are shown in columns labeled "CART Imp." The importance ranking assigns the single most important variable a rank of 100%, and each other variable is assigned a lesser rank based on its relative effectiveness in reducing the total variance. The ranking is rather qualitative and does not depend on what other variables are simultaneously considered, unlike the TACMVS ranking. The variable ranked 100% by CART can be compared to the first variable chosen by TACMVS, but second and subsequent variables should not be compared.

The best dependent variable was selected on the basis of the following considerations:

- comparison of the TACMVS cumulative R^2 values for the five most sensitive independent variables; the higher the R^2, the greater fraction of the data range that is explained by a model using those variables
- comparison of the coefficients of variance from CART results; the coefficient of variance for a CART run was calculated from the pooled variance of the final CART groupings, and a smaller number indicates reduced scatter (see Table 4-3)

The best dependent variable for modeling recovery in ΔUSE is clearly the final value of the upper shelf energy after irradiation and annealing, USE_{ia}. An independent evaluation by direct testing of various correlation functions and variable sets produced the same conclusion.

4.1.2 Correlations Among "Independent" Variables

Correlations among the independent variables were investigated first using the TACMVS computer code. As expected, there are a number of intermediate and strong correlations among various chemistry variables. For the upper shelf energy data, strong correlations ($R^2 \geq 0.8$) between P and Cr and between Cr and Mn were found. There is also a strong correlation between ϕt and t_i, reflecting the narrow range in flux and a limited amount of independent flux data. Note that strong correlations also exist among some USE quantities used as independent variables, such as USE_u and USE_i. The correlations are shown graphically in Figure 4-1. The significance of the identification of correlations among independent variables is that correlated variables ideally should not be used in the same model, since their effects are partially confounded. When it is necessary to use correlated variables, the modeling and interpretation requires greater care.

4.1.3 Pattern Recognition and Transformation Analysis

The most important independent variables indicated by

Table 4-1. TAC and CART Results for USE Recovery, Including Cu Combinations

USE_{ia}				ΔUSE_a				ΔUSE_{resid}				$fUSE_{recov}$			
TAC		CART		TAC		CART		TAC		CART		TAC		CART	
X	R^2	X	Imp	X	R^2	X	Imp	X	R^2	X	Imp	X	R^2	X	Imp
USE_i	0.90	USE_u	100	ΔUSE_i	0.43	ΔUSE_i	100	ΔUSE_i	0.42	ΔUSE_i	100	ΔTT_i	0.49	USE_i	100
USE_u	0.94	USE_i	97	fTT_{recov}	0.56	T_a	58	$T_a lnt_a$	0.59	T_a	79	Mn	0.57	ΔTT_i	18
T_a	0.95	TT_i	62	Cr	0.65	$Cu(T_a-T_i)$	47	Cr	0.69	TT_{ia}	68	Mo	0.63	fTT_{recov}	6
P	0.96	Si	54	TT_u	0.72	$T_a lnt_a$	45	fTT_{recov}	0.78	ΔTT_{resid}	66	Cr	0.67	ΔTT_{resid}	5
$T_a lnt_a$	0.97	TT_u	48	ΔTT_{resid}	0.73	fTT_{recov}	39	T_a	0.76	$T_a lnt_a$	62	S	0.77	Mo	5

Table 4-2. TAC and CART Results for USE Recovery, Including T_a Combinations

USE_{ia}				ΔUSE_a				ΔUSE_{resid}				$fUSE_{recov}$			
TAC		CART		TAC		CART		TAC		CART		TAC		CART	
X	R^2	X	Imp	X	R^2	X	Imp	X	R^2	X	Imp	X	R^2	X	Imp
USE_i	0.90	USE_u	100	ΔUSE_i	0.43	ΔUSE_i	100	ΔUS_i	0.42	ΔUSE_i	100	ΔTT_i*T_a	0.49	USE_i	100
USE_u	0.94	USE_i	97	fTT_{recov}	0.56	ΔTT_i*T_a	56	$T_a lnt_a$	0.59	T_a	76	Mn	0.57	ΔTT_i	18
T_a	0.95	USE_u/T_a	94	Cr	0.65	T_a	53	Cr	0.69	TT_{ia}	68	Mo	0.63	ΔTT_i*T_a	18
P/T_a	0.96	TT_i	62	TT_u	0.72	fTT_{recov}	44	fTT_{recov}	0.78	ΔTT_{resid}	65	Cr/T_a	0.70	fTT_{recov}	6
$T_a lnt_a$	0.97	Si	54	ΔTT_{resid}	0.73	$T_a lnt_a$	42	T_a	0.76	$T_a lnt_a$	61	S	0.76	ΔTT_{resid}	5

Table 4-3. Pooled Coefficients of Variance for USE from Final CART Groupings

Dependent variable	Including Cu combinations	Including T_a combinations
USE_{ia}	0.09	0.09
ΔUSE_{ia}	0.37	0.23
ΔUSE_{resid}	1.11	0.86
$fUSE_{recov}$	0.21	0.22

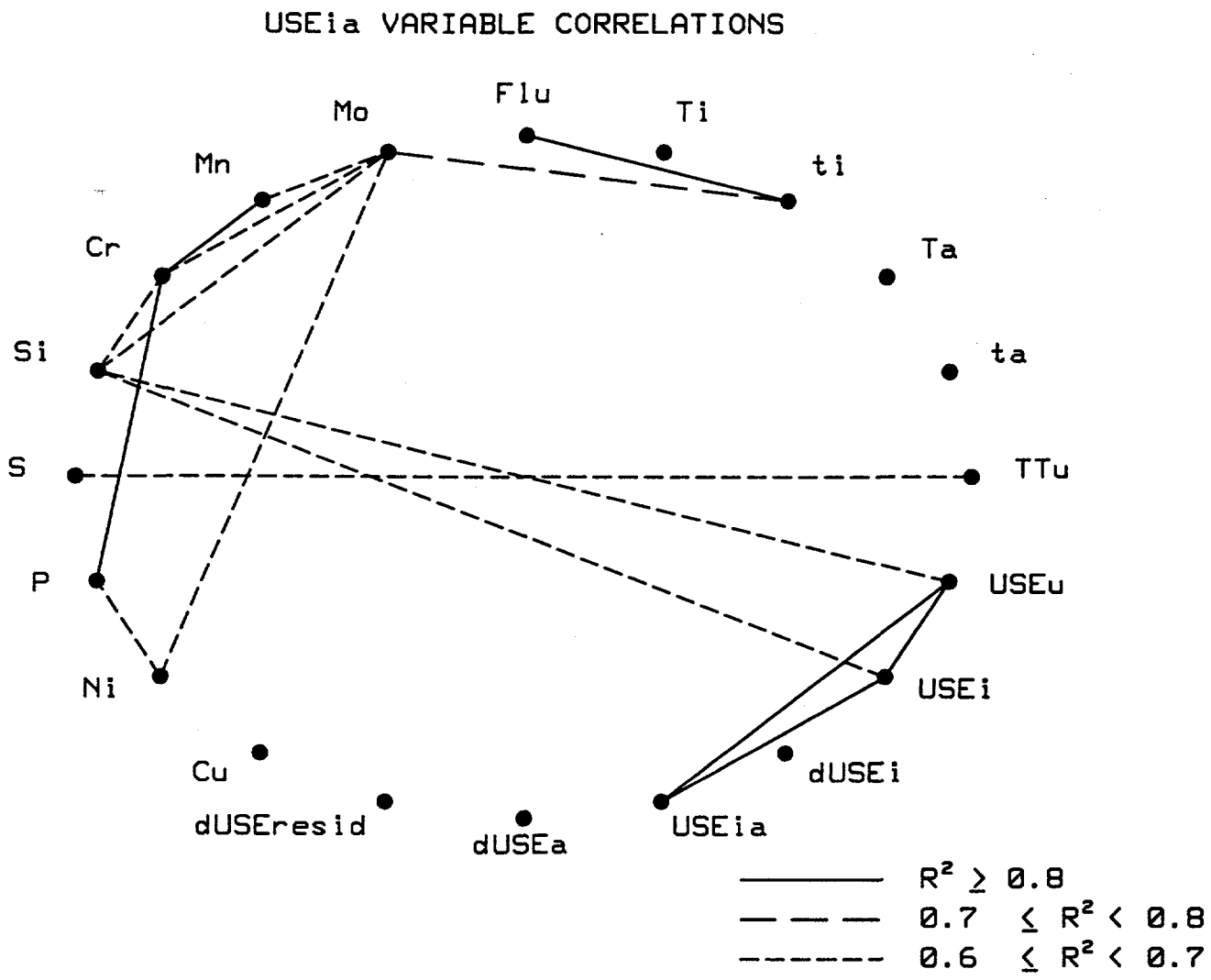

Figure 4-1 Correlations Among USE Variables

TACMVS and CART runs (See Tables 4-1 and 4-2) were used in TAC runs for USE_{ia}. For example, Figure 4-2 shows TAC results for USE_{ia} versus USE_i, USE_u, and $USE_u/[T_a ln(5.6E9t_a)]$. These variables and combinations of variables were identified by previous iterations of TAC runs. On these plots, the vertical scale is non-dimensionalized in standard deviations of the dependent variable (USE_{ia}). Thus, in Figure 4-2, the value of upper shelf energy after irradiation, USE_i, accounts for a three standard deviation range in the raw data, from $-\sigma$ to $+2\sigma$. The functional forms of all variables are approximately linear, indicating that the model form should contain linear terms in these variables. When potentially important additional independent variables such as fluence were added to the TAC run shown, the traces were nearly horizontal. The nearly-horizontal traces on TAC plots indicate little effect of the additional variables on USE_{ia} given that USE_u, USE_i, and $USE_u/T_a ln(5.6E9t_a)$ are in the model. Possible reasons for the lack of strong fluence and composition effects are given in the Discussion section.

4.1.4 Upper Shelf Energy Recovery Model

The SURFIT nonlinear least squares code was used to calibrate multivariable models for predicting recovery in USE. Using the TAC and CART results discussed above, the following preliminary model was developed (Eason et al.,1993):

$$USE_{ia} = 0.602\,USE_i + \left[1.14 - \frac{22{,}900}{T_a \ln(5.55\times10^9 t_a)}\right] USE_u + 6.83 \qquad (4\text{-}1)$$

where all upper shelf quantities are in ft-lb units, T_a is in °R, and t_a is in hours. This model had a standard error of 5.8 ft-lb, indicating an excellent fit, especially since measurement error alone would not be expected to be much less.

The preliminary model in Equation 4-1 was improved by mechanistic considerations and additional detailed analysis. An iterative series of data and residual plots was used to help determine if and how Cu, T_a, and t_a should appear in the recovery model. First, average values of the recovery (ΔUSE_a) were used to establish a crude T_a dependence trend. Data plots as well as TAC results showed that ΔUSE_a increased approximately linearly with ΔUSE_i. At lower T_a (650 and 700°F) the data fell into two groups of full or partial recovery. At 850°F the two groups were full recovery or over-recovery. The intermediate 750°F anneals showed all three recovery conditions. These population groupings were found to depend primarily on Cu as shown in Figure 4-3. Residual trends from a model that included T_a and ΔUSE_i terms were found to depend on T_a. Residual trends from a model with T_a, ΔUSE_i, and Cu terms showed an additional, independent T_a sensitivity, consistent with the presence of multiple defects. The data trends also showed that ΔUSE_i plays a role in recovery. Finally, analysis of both the USE data and hardness data base suggests that the effect of t_a can be accounted for using an exponential function in the form $[1-Cexp(-t_a/t_r)]$, where t_r is the relaxation time.

A decaying exponential function of t_a, a $Cu(C_1T_a - C_2)$ term, and a linear T_a term were investigated. Adding the $Cu(C_1T_a - C_2)$ term to Equation 4-1 produced a slight improvement in the standard error of the model. Adding a linear T_a term, given that a CuTa term was already in the model, produced no improvement in the model standard error, but the multiple-defect model of annealing mechanisms makes its use appealing. Accounting for the t_a effect by an exponential term instead of the $T_a ln t_a$ term also produced no improvement of the model standard error; however, since the exponential function agrees with both the USE trends and the hardness trends, it is believed to be a better representation of the effect of annealing time. The following is the final USE_{ia} model fitted using SURFIT:

$$USE_{ia} = USE_i + \left[1 - 0.586\exp\left(\frac{-t_a}{15.9}\right)\right] \times \left[0.570\,\Delta USE_i + \left(0.120\,T_a - 104\right)Cu + 0.0389\,T_a - 17.6\right] \qquad (4\text{-}2)$$

where USE_i and ΔUSE_i are in ft-lb, T_a is in °F, t_a is in hours, and Cu is in wt%. Equation 4-2 yields a standard error of 5.1 ft-lb.

The data used to calibrate Equation 4-2 include 113 points for which all the variables are available; five points that could have been used were omitted from the calibration. Four of these were points with higher USE after irradiation ($USE_i > USE_u$); all four were from the same experiment. The fifth point removed showed a large over-recovery ($USE_{ia} >> USE_u$) and initially showed up as an outlier; upon closer examination, it was noted that this is the only point from a 650°F anneal for which over-recovery occurred. (Including or excluding this point in the calibration has a very small effect on the fitting parameters and the standard error).

Comparing the standard errors of Equations 4-1 and 4-2 indicates no statistically significant difference based on F-tests at $\alpha = 0.05$. However, Equation 4-2 is preferred for its ability to capture the trends shown in Figure 4-3 and its slightly smaller standard error, even though we cannot prove statistically that it is a significantly better fit. Possible reasons for the relatively small sensitivity of standard error to the difference in the form of Equations 4-1 and 4-2 are given in the Discussion section.

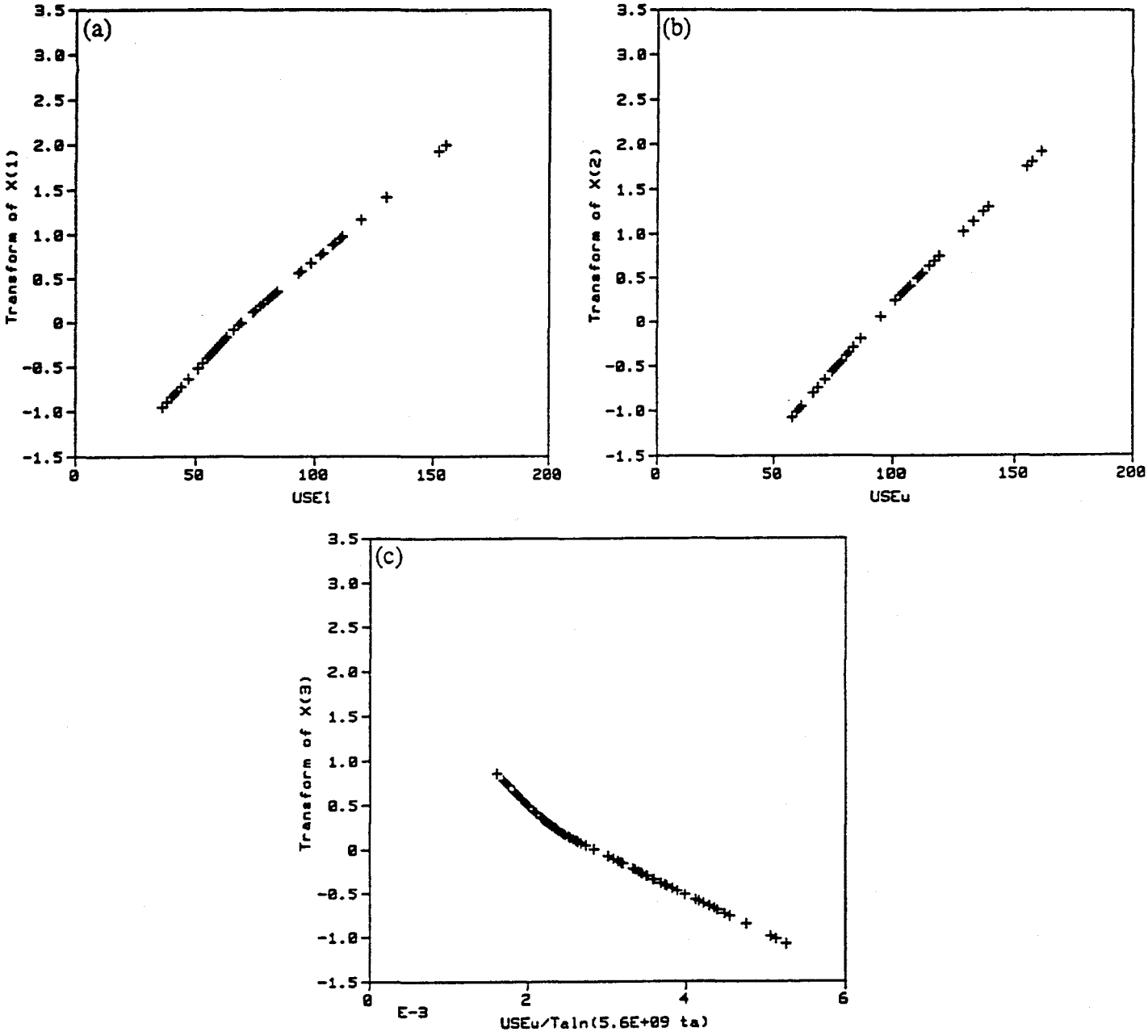

Figure 4-2 Preliminary TAC Results for USE_{ia}

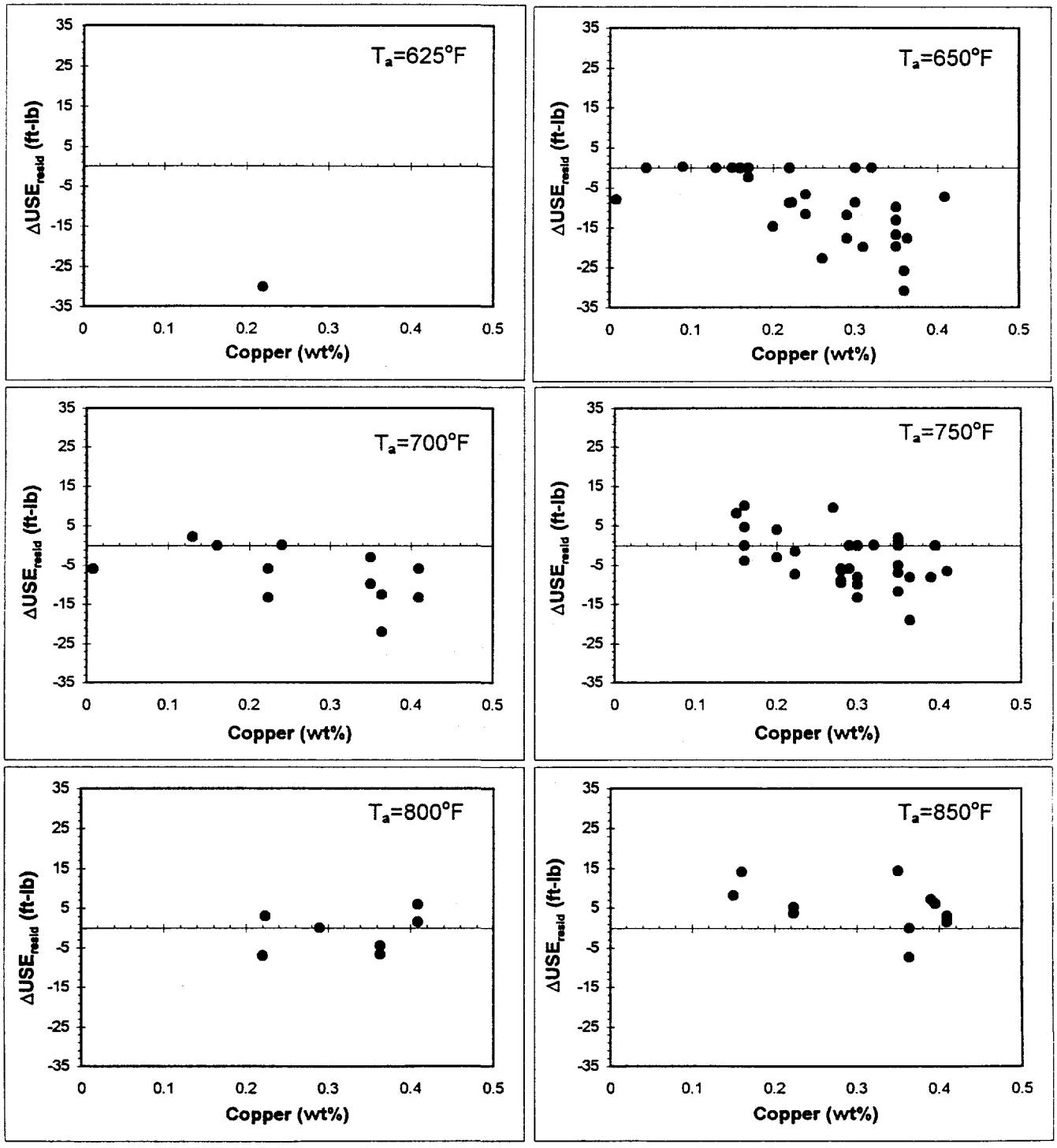

Figure 4-3 Trends in USE Recovery with Cu and T_a

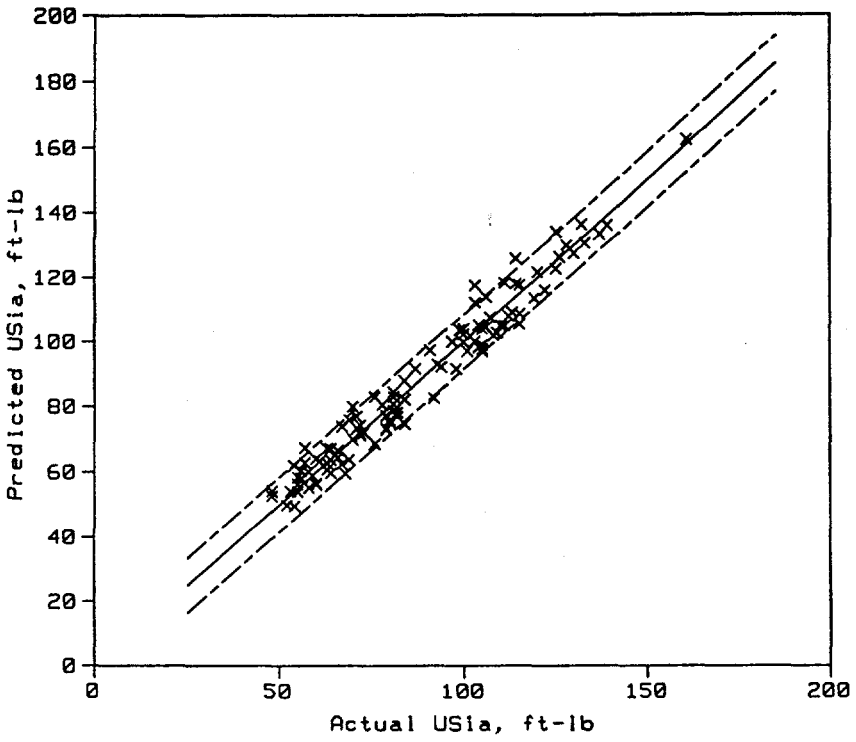

Figure 4-4 Predicted vs. Actual USE_{ia} After Annealing, Eq. 4-2

The key trends reflected in the data and represented in Equation 4-2 are:

- for long annealing times (t_a > 50 h), the amount of annealing recovery $\Delta USE_a = USE_{ia} - USE_i$ is directly proportional to the drop in upper shelf energy due to irradiation, ΔUSE_i
- higher Cu makes the irradiation effect more resistant to recovery at low T_a
- recovery increases with increasing T_a

These trends are certainly expected on a physical basis. For example, similar trends are manifested, albeit in a different quantitative manner, in the behavior of shift. Hence, inclusion of these terms is likely to provide a more reliable basis for data interpolation and extrapolation, despite the lack of sensitivity in the available data base. The motivation for addition of a separate T_a term from patterns in the USE data base is less apparent. However, it derives from the notion of copper-dependent and copper-independent hardening features recovering over different temperature ranges. That is, even with no copper, some effect of T_a would be expected.

Note that over-recovery (USE_{ia} > USE_u) is possible using Equation 4-2. Such over-recovery actually occurs in the data base for 24 points.

The goodness of fit of Equation 4-2 is demonstrated graphically in Figures 4-4 and 4-5. Figure 4-4 shows the actual USE_{ia} versus the predicted USE_{ia} with bounds that enclose 90% of the data. For Figure 4-5, the USE_{ia} data were normalized to "standard conditions" of the other independent variables, as if all tests were conducted at the same conditions. To obtain these plots, the data are adjusted using the model to minimize the scatter about the model. For example, the normalized plot of USE_i versus USE_{ia}, Figure 4-5a, was obtained by the following formula:

$$USE_{ia}|_{norm} = USE_{ia}|_{data} + \left(USE_{ia}|_{sc} - USE_{ia}|_{mc} \right) \quad (4\text{-}3)$$

where

$USE_{ia}|_{norm}$ = the plotted (normalized) value of USE_{ia}
$USE_{ia}|_{data}$ = the data value of USE_{ia}
$USE_{ia}|_{sc}$ = the model value of USE_{ia} at the measured value of USE_i and standard conditions of ΔUSE_i, T_a, t_a, and Cu
$USE_{ia}|_{mc}$ = the model value of USE_{ia} at the measured values of USE_i, ΔUSE_i, T_a, t_a, and Cu

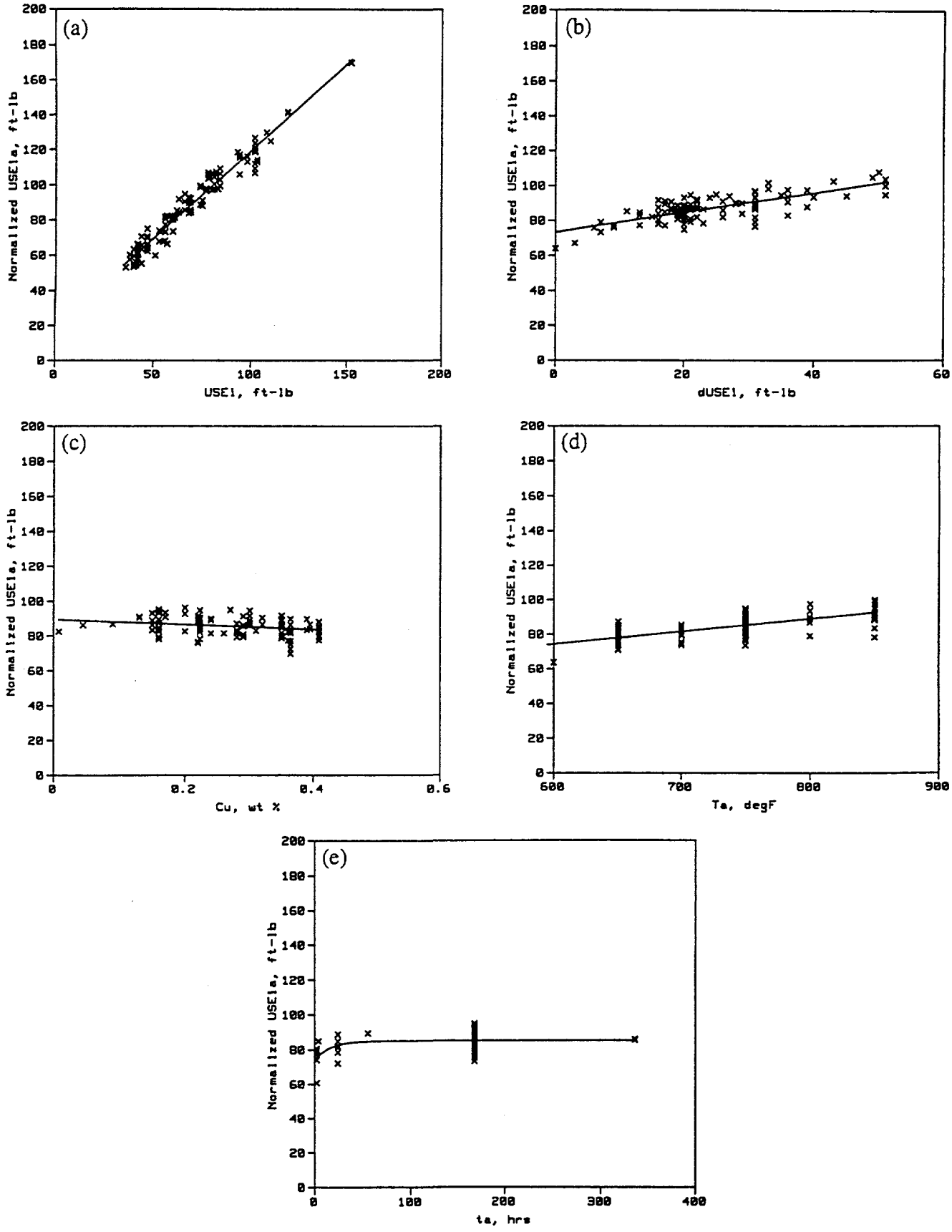

Figure 4-5 Normalized USE_{ia} After Annealing for Upper Shelf Model (Eq. 4-2)

Standard conditions were defined as

USE_i = 66 ft-lb
ΔUSE_i = 21 ft-lb
T_a = 750 °F
t_a = 168 h
Cu = 0.29 wt%

This normalizing procedure makes it possible to visually assess the trends and the quality of fit to a multivariable model. Without such a procedure, the apparent scatter arising from different test conditions of the variables not being plotted makes any assessment of trends difficult.

The trends displayed in Figure 4-5 are displayed in a different form in Figure 4-6, where the dependent variable is $\Delta USE_a = USE_{ia} - USE_i$. The plots look a little different, but they portray the same information. For instance, if Cu varies over the range 0.1 to 0.4 wt%, with all other variables fixed, the result is a 4 ft-lb change in both USE_{ia} and ΔUSE_a. Similarly, over the range $650 \le T_a \le 850$°F, with all other variables fixed, the result is a 15 ft-lb change in both USE_{ia} and ΔUSE_a. The apparent greater effects of these variables in the ΔUSE_a plots in Figure 4-6 is caused by the different scales (the eye compares the same 4 or 15 ft-lb change to average values near 20 ft-lb for ΔUSE_a versus 100 ft-lb for USE_{ia}).

The following expression may be used to convert Equation 4-2 to the residual fraction of the drop in USE:

$$fUSE_{resid} = \frac{USE_u - USE_{ia}}{USE_u - USE_i} \qquad (4\text{-}4)$$

Note that $fUSE_{resid}$ is a function of $\Delta USE_i = USE_u - USE_i$.

4.2 Transition Temperature Shift Recovery

4.2.1 Selection of Dependent Variable

The candidate dependent variables considered for TTS are defined in Table 2-3. Results of TACMVS and CART for the various dependent variables are shown in Tables 4-4 through 4-6. Differences among the dependent variable formulations are less significant for TTS than they are for USE. For modeling recovery in TTS, both the final value (TT_{ia}) and the shift (ΔTT_a) can be predicted well, although the final value TT_{ia} shows slightly better results. To obtain fits with minimum scatter and remain consistent with the USE model, TT_{ia} was used as the dependent variable for most model-building purposes. In all cases, the correlation forms for TT_{ia} included linear TT_i and ΔTT_i terms with coefficients of one. Thus the model in TT_{ia} form can be converted algebraically to other forms, including the fractional recovery. The fractional recovery does not depend explicitly on TT_i and ΔTT_i, which permits a direct comparison of the Charpy shift correlation with surrogate hardness data and other types of embrittlement data. This feature is used below for calibrating the flux effect.

4.2.2 Correlations Among "Independent" Variables, Variable Importance, and Pattern Recognition

A number of intermediate to strong correlations were found among chemistry variables, such as Mn and Mo, and among TT quantities used as independent variables, such as TT_i and ΔTT_i. Intermediate correlations were found between Mo and T_a. The correlations are shown graphically in Figure 4-7.

TAC runs for TT_{ia} were made using the most important independent variables indicated by TACMVS and CART (see Tables 4-4 and 4-5). TAC plots are shown in Figure 4-8. These plots show that TT_{ia} is roughly linearly related to TT_i, ΔTT_i, and the products ΔTT_i times $T_a ln t_a$ and $(T_a - T_i)$. The curve showing the product of ΔTT_i and $Cu^{0.5}$ is nonlinear, which indicates a saturation effect of Cu.

4.2.3 Transition Temperature Shift Recovery Model

The TAC and CART results led to the following preliminary model for TT_{ia} for all T_a:

$$TT_{ia} = TT_i - \Delta TT_i\left[3.81\text{x}10^{-5} T_a \ln t_a + 2.76\text{x}10^{-3}\left(T_a - T_i\right) - 0.704\,Cu^{0.396} + 0.250\right] \qquad (4\text{-}5)$$

with a standard error of 18.9°F. Starting from this preliminary correlation and the physical knowledge summarized in Section 1.3, several iterations of pattern recognition evaluations, statistically-based model development, analysis of subsets of data split by T_a, Cu, and other variables, and physically-motivated modeling efforts were conducted. More realistic nonlinear forms for the interactions of T_a, Cu, T_i, and t_a were found, and the fact that over-recovery does not occur in the shift recovery data was accommodated by the use of a *tanh* function. The *tanh* function also captures the nonlinearity in fractional annealing recovery with increasing annealing temperature. The final result of the collaborative analysis is the following *tanh* model, calibrated using SURFIT:

$$TT_{ia} = TT_i - \Delta TT_i\left[0.5 + 0.5 \tanh\left(\frac{a_1 T_a - a_2}{a_3}\right)\right] \qquad (4\text{-}6)$$

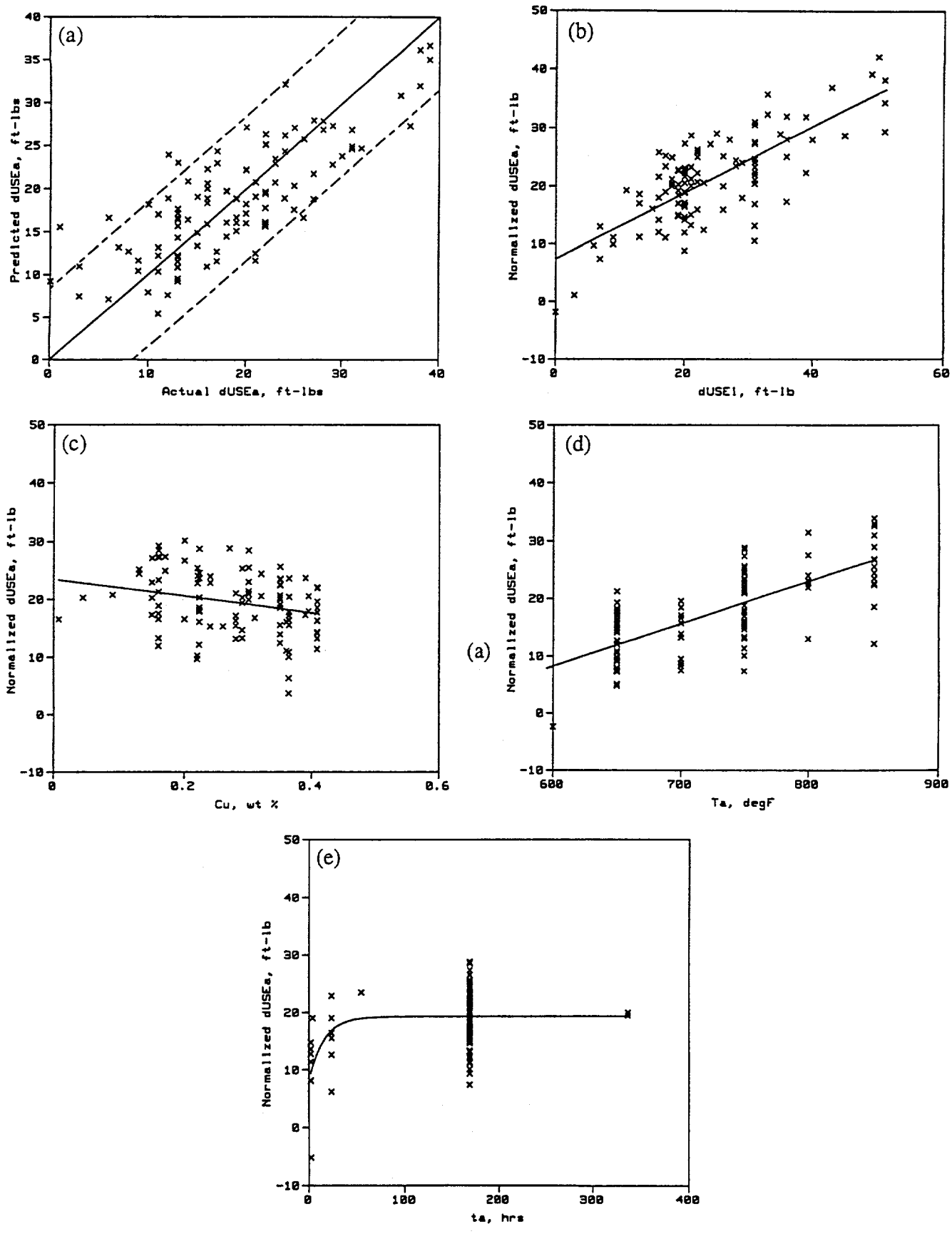

Figure 4-6 Normalized ΔUSE_a Due to Annealing, for Upper Shelf Model (Eq. 4-2)

Table 4-4. TAC and CART Results for TTS Recovery, Including Cu Combinations

TT_{ia}				ΔTT_a				ΔTT_{resid}				fTT_{recov}			
TAC		CART		TAC		CART		TAC		CART		TAC		CART	
X	R^2	X	Imp	X	R^2	X	Imp	X	R^2	X	Imp	X	R^2	X	Imp
TT_i	0.64	TT_i	100	ΔTT_i	0.71	ΔTT_i	100	$Cu*\Delta TT_i$	0.41	T_a	100	$fUSE_{recov}$	0.46	T_a	100
$fUSE_{recov}$	0.79	TT_u	95	T_a	0.78	TT_i	69	T_a	0.77	ΔUS_{resid}	78	T_a	0.71	$T_a lnt_a$	99
T_a	0.89	S	75	$CuT_i lnt_i$	0.86	T_i	51	$fUSE_{recov}$	0.81	ΔTT_i	72	Ni	0.77	$fUSE_{recov}$	70
Cr	0.92	ΔTT_i	74	Ni/Cu	0.90	$T_i lnt_i$	42	ϕt	0.86	$Cu(T_a-T_i)$	63	TT_u	0.81	$T_i lnt_i$	62
ΔUSE_{resid}	0.92	T_i	56	Si	0.91	$T_a lnt_a$	38	Cr	0.89	TT_i	61	Cu*Ni	0.82	$Cu(T_a-T_i)$	51

Table 4-5. TAC and CART Results for TTS Recovery, Including T_a Combinations

TT_{ia}				ΔTT_a				ΔTT_{resid}				fTT_{recov}			
TAC		CART		TAC		CART		TAC		CART		TAC		CART	
X	R^2	X	Imp	X	R^2	X	Imp	X	R^2	X	Imp	X	R^2	X	Imp
TT_i	0.64	TT_i	100	ΔTT_i*T_a	.73	ΔTT_i*T_a	100	ΔUSE_{resid}	0.39	T_a	100	$fUSE_{recov}$	0.46	$T_a lnt_a$	100
$fUSE_{recov}$	0.79	TT_u/T_a	100	$Ni*T_a$	0.81	ΔTT_i	90	Cr/T_a	0.64	ΔUSE_{resid}	85	T_a	0.71	$T_i lnt_i$	82
T_a	0.89	TT_u	96	t_i	0.84	TT_i	62	ΔTT_i	0.77	Mn/T_a	84	Ni	0.77	T_a	80
Cr	0.92	S/T_a	79	$T_a lnt_a$	0.86	T_i	52	T_a	0.82	ΔTT_i	78	TT_u/T_a	0.81	$fUSE_{recov}$	80
ΔUSE_{resid}	0.92	ΔTT_i	75	Cu	0.88	S/T_a	38	Ni/T_a	0.87	TT_i	75	$Ni*T_a$	0.82	ΔTT_i*T_a	72

Table 4-6. Pooled Coefficients of Variance for TT from Final CART Groupings

Dependent variable	Including Cu combinations	Including T_a combinations
TT_{ia}	0.05	0.06
ΔTT_a	0.24	0.24
ΔTT_{res}	0.41	0.34
fTT_{recov}	0.23	0.34

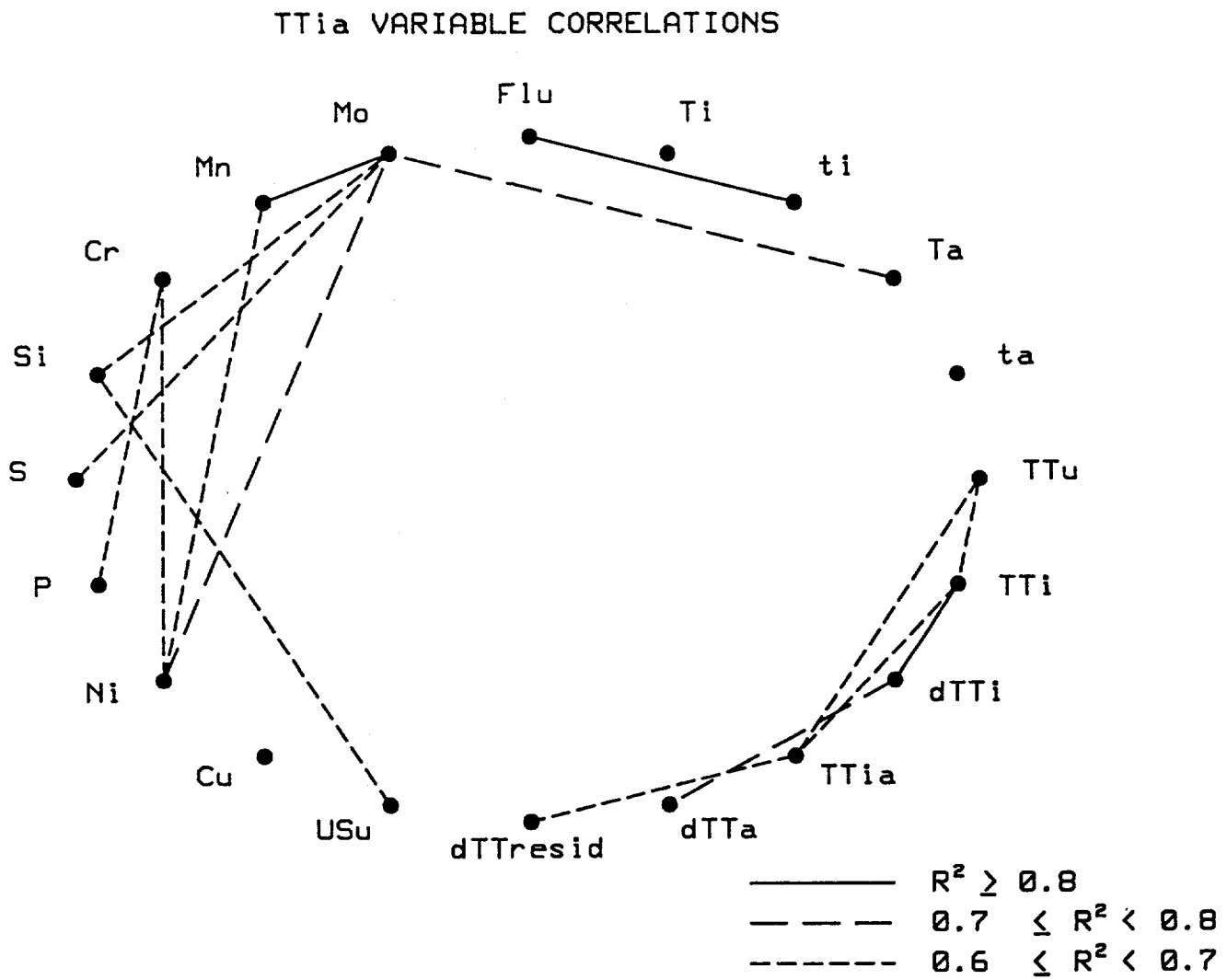

Figure 4-7 Correlations Among TT Variables

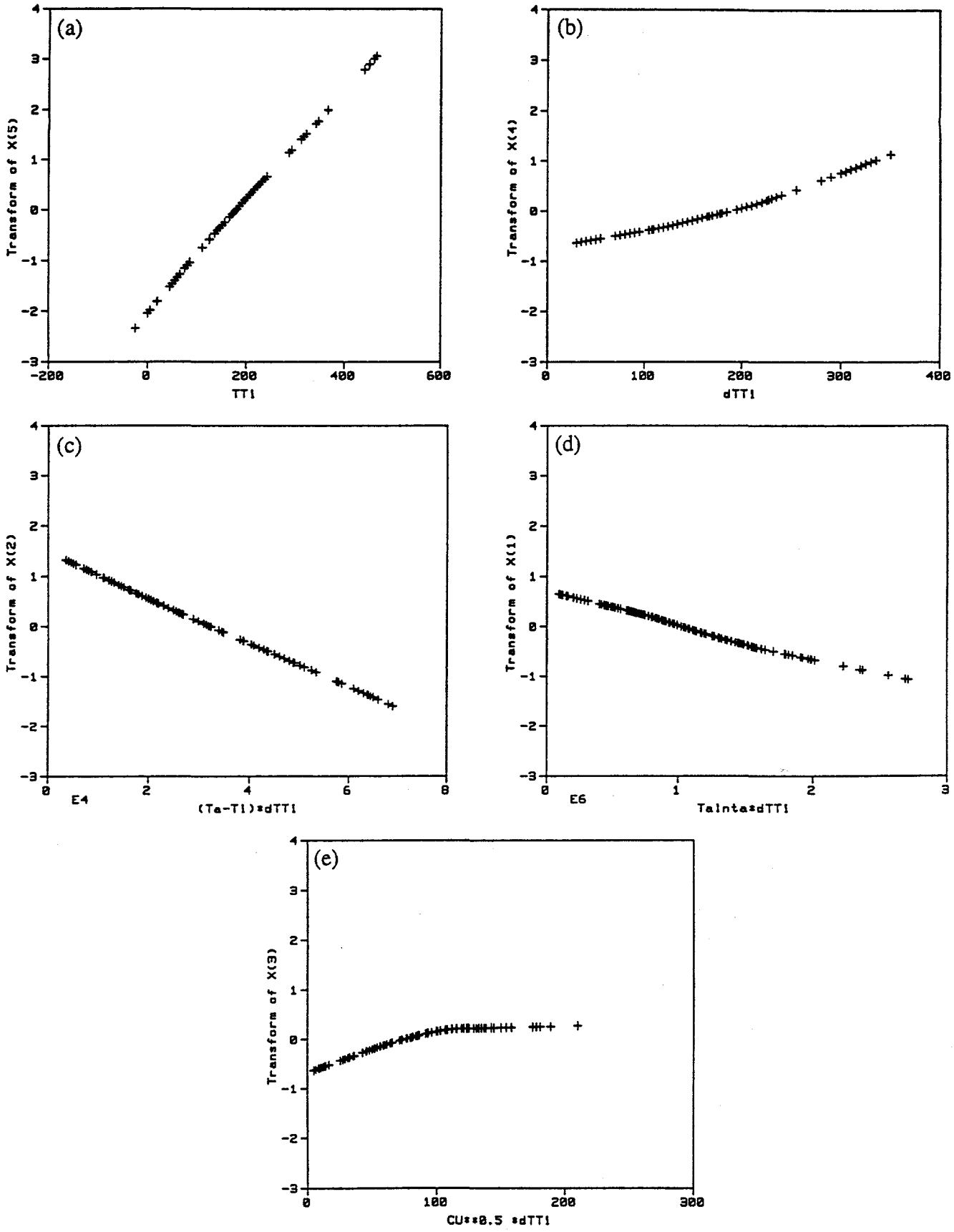

Figure 4-8 Preliminary TAC Results for TT_{ia}

where

$$a_1 = 1 + 0.0151 \ln t_a - 0.424 Cu^{(3.28 - 0.00306 T_a)} \quad (4\text{-}7)$$

$$\text{where } Cu = \min \begin{cases} Cu_{\text{measured}} \\ 0.30 \text{ wt \%} \end{cases}$$

$$a_2 = 0.584 (T_i + 637) \quad (4\text{-}8)$$

$$a_3 = 95.7 \quad (4\text{-}9)$$

and TT_{ia}, TT_i, ΔTT_i, T_a, and T_i are in °F, t_a is in hours, and Cu is in wt%. The standard error of the model in this form is 16.9°F, using the 153 data points for which the dependent variable and all independent variables in the model were available; one point that was initially an outlier and biased the fit was omitted (i.e., calculated TT_{ia} is more than $4S_e$ from the actual TT_{ia}).

The above model has an upper limit on the amount of copper that affects the annealing process, as shown in Equation 4-7. Matrix copper content depends on time and temperature history during tempering and stress relief treatments as well as the alloy composition and microstructure. Unpublished analytical electron microscopy measurements by Pythian, Odette, and co-workers show matrix copper contents of about 0.3±0.02 wt% following typical stress relief treatments in the range of about 1112 to 1166°F for times up to 80 h. These values are slightly in excess of the estimated solubility limits of copper; hence using 0.3 wt% represents a reasonable estimate of the maximum effective concentration of this element. The maximum copper concentration may vary from one vessel to another, depending on stress relief heat treatment conditions.

During the fitting process, several models were fitted with different Cu_{max} to check the sensitivity to this parameter and to attempt to find a statistically optimal value. The standard errors for all these models, over the range $0.26 \le Cu_{max} \le 0.34$ wt%, are not significantly different. For this reason, and the likelihood that the minor differences observed in S_e were unduly influenced by a few points, the attempt to find a statistically optimal value of maximum copper was abandoned. The value Cu_{max} = 0.3 wt% for the model was chosen for physical reasons as a good average value for the stress relief temperatures that were commonly used during fabrication of the existing pressure vessels. It is also a good value from a statistical point of view.

It should be emphasized that Equation 4-7 does not reflect a global conclusion that the maximum effective copper is 0.3 wt% in all cases. Indeed, there may be important instances in which the effective maximum Cu deviates from the nominal value of 0.3 wt%. If a case can be made for lower Cu_{max} for a particular application, it is suggested that Equation 4-7 should be used with the lower estimate replacing the 0.3 wt%. This represents an interpolation within the present data base for Cu < 0.3 wt%. In cases where the maximum effective copper content is believed to be more than 0.3 wt%, it is recommended that the higher estimate of Cu_{max} be used in Eq. 4-7, which represents an extrapolation of the trends observed in this study.

A possible effect of flux is suggested by the Charpy annealing data and the physical considerations outlined in Section 1.3. The UCSB and Westinghouse microhardness data base contains a broader range of flux and shows a clear trend -- annealing recovery decreases with decreasing flux for anneals at 650 and 750°F but not at 850°F, as shown in Figure 4-9. Figure 4-9 shows that a flux term is needed to avoid over-prediction of recovery at low fluxes for $T_a \le 750$°F, but not for $T_a \ge 850$°F. Recognizing that the expression in square brackets in Equation 4-6 is the fractional shift recovered by annealing, fTT_{recov}, it is possible to expand the modeling data base with some low flux hardness data -- specifically, Westinghouse power reactor data (Mager and Lott, 1989) -- and calibrate a flux effect. The assumption is made that annealing produces the same fraction recovered for hardness as for Charpy TTS. This assumption is necessary, because Charpy recovery data are not available at power reactor fluxes, but it is also justified by the observed consistency of hardness and shift data.

To account for the flux effect at low T_a, a flux term was added to Equation 4-8 such that

$$a_2 = 0.584 T_i - 15.5 \ln \phi + 833 \quad (4\text{-}10)$$

where ϕ is in units of $n/(cm^2\text{-}s)$. The coefficient on $ln\phi$ and the constant term (+833) in Equation 4-10 were calibrated to the Westinghouse power reactor hardness data plus Charpy recovery data with $T_a \le 750$°F, while all other parameters of the model were held fixed, as in Equations 4-7 through 4-9. Figure 4-10 shows the resulting plot of normalized fraction recovered versus flux for the $T_a \le 750$°F data.

Figure 4-10 shows good agreement between the hardness and Charpy data at lower annealing temperatures ($T_a \le 750$°F) when the flux effect in Equation 4-10 is used. Figure 4-11 shows good agreement at higher annealing temperatures ($T_a \ge 800$°F) without the flux term (i.e., using Equation 4-8). To have the best model over the full range of T_a, we recommend using Equation 4-10 for $T_a \le 750$°F and Equation 4-8 for $T_a \ge 800$°F.

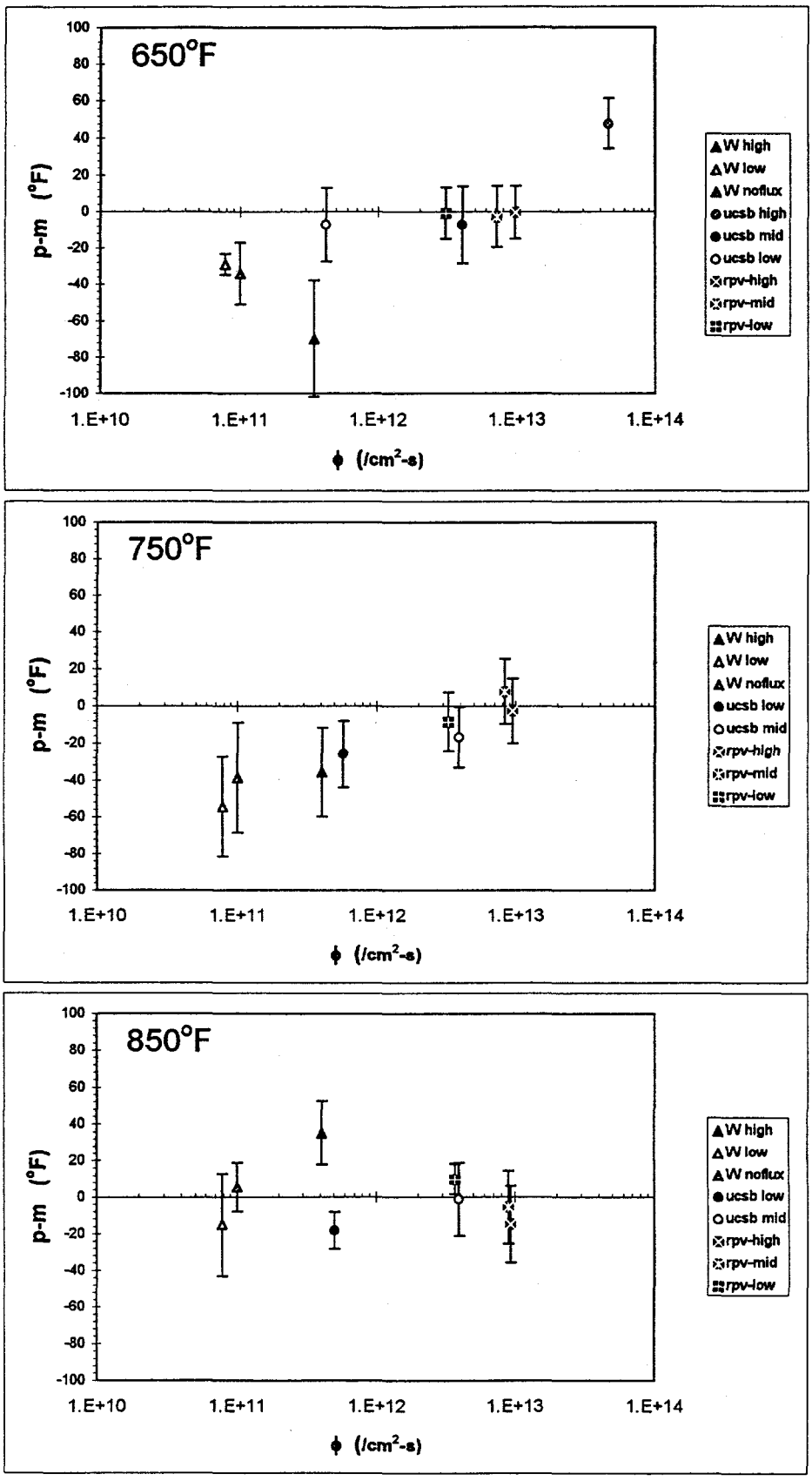

Figure 4-9 Flux vs. T_a Trends, Residuals from Eq. 4-6 through 4-9

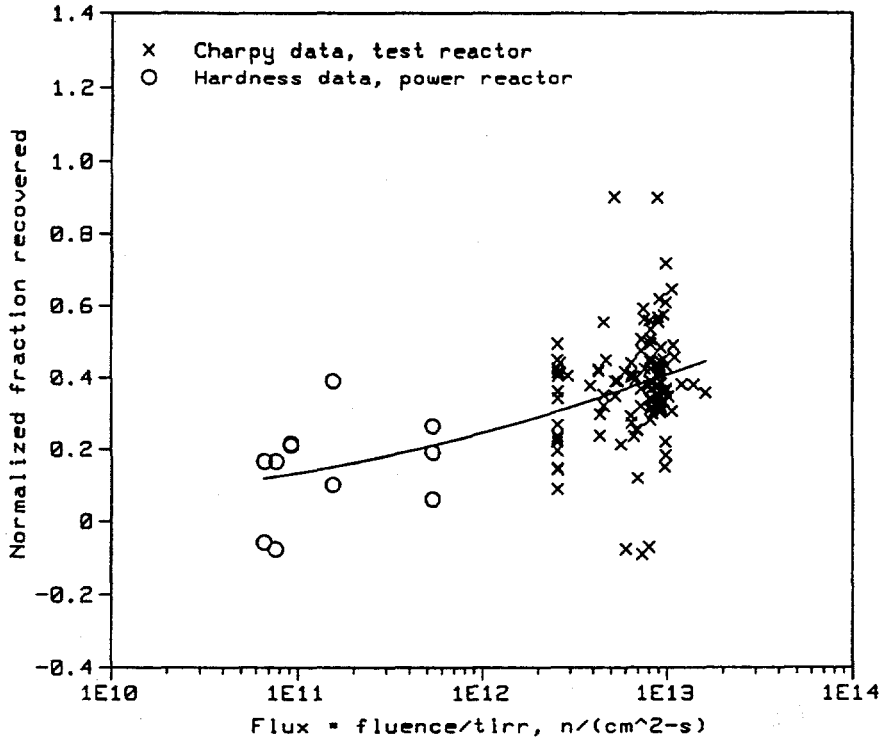

Figure 4-10 Charpy and Power Reactor Hardness Data vs. Flux Term (Eq. 4-10), $T_a \leq 750°F$

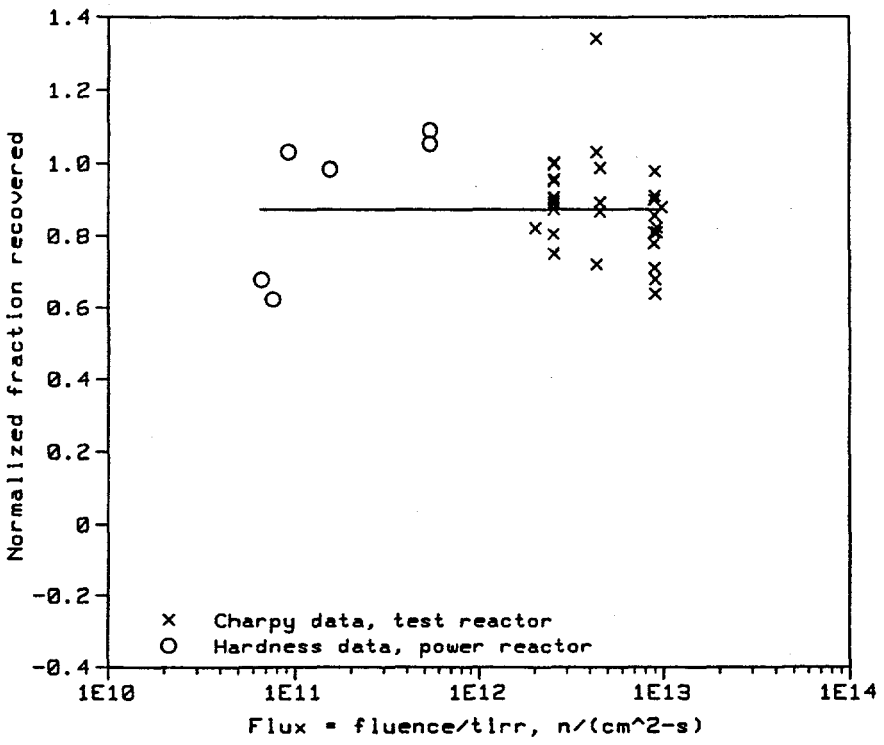

Figure 4-11 Charpy and Power Reactor Hardness Data without Flux Term (Eq. 4-8), $T_a \geq 800°F$

Annealing treatments between 750°F and 800°F should be avoided pending additional data; there are neither Charpy nor hardness data in that range to help determine the shape of the transition from flux-dependent to flux-independent behavior, or the range in temperatures over which such transitions occur. The treatment of flux given here must be considered preliminary and should be revisited if additional data become available or new fundamental insights into irradiation and annealing mechanisms are discovered. It is probable that the transition range depends on other irradiation, metallurgical and annealing variables.

Actual versus predicted TT_{ia} and normalized plots using Equations 4-6 through 4-10 are shown in Figures 4-12 and 4-13, where the a_2 term of Equation 4-6 is calculated from Equation 4-8 for $T_a \geq 800°F$ and Equation 4-10 for $T_a \leq 750°F$. The standard error of the Charpy data is 17.2°F for 151 data points. Based on an F-test, this standard error is not statistically different from the standard error of 16.9°F obtained when Equation 4-8 is used for all T_a. Thus, while the best fit to the Charpy data (Equation 4-6 through 4-9) does not include a flux term, adding a flux term to agree with hardness data does not compromise the fit to the Charpy data.

The method of normalization used for Figures 4-10, 4-11, and 4-13 was the same as that described by Equation 4-5. Standard conditions for the normalized plots were defined as:

TT_i = 178°F
ΔTT_i = 167°F
T_a = 663°F for Figure 4-10, 850°F for Figure 4-11, 750°F for Figures 4-13 and 4-14
t_a = 168 h
T_i = 550°F
Cu = 0.223 wt%
ϕ = 8.07×10^{12} n/(cm^2-s)

As previously mentioned, the quantity in brackets in Equation 4-6 is the fraction of the TTS that is recovered by annealing, which is equal to $1 - fTT_{resid}$; so residual fraction can be expressed:

$$fTT_{resid} = 0.5 - 0.5 \tanh\left(\frac{a_1 T_a - a_2}{a_3}\right) \quad (4\text{-}11)$$

The above models can be converted easily to predict absolute recovery of TTS due to annealing using $\Delta TT_a = TT_i - TT_{ia}$. Actual versus predicted ΔTT_a and normalized plots for the models in this form are shown in Figure 4-14.

4.2.4 Physically-Motivated TTS Recovery Model

A physically-motivated model without a flux term was developed in parallel with the statistical model without a flux term, i.e., Equations 4-6 through 4-9. The purpose was to help with the development and evaluation of the statistical model, rather than to derive a detailed model describing all of the thermodynamics, kinetics, and structural property physics involved in annealing. Such detailed models have been derived and are under continuing development, including mechanistic elaboration of flux effects, as will be described in a thesis being prepared by one of the authors (E. Mader). The thesis will include a very extensive microstructural data base, detailed kinetic, thermodynamic, and micromechanical models, and comparisons of the physical and correlation models to the embrittlement and annealing data base. For the present purposes, it was sufficient to develop a formulation that is physically motivated, does not violate our basic understanding of embrittlement and recovery processes, and is broadly consistent with trends in hardness and other surrogate data.

A simplified, physically-based model has been constructed to reflect the recovery of two independent defect features -- namely the matrix defects (MD) and copper rich precipitates (CRP) – in terms of the fractional residual shift, fTT_{resid},

$$fTT_{resid} = \frac{C_1 A_{md} + \sqrt{Cu}\, A_{crp}}{C_1 + \sqrt{Cu}} + \nu T_i + \kappa t_a \quad (4\text{-}12)$$

where T_i is in °R, t_a is in hours, and Cu is in wt%. Here the A_{md} and A_{crp} are separate annealing functions for the MD and CRP (discussed below), where C_1 reflects their relative contributions. For simplicity, the effects of T_i and t_a have been included as separate correction terms (υT_i and κt_a). Alternatively, their effects could be included in the C_1 and $A_{crp/md}$ functions respectively.

The A_{md} is expected to depend only on T_a. For a specified t_a (or lnt_a) a first order annealing model suggests that a good representation is

$$A_{md}(T_a) = \sqrt{\exp\left[-\exp\left(-\frac{T_{rmd} + \Delta T_{md} - T_a}{\Delta T_{md}}\right)\right]} \quad (4\text{-}13)$$

where all temperatures are in °R, T_{rmd} is a reference value defining the minimum recovery temperature, and ΔT_{md} is the measure of the recovery temperature interval for the MD. The square root reflects the corresponding dependence of hardening and shift on the number density

of MD. While the CRP processes (dissolution and coarsening) certainly do not follow such simple first order recovery, the double exponential remains a convenient formulation. However, in this case the effect of the Cu content on the CRP recovery must be included. This effect is related to the solubility of Cu in equilibrium with small, coherent body-centered cubic (bcc) CRP; this solubility is much higher than the solubility of Cu in equilibrium with bulk face-centered cubic (fcc) Cu. Thus the recovery temperature interval is expected to decrease with increasing Cu, and

$$A_{crp}(T_a, Cu) = \sqrt{\exp\left[-\exp\left(-\frac{T_{rcrp} + \Delta T_{crp} - T_a}{\Delta T_{crp}}\right)\right]} \quad \textbf{(4-14)}$$

where

$$\Delta T_{crp} = 1 + C_2 Cu \quad \textbf{(4-15)}$$

The irradiation temperature dependence term was derived by making use of the observation that T_i affects the as-irradiated hardening much more than subsequent annealing. Thus Equation 4-12 was modified to the form

$$f'_{resid}(T_i) = \frac{C_1 A_{md} + \sqrt{Cu}\, A_{crp}}{C_1\left[1 + C_3(T_i - 1010)\right] + \sqrt{Cu}} \quad \textbf{(4-16)}$$

However, rather than this nonlinear form, it is better to use a linear temperature term over the interval with most of the data, namely T_i = 960 to 1010°R. Thus, taking $\{ [f'_{resid}(1010) - f'_{resid}(960)] / 50 \} (T_i - 1010)$, and after some manipulation,

$$\nu T_i = \frac{C_1 A_{md} + \sqrt{Cu}\, A_{crp}}{(C_1 + \sqrt{Cu})(C_1 C_3 + \sqrt{Cu})}\left[C_1\left(\frac{1 - C_3}{50}\right)\right](T_i - 1010) \quad \textbf{(4-17)}$$

Finally, the effect of t_a on fTT_{resid} is well represented by the expression

$$\kappa t_a = C_4 T_a\left[\ln(168) - \ln t_a\right] \quad \textbf{(4-18)}$$

This allows fTT_{resid} to rapidly drop to a T_a-dependent level followed by a much slower rate of decrease as manifested in both the shift and hardness data bases.

The reference T_{rmd} and T_{rcrp} were set to 1010 and 1110°R, respectively. The value for the MD is the nominal irradiation temperature. The value for the CRP is based on microstructural observations showing minimal CRP recovery at 650°F (1110°R). This leaves five physically meaningful fitting parameters: C_1 (the MD weighting function), ΔT_{md} (the MD recovery temperature interval), C_2 (the Cu-dependent CRP recovery temperature interval), C_3 (the T_i sensitivity parameter), and C_4 (the T_a/t_a recovery kinetics term).

The fitting parameters for all 151 records with Cu and shift data, T_a (from 1085 to 1310°R), and t_a are:

$C_1 = 0.352$
$C_2 = 389.5$
$C_3 = 0.594$
$C_4 = 3.82 \times 10^{-5}$
$\Delta T_{md} = 70$°R
$Cu_{max} = 0.3$ wt%

Using these parameters in Equation 4-12 yields an average bias of 0°F and a standard deviation of 17.7°F in ΔTT_a. A plot of the predicted versus measured TT_{ia} is shown in Figure 4-15.

Comparisons were made between the physically-motivated model and the hardness and Charpy fitting data and the supplemental shift data. Extensive residual analysis was conducted for both the Charpy and hardness data bases. The results are summarized as follows:

- the physically-motivated model produced excellent fits to all data sources, with standard errors essentially identical with those produced by the *tanh* model (Eqs. 4-6 through 4-10)

- plots of predicted minus measured (p-m) property changes after irradiation and annealing versus all available variables revealed no systematic trends

Figure 4-16 summarizes a number of the trends from the physically based model in terms of the fractional property (f_{resid} = fTT_{resid} or fH_{resid}) after irradiation and annealing. Figure 4-16a shows the recovery versus T_a for Cu = 0, 0.1, 0.2, and 0.3, where the matrix defect is shown as a dotted line and the CRP as the dashed line. Figure 4-16d shows f_{resid} versus copper for T_a = 649, 752, and 842°F. These results demonstrate that at high copper contents the predominant hardening is from the CRP and that the CRP contribution is much more resistant to annealing than the MD. At lower copper contents, the CRP contribution decreases along with its annealing stability, and it is difficult to separate the MD and CRP contribution due to the similarity (non-orthogonality) of the respective annealing functions. Figures 4-16b and 4-16c show f_{resid} versus T_i and t_a, respectively, at T_a = 649, 752, and 842°F; f_{resid} increases with increasing T_i but more slowly at higher T_a, both as expected from the discussion in Section 1.3. The rapid drop in f_{res} versus t_a with annealing temperature is also rationalized based on the presence of matrix defects with a range of thermal stability and

relatively rapid dissolution and coarsening kinetics of the CRP component at high T_a. Thus the calibrated two-defect model appears to be consistent with current understanding of both embrittlement and annealing mechanisms.

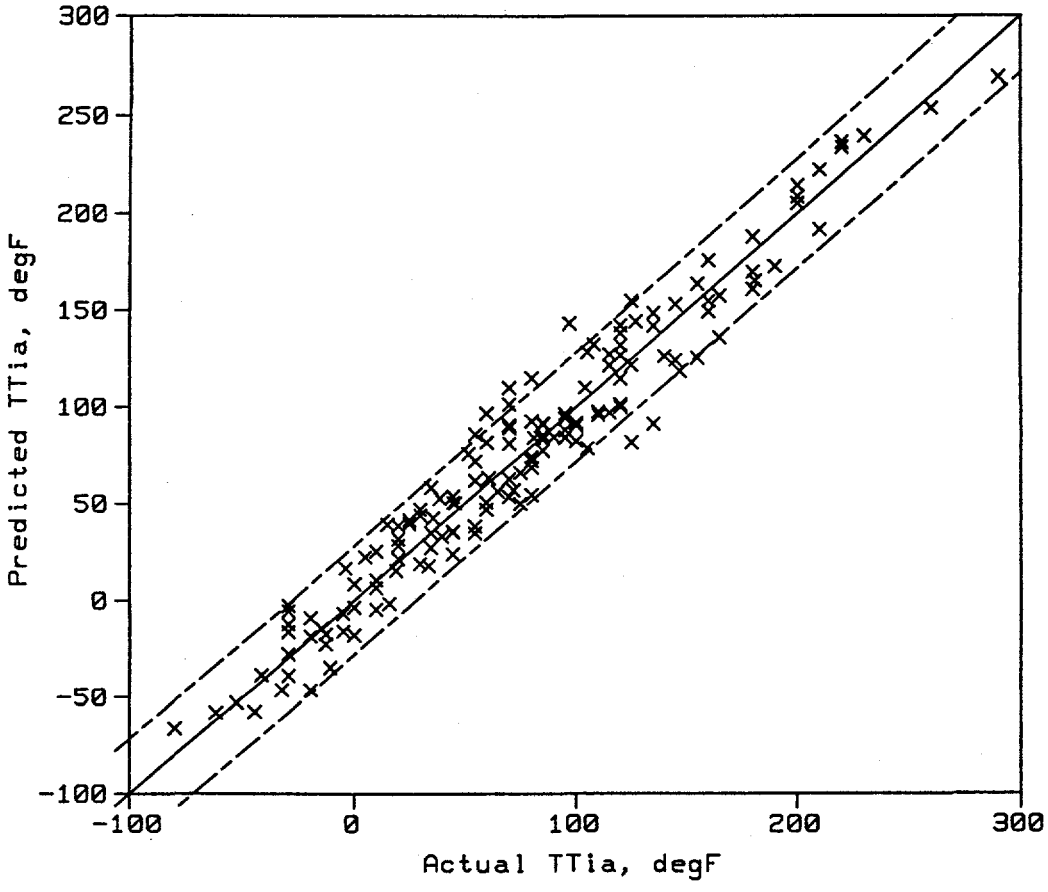

Figure 4-12 Predicted vs. Actual TT_{ia} After Annealing, *tanh* Model

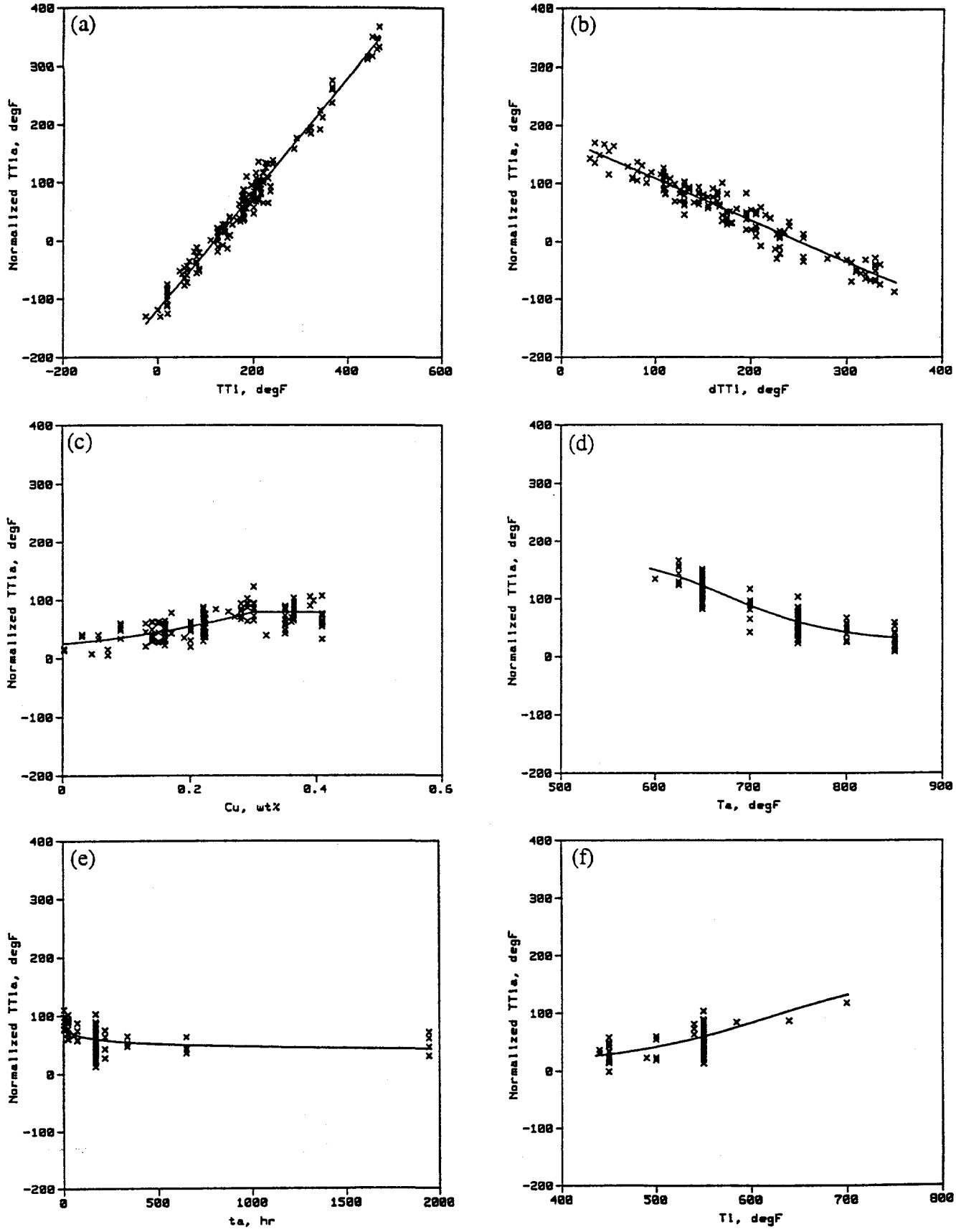

Figure 4-13 Normalized TT_{ia} After Annealing, *tanh* Model

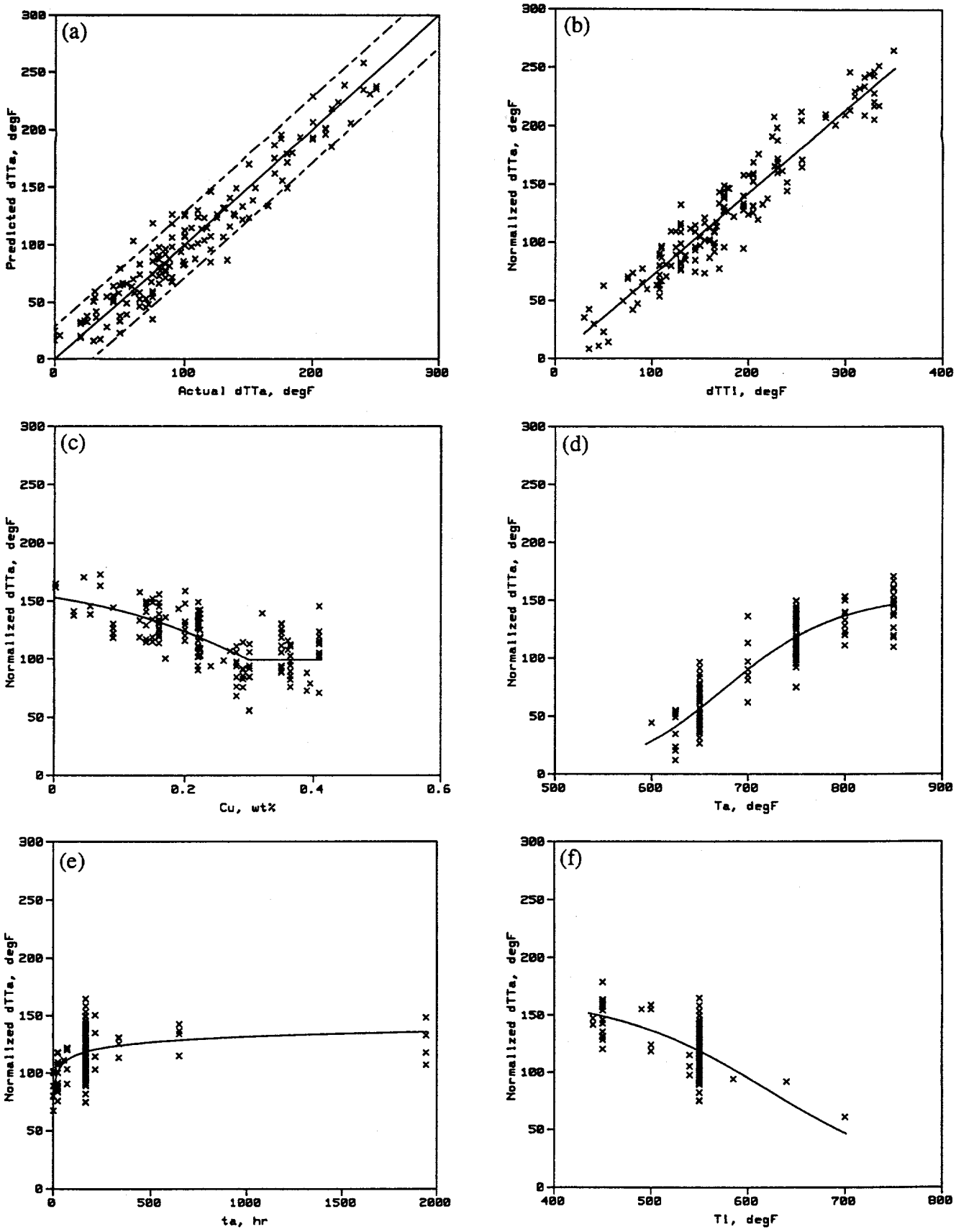

Figure 4-14 Normalized ΔTT_s Due to Annealing, *tanh* Model

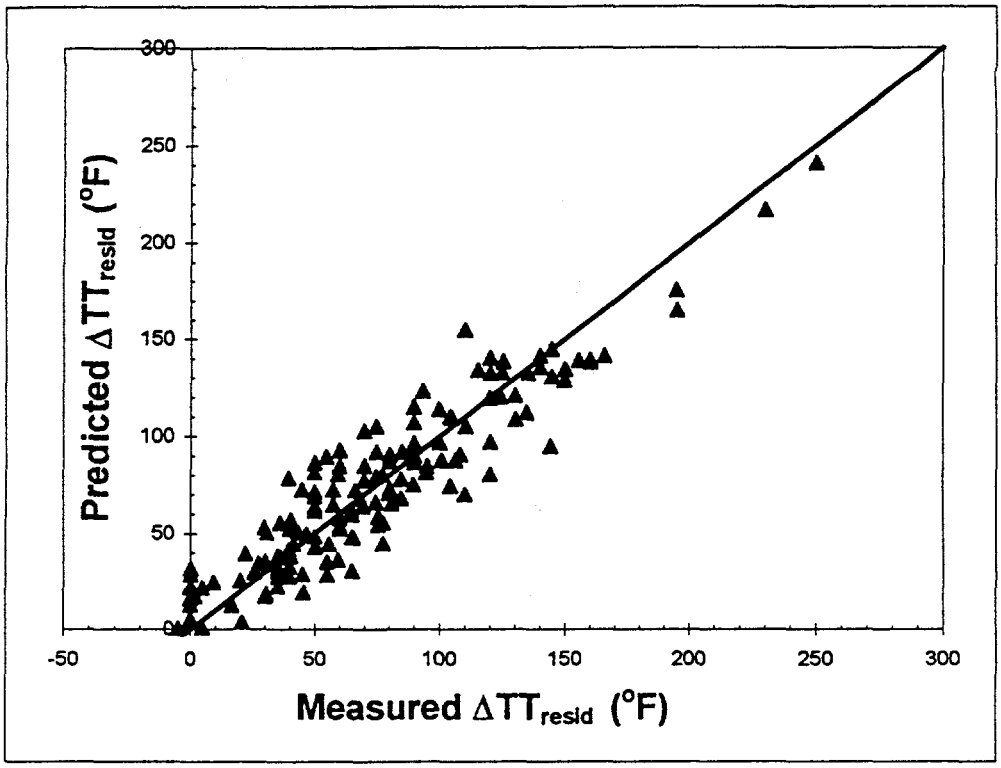

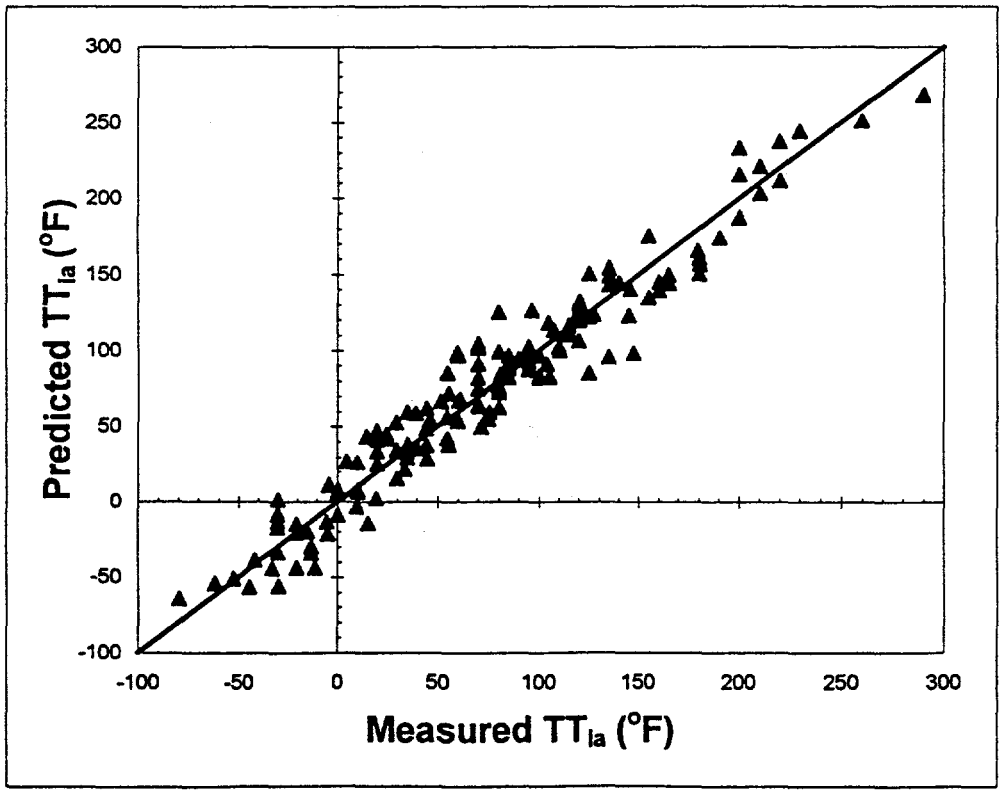

Figure 4-15 Predicted vs. Actual ΔTT_a and TT_{la}, Physically-Motivated Model

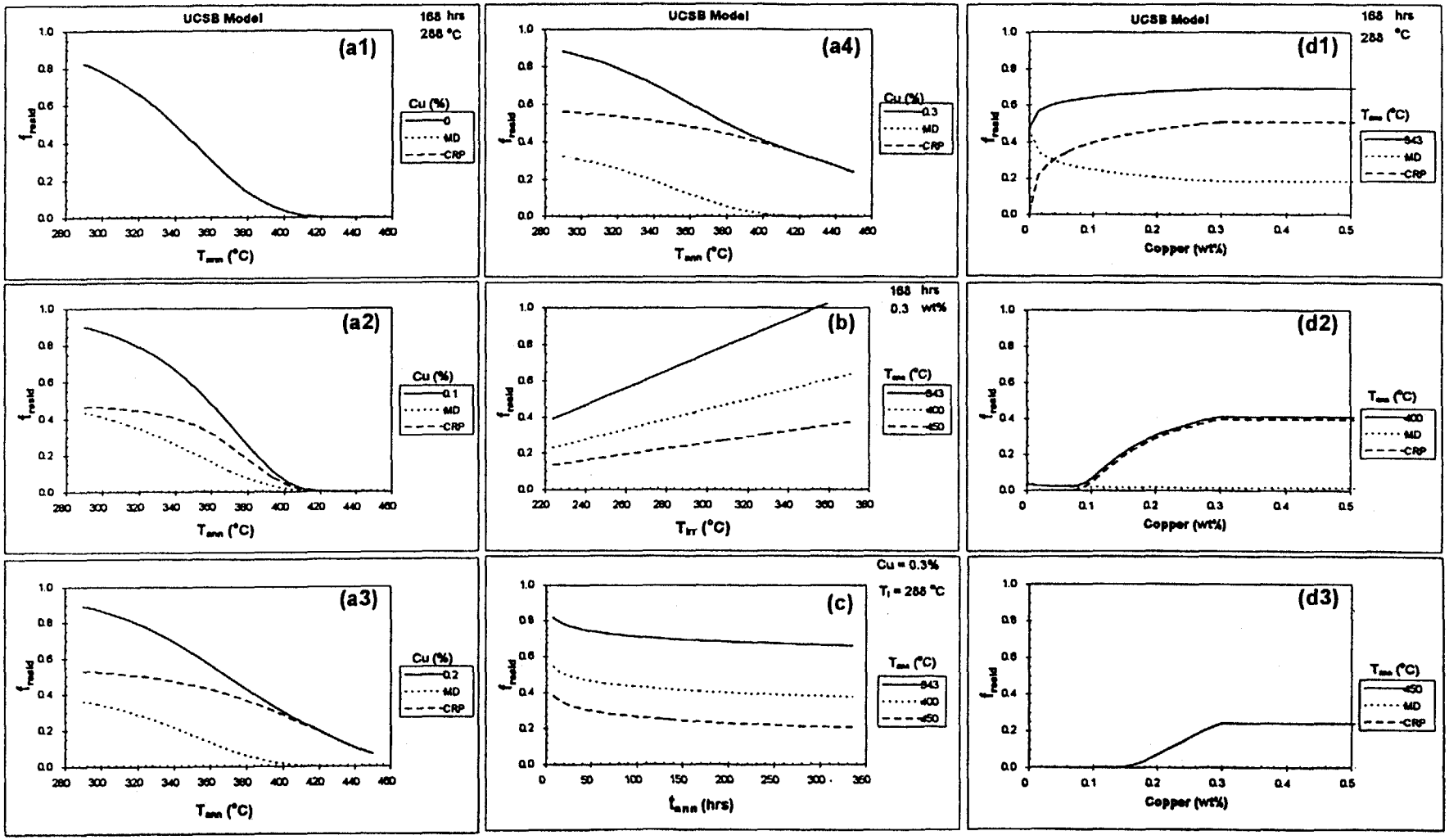

Figure 4-16 Trends in fTT_{resid} or fH_{resid} from Physically-Motivated Model

5 DISCUSSION

5.1 Upper Shelf Energy Recovery Model

The upper shelf energy model in Equation 4-2 is remarkably effective, accounting for 96% of the range in the available data ($R^2 = 0.96$). The residuals relative to the model (predicted-measured = p-m) show no trends that have been missed, as shown in Figure 5-1. The standard error, at 5.1 ft-lb, is not substantially different from the level of error expected in repeated Charpy tests of the same heat at the same conditions. It is difficult to improve upon a model that can predict the annealed upper shelf energy for a range of irradiation, material, and annealing conditions with no more uncertainty than repeated measurements.

In the process of developing Equation 4-2, several correlation models were calibrated with varying forms and complexity. An interesting observation was that all such models were quite effective in predicting the annealed value USE_{ia}, even though they had rather different fitting forms and did not include the same variables. The worst of the models had only slightly higher standard error (6.5 versus 5.1 ft-lb) and slightly lower R^2 (0.92 versus 0.96) than the best of the models, and that worst-case model did not include either T_a or Cu, which clearly have effects (see Figure 4-3). This situation was evident both in the least square fits and the TAC runs; for instance, the first two columns of Tables 4-1 and 4-2 show that the correlation of USE_{ia} with USE_i is very strong (R^2=0.9) if USE_i is the only independent variable. The fit improves to $R^2 = 0.92$ if USE_u or ΔUSE_i is added. With such a high correlation using only the endpoints of the irradiation process (USE_u and USE_i), models with additional variables are refinements of an already good model.

There are several possible explanations for this observation. One partial explanation is that there is substantial recovery in upper shelf energy drop due to irradiation in most of the annealing experiments, generally ranging from 40% to more than 100% recovery. Thus the predicted upper shelf energy after annealing should be less sensitive to the annealing and material variables than if the range were 0-100%. But 40-100% recovery is still a broad range, corresponding to ΔUSE_a ranging from near zero to about 40 ft-lb. This partial explanation does not explain why the amount of recovery can be predicted within that range with a standard error S_e = 6.5 ft-lb by knowing only USE_u and USE_i.

A second partial explanation is that the drop in upper shelf energy due to irradiation depends on fluence, material composition, irradiation temperature, and other variables that also affect the effectiveness of annealing. So the effects of such variables are implicitly included in ΔUSE_i, even when they are not explicitly modeled. This partial explanation does not account for the predictive power of ΔUSE_i without considering annealing temperature T_a, which is not implicitly included.

The third partial explanation is based on the relative magnitudes of the effects of the modeling variables compared to the scatter in the data. For reasons that are not well understood, the copper content and annealing temperature are less sensitive variables than the end conditions USE_u and USE_i (or ΔUSE_i). This fact is evident in the USE_{ia} plots, Figure 4-5, or the ΔUSE_a plots, Figure 4-6. For example, on Figure 4-6b, the range of ΔUSE_i (0 to 50 ft-lb) corresponds to a range of about 30 ft-lb in the expected value of ΔUSE_a. The full ranges of T_a and Cu correspond to changes in the expected value of ΔUSE_a of about 15 and 4 ft-lb, respectively. By comparison, the scatter at any condition is approximately $\pm 2S_e$, a range of 20 ft-lb. So the effects of T_a and Cu are smaller than the scatter.

Whatever explanation or combination of explanations is accepted, the fact that several different models have standard errors that are 1) comparable to experimental error and 2) not significantly different on a statistical basis means that statistical proof of which model is best is not possible. Equation 4-2 has the smallest numerical value of S_e of the various models fitted, and it reflects the trends that are evident in the data. It also reflects the mechanistic concept of Cu-dependent and Cu-independent features that recover to varying degrees depending on temperature. For these reasons, Equation 4-2 is recommended for use over the range of application discussed in Section 5.4.

Unfortunately, no surrogate data are available to address the low flux regime for the USE recovery model (like the hardness recovery data used for the TTS recovery model). So USE recovery data were analyzed to investigate the existence of a flux effect analogous to the one found for TTS recovery. Residual and normalized plots versus flux for the USE recovery model were generated for various subsets of data corresponding to different T_a. No consistent trend in the data was found, so that no flux effect could be inferred from the USE recovery data. By contrast, in the TTS recovery data, a trend with flux is apparent, even without considering the hardness data that

were needed to calibrate a model of the trend.

5.2 Transition Temperature Recovery Model

Transition temperature recovery can be modeled well using the *tanh* model. The standard error of the model, including the flux term for $T_a \leq 750°F$, is 17.2°F over the range of conditions shown in Table 5-1. This is comparable to the standard deviation of TT measurements on a single, well-characterized unirradiated weld (σ= 17°F for twenty locations in a beltline weld, NUREG/CR-5914). From a practical point of view, this means that the expected error from using the model to estimate TT after irradiation and annealing is not much different from the uncertainty in the original, unirradiated value due to variations within the weld. That is believed to be a practical level of overall accuracy. At $R^2 = 0.94$, the correlation coefficient is almost as high as for the upper shelf model.

Many evaluations of quality of fit have been made during this project, including the normalized plots already displayed and the values of standard error and R^2. The following subsections present additional evidence of the quality of fit of the *tanh* model.

5.2.1 Comparison with Physically-Motivated TTS Recovery Model

Figure 5-2 compares the physically-motivated model (solid line in most plots) with the *tanh* model, Equations 4-6 to 4-9 (dashed lines in most plots). Both models in this comparison lack flux terms. Overall, the agreement is excellent, which is not surprising since the two approaches evolved in an iterative fashion and were calibrated on the same data base. The good agreement demonstrates that while Equations 4-6 to 4-9 provide a simple, analytic representation of annealing behavior, they also effectively and robustly mimic the behavior of the more complex physically-motivated model. Where minor differences are evident, such as Cu ≤ 0.15 wt%, there are few Charpy data available to prove which model is more accurate. The differences in any case are small compared to scatter.

5.2.2 Residuals and Subsets of the Charpy Data

Figure 5-3 shows predicted minus measured (p-m) residual plots for the *tanh* model both for variables included and not included in the model. No significant trends could be detected, suggesting that the model is not missing important effects.

Further evaluation of single-variable subsets or data groupings that attempt to isolate single-variable trends in the residuals for the *tanh* model did not reveal any significant un-modeled effects of the T_i, T_a, and Cu variables included in the model. Corresponding evaluations of the effects of the P and ϕt variables not included in the *tanh* model yielded similar conclusions.

Three subsets of data involving single or quasi-single variable differences in nickel content reported by Hawthorne (materials 5C-D, 6A-B-C, WW7-W8A-W9A) indicated a slight, systematic trend: decreasing fractional recovery with increasing nickel. At 750°F the effect is approximately $\Delta fTT_{recov}/\Delta Ni$ = -0.2, and the effect is approximately half as strong at 850°F. A slight Ni effect is also evident in TAC runs on fTT_{resid} over the entire Charpy data base, but not in the predicted minus measured residuals (see Figure 5-3, Ni plot). The insensitivity of fTT_{resid} to Ni was also indicated in the model calibration process by adding a Ni term to Equation 4-6 and observing no improvement in the standard error. But this fact does not prove there is no nickel effect on annealing, since the effect of Ni on embrittlement is implicitly contained in ΔTT_i used in Equation 4-6. If TT_i is higher due to nickel, then TT_{ia} will also be higher, even if fTT_{resid} is independent of Ni. Indeed these implicit effects probably account for most of the effect of Ni. However, the implicit effect does not explain the trend in the subset of data cited above, which despite its small size, is probably best capable of identifying a Ni effect if one exists. These data suggest that higher nickel makes steels slightly more resistant to annealing than indicated by the effect on ΔTT_i alone. Thus, either the effect of Ni on fTT_{resid} indicated here does not occur in other cases, or it is confounded by other variables in the overall data base. Since the shift data base is very limited in the regime where a Ni effect would be most significant (high nickel and copper), additional experiments will be needed to resolve this question.

5.2.3 Hardness Data Base

Direct application of the *tanh* model to the completely independent and largely controlled hardness data base yielded remarkable agreement, as shown in Figure 5-4. Seven (7) outliers were excluded from Figure 5-4, with predicted minus measured errors of more than 16 DPH. The average bias of the outliers was only 1 DPH. Four of the seven excluded data points were for low temperature 650°F anneals, and in six of the seven cases, other data points for the same irradiated steel with slightly different annealing times or temperatures were in much better agreement with the *tanh* model predictions. No systematic bias is indicated by any of these isolated data points. The mean bias is only -1.0 DPH, and the standard

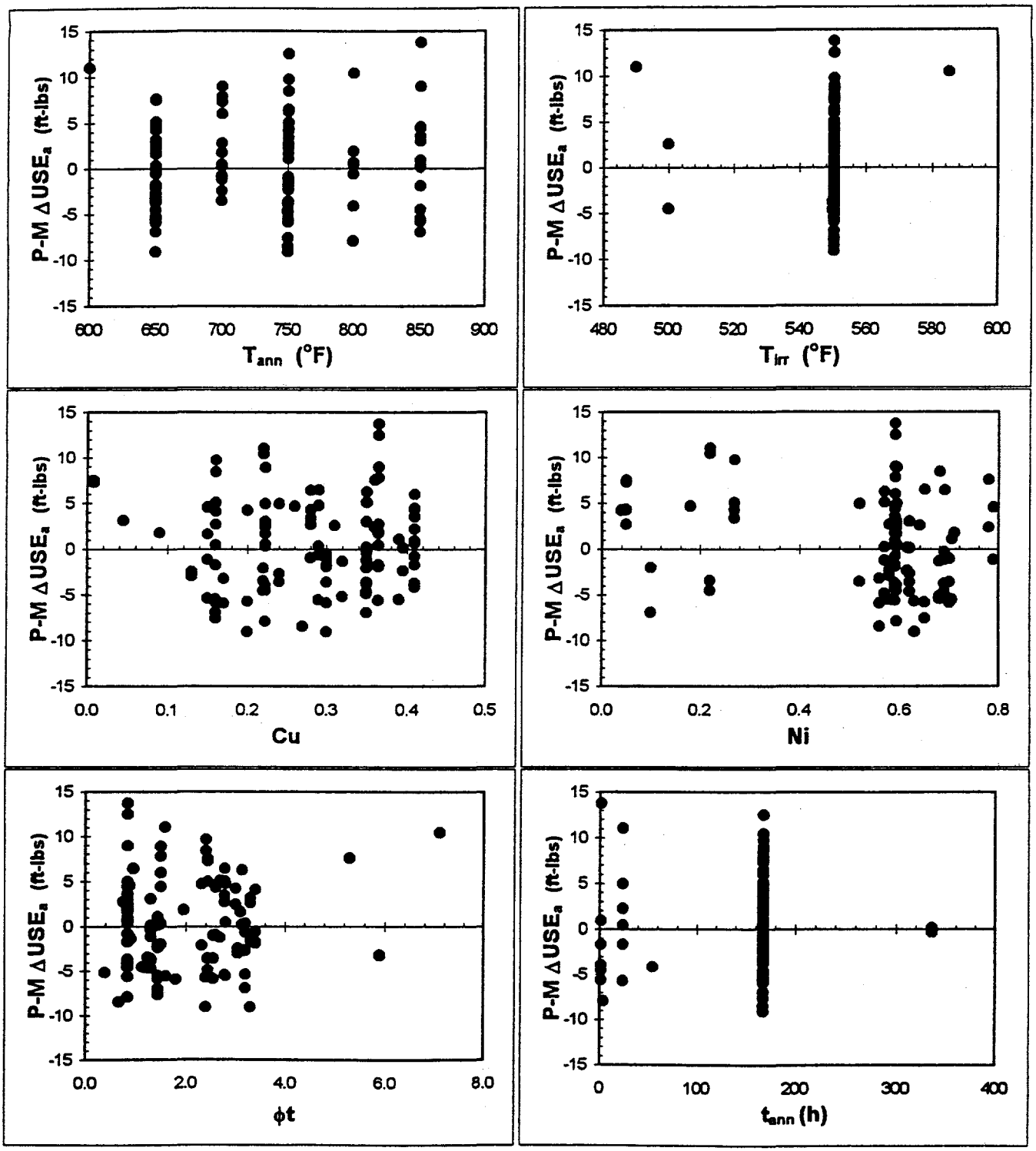

Figure 5-1 Predicted Minus Measured Residuals, Upper Shelf Model, Equation 4-2

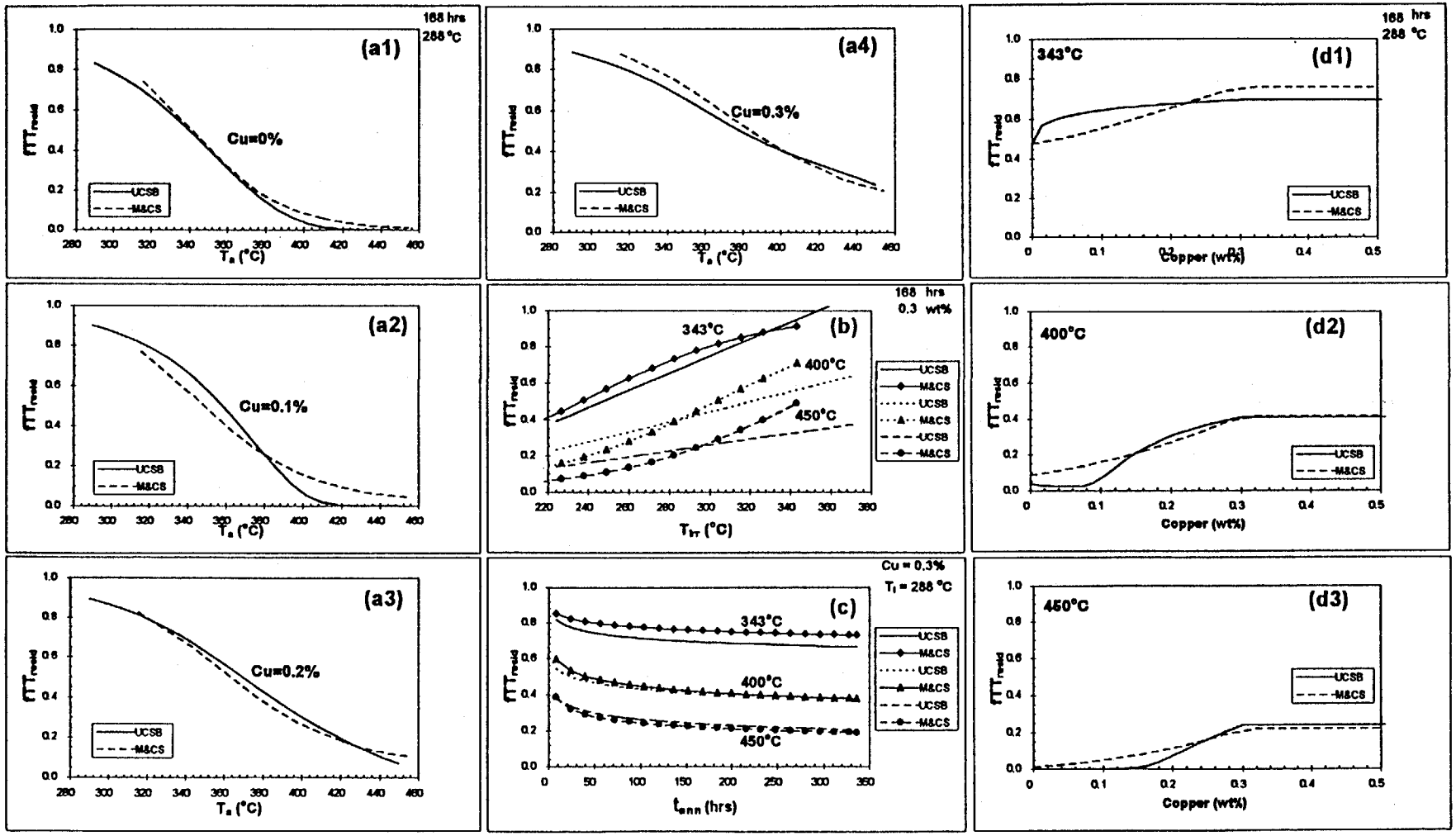

Figure 5-2 Comparison of Trends in Physically-Motivated and *tanh* Shift Models

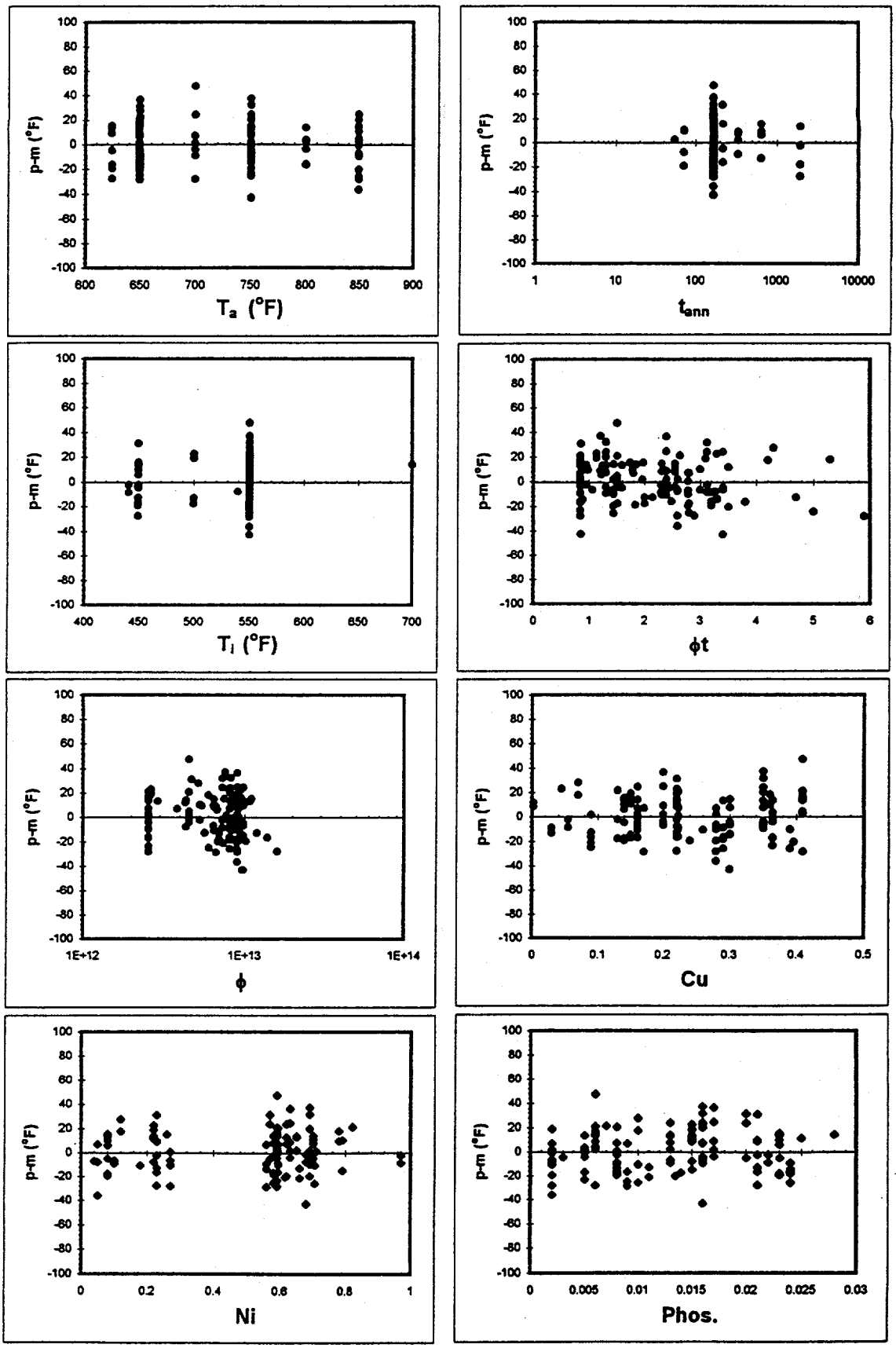

Figure 5-3 Predicted Minus Measured Residuals, *tanh* shift model, Eqs. 4-6 through 4-10

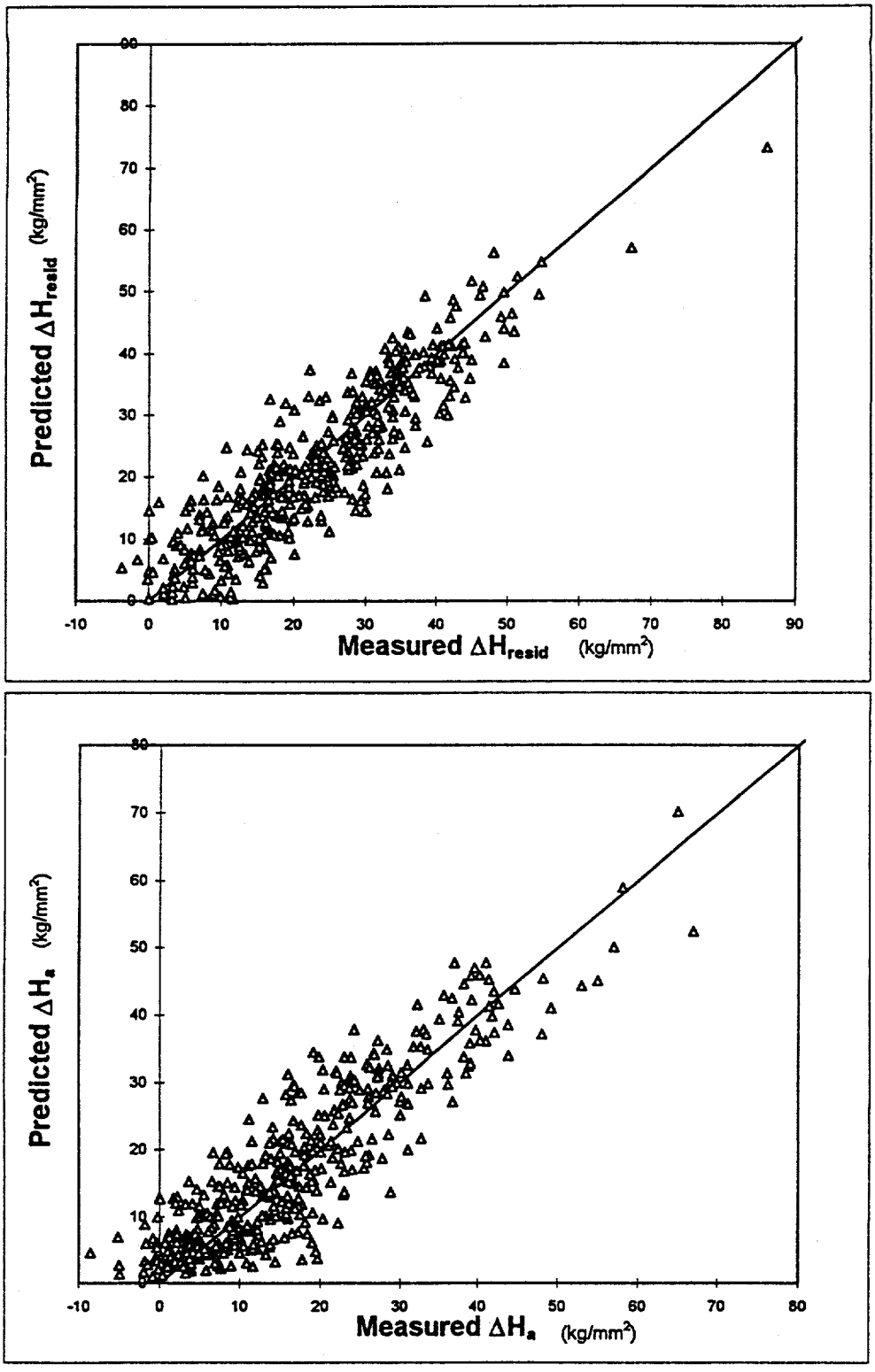

Figure 5-4 Predicted vs Measured Residual Hardness and Hardness Recovered by Annealing, *tanh* Shift Model

deviation is 5.9 DPH. With outliers included, the bias is unchanged, and the standard deviation increases to 6.4 DPH. Using a nominal conversion factor of 3.6, these hardness values are roughly equivalent to shift values of -4 and 21°F, respectively. Figure 5-5 shows the corresponding residual plots. The most significant deviation is for the 650°F anneal of the high copper-high nickel alloy. The implications of this deviation to the limitations of the data base will be discussed further below. However, overall these results demonstrate that microhardness is an excellent surrogate for evaluating general trends in transition temperature recovery due to annealing.

5.2.4 Literature TTS and Surrogate Data

Figure 5-6 compares supplementary shift data from the literature for predicted versus measured annealing recovery (ΔTT_a) for the *tanh* model. These data were not used in fitting, so they provide independent validation. For the 25 data points the average bias is -1.9°F and the standard deviation 16.8°F. A data point for a 650°F anneal of the Midland beltline weld appears to be an outlier with a predicted minus measured TT_{ia} of -61°F. Reasons for this possible discrepancy are under investigation. Without this data point, the average bias and standard deviation are -4.5 and 10.6°F respectively. Notably, the high temperature (850°F) anneals of the high nickel-intermediate copper welds fell within ±7.1°F of the correlation prediction with an average bias of 0.4°F. These results add further support to the *tanh* model.

5.2.5 Effect of Cu, Ni, P, and Fluence

While trends in VVER steels in the literature and theoretical considerations suggest an effect of P or ϕt on fTT_{resid}, the data base examined in this study did not reveal any systematic trends in these variables. Some subsets of shift and hardness data did suggest a slight effect of nickel on fractional recovery data that was not apparent in the overall TT_{ia} data, as discussed above. Given the minimal coverage of the data base at high Ni, this is a matter of some concern, and acquiring additional data for these steels should be a high priority. Fortunately, the data trends show that effects associated with the secondary variables (if real) decrease with increasing T_a and probably can be safely neglected for high temperature anneals (around 850°F).

Using the Charpy data base, Ni and P were not found to be important for predicting USE_{ia} or TT_{ia} after annealing. Adding Ni to the USE and TT recovery models resulted in no improvement, and no effect of Ni was found in the p-m residuals. No effect of P on USE_{ia} or TT_{ia} was found in any phase of the statistical analysis. Subsets of data from several studies originally designed to look at effects of Cu and P were also analyzed separately, but only Cu proved to be important to USE_{ia} or TT_{ia}, given the other variables already in the models. The possibility of a synergistic effect of Cu and Ni was investigated, but it was not supported by the overall data base. It is worth noting again that the first-order effects of composition variables are implicit in the irradiated TTS and ΔUSE variables.

5.2.6 Effect of Flux

The effects of ϕ are a major concern, since the annealing predictions are derived from high ϕ test reactor irradiations and will be applied to low ϕ power reactor conditions. The spread in the Charpy TTS data is too small to yield reliable predictions over the ϕ range from test reactors to power reactors. However, encouraged in part by the consistency of the trends, ϕ can be evaluated over a much larger range by combining the TTS and hardness data bases and extending the latter to include very high data (~$5x10^{13}$ n/cm^2-s) from the UCSB data base and much lower data from annealing studies on surveillance specimens (Mager and Lott, 1989). The latter data were used to calibrate the flux term of the *tanh* model; no other hardening data were used in the calibration.

Figure 5-7 shows the trends in the complete hardness and shift data base as a function of flux for the *tanh* model using the flux term at and below 750°F. The bars represent standard deviations about the average residual shift or hardening fraction for a large number of data points. The "scatter" includes a range of other variables not plotted here. These results reinforce the conclusion that annealing is more sensitive to variables such as ϕ at low T_a. They also support the flux term, Equation 4-10, for low T_a.

Note that the very high flux data at $5x10^{13}$n/cm^2-s in Figure 5-7 fall substantially below the flux-dependent *tanh* prediction. This is associated with the significant retardation of CRP development at very high damage rates, as discussed in Section 1.3, so that MD are the dominant embrittlement features. Hence at higher fluences, with CRP micostructures approaching full decomposition, the differences due to flux would be expected to be reduced. At sufficiently high fluence, the effect of flux is believed to depend primarily on the matrix defect component.

Lower fluxes would reduce the contribution of matrix defects and increase their thermal stability, at least at lower annealing temperatures. Thus, the effect of flux is expected to be qualitatively analogous to the inverse of the effect of irradiation temperature: fTT_{resid} increases with lower flux and higher irradiation temperatures, with

larger effects at lower T_a. The data strongly support the minimal effect of flux for T_a of 850°F. There is a small residual effect of the irradiation temperature for high flux irradiation with $\Delta fTT_{resid}/\Delta T_i \cong 10^{-3}$. However, the evaluation of the flux effect must be considered tentative and should be subject to additional confirmation.

5.2.7 Annealing Time

The *tanh* model provides a good fit to the Charpy shift data base for all annealing times. However, comparison of the model to the hardness data base at times less than 50 h showed a systematic over-prediction of recovery. While no definitive conclusions can be drawn from this comparison, the short-time hardness recovery data base is much larger than the short-time shift recovery data base. To avoid the region of discrepancy, the *tanh* model should be applied at annealing times of 50 h or more.

5.3 Recovery of ΔUSE versus TTS

Test results in the annealing data base indicate that upper shelf energy *generally* recovers more completely than transition temperature, when the same materials are exposed to the same treatments. This is shown graphically in Figure 5-8, which shows the percent recovery for ΔUSE versus TTS. For plotting purposes, over-recovery is shown as 100% recovery on this plot. Figure 5-8 includes 98 points for which TT and USE recovery are both in the data base; the four points for which USE increased due to irradiation are omitted, as are the first point in the data base (an outlier for the TT recovery fits) and the point for which T_a = 650°F and $USE_{ia} >> USE_u$ (an outlier for the USE recovery fits). The point on Figure 5-8 with less than 5% recovery of USE and nearly 60% recovery of TTS is suspect; it is a 1.5 hr anneal at 850°F. The same material annealed 1.5 hr at 750°F is in the scatter above the dashed line in Figure 5-8.

Of the 113 points in the Charpy annealing data base for which fraction recovery in USE is available (not counting the four points for which $USE_i > USE_u$), 24 points show over-recovery. For this reason, the USE model (Eq. 4-2) may predict over-recovery for some combinations of independent variables. In contrast, over-recovery of TTS does not occur in the annealing data base. This led to the development of the *tanh* model form of Equation 4-6, which does not predict over-recovery for any combination of variables.

The over-recovery of USE at high T_a is somewhat puzzling. However, we offer two hypotheses that may help guide further research. The first is based on possible effects of coarsened copper-rich precipitates on increasing the strain hardening relative to unirradiated alloys. Increased strain hardening can lead to an increase in the USE. A second possible explanation is that small solute clusters form upon slow cooling from stress relief temperatures, causing a slight increase in strength and corresponding decrease in ductility associated with an enhanced propensity towards flow localization. High temperature anneals could dissolve such features, thus also leading to increased USE. The observation that over-recovery occurs at all Cu levels may lend support to the latter hypothesis.

We believe the apparent differences between the USE and TT recovery behavior are real and reflect the fact that a different balance of pre-existing (i.e., small solute clusters) and irradiation-induced features mediate the different Charpy test parameters. Whereas the shifts are most sensitive to the elevation of yield stress, or hardening, USE reductions are most sensitive to finer, less stable features that reduce ductility.

5.4 Ranges of Validity of Models

The models are curve fits, valid only within the ranges of data used to create them. Table 5-1 shows the ranges of the independent variables without regard to variable combinations or interactions and "clumping" within the data base. Staying within the limits of Table 5-1 is a necessary but not sufficient condition for validity.

Complete mapping of the range of validity in multivariable space, considering interactions and areas of clumping or sparse data, is extremely difficult. The application ranges based on T_a in Table 5-2 are guided by physical considerations. The limits for Ni and ϕ for $T_a \geq 800$°F have been established based on limited hardness data. Clearly, these conclusions must be verified by further experimental research, including developing an extended shift data base. Additionally, comparisons of the correlations for $T_a \leq 750$°F with data from the literature suggest some caution should be used in applications, even within the specified limits. Finally, while the USE model can be used in conjunction with the TTS model, we recommend that the TTS model not be applied for conditions with $USE_i > 155$ ft-lb or $USE_i < 36$ ft-lb, the range of the Charpy data base.

The validity range for flux presents a special problem. Based on excellent correspondence between hardness data and TTS data at test reactor flux levels and the trend in hardness data, we recommend use of the TT model with the flux term down to power reactor flux levels, nominally as low as 5×10^{10} n/(cm^2-s) (E>1MeV). Estimates for even lower flux levels are not precluded but should be viewed as pure extrapolation. But there is no confirmation of a flux trend in Charpy data at power reactor fluxes, either for TTS or USE. Thus the flux term in the shift model and the lack of a flux term in the USE

model must be considered best engineering judgement with the present state of knowledge. Further experimentation and analysis on this issue is sorely needed.

Table 5-1. Ranges of Independent Variables used to Calibrate Models

USE_{ia}			TT_{ia}		
Variable	Min	Max	Variable	Min	Max
USE_i, ft-lb	36	155	TT_i, °F	-25	465
ΔUSE_i, ft-lb	0	51	ΔTT_i, °F	30	350
T_a, °F	600	850	T_a, °F	600	850
t_a, h	2	336	t_a, h	2	1944
Cu, wt%	0.008	0.409	Cu, wt%	0.002	0.409
			T_i, °F	430	700
			ϕ, n/(cm^2-s)	$5x10^{10}$	$2x10^{13}$

Table 5-2. Model Application Ranges

T_a	Cu	T_i	t_a	Ni	ϕt	ϕ
≤ 750°F	> 0.05 wt%	500-600 °F	> 50 h	< 0.8 wt%	0.5 - $5x10^{19}$ n/cm^2	≥ $5x10^{10}$ n/(cm^2-s)
≥ 800°F	> 0.15 wt%	500-600 °F	> 50 h	< 1.2 wt%	0.5 - $5x10^{19}$ n/cm^2	≥ $5x10^{10}$ n/(cm^2-s)

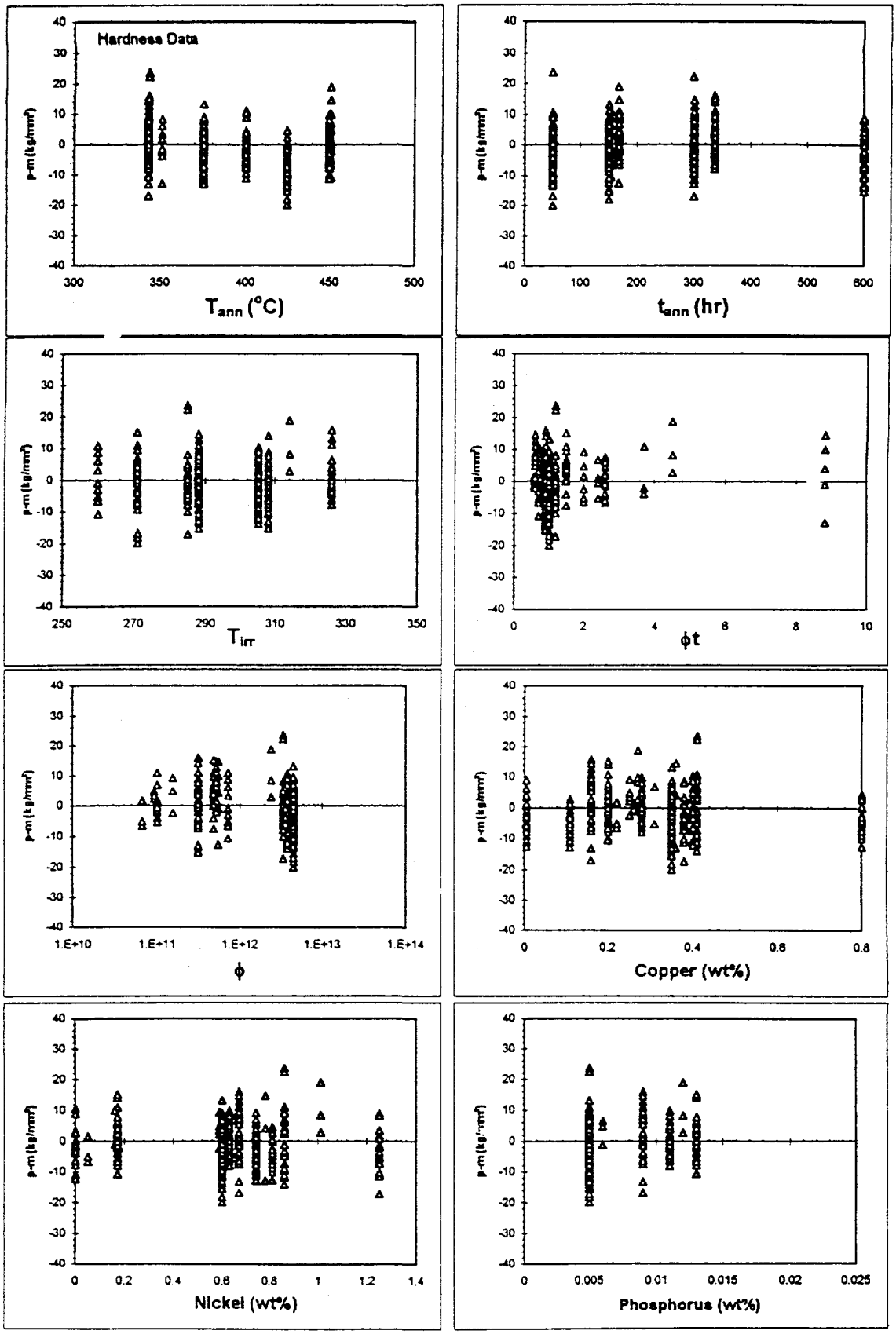

Figure 5-5 Predicted Minus Measured Residuals, *tanh* Model Applied to Hardness Data

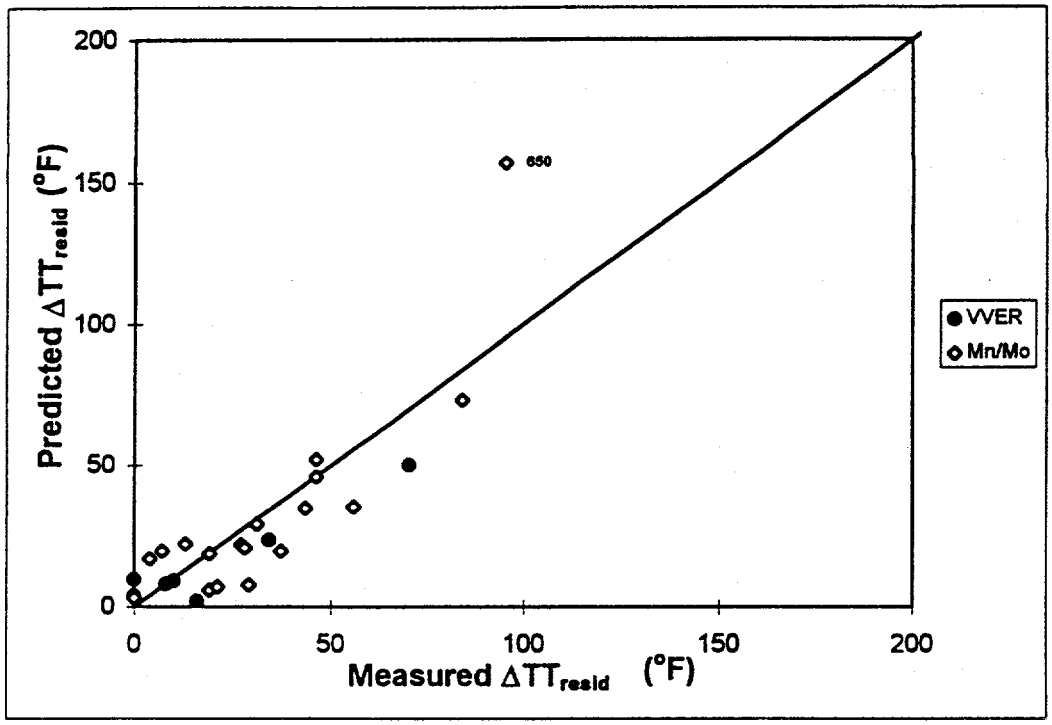

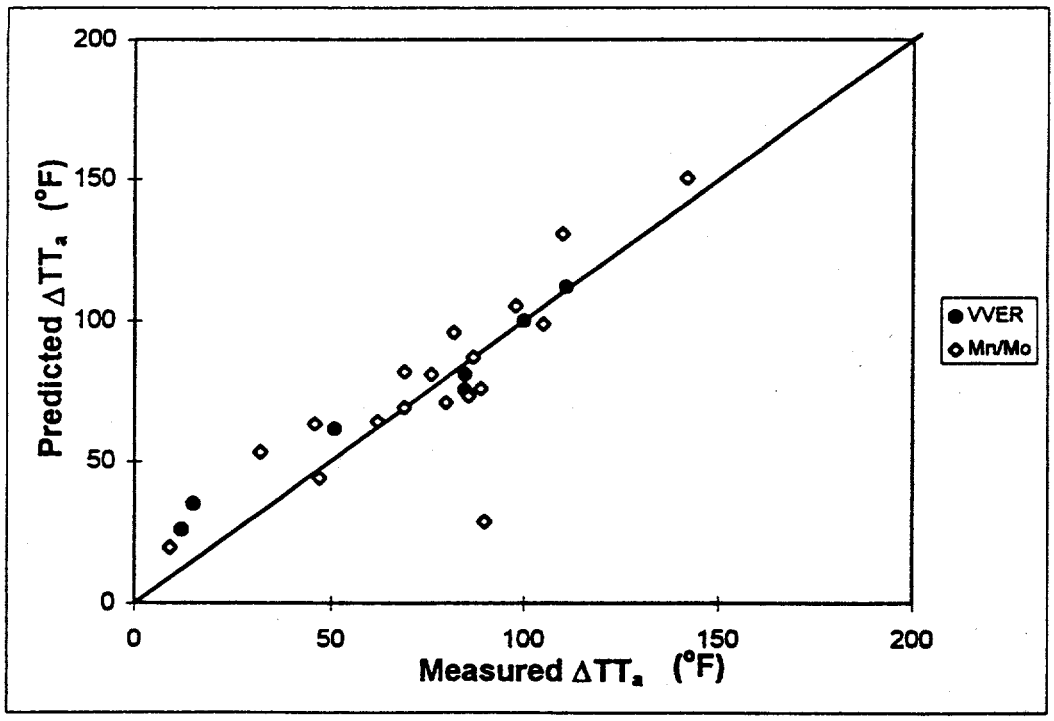

Figure 5-6 Predicted vs. Measured TT_{ta} and ΔTT_a, *tanh* model on Literature Shift Data

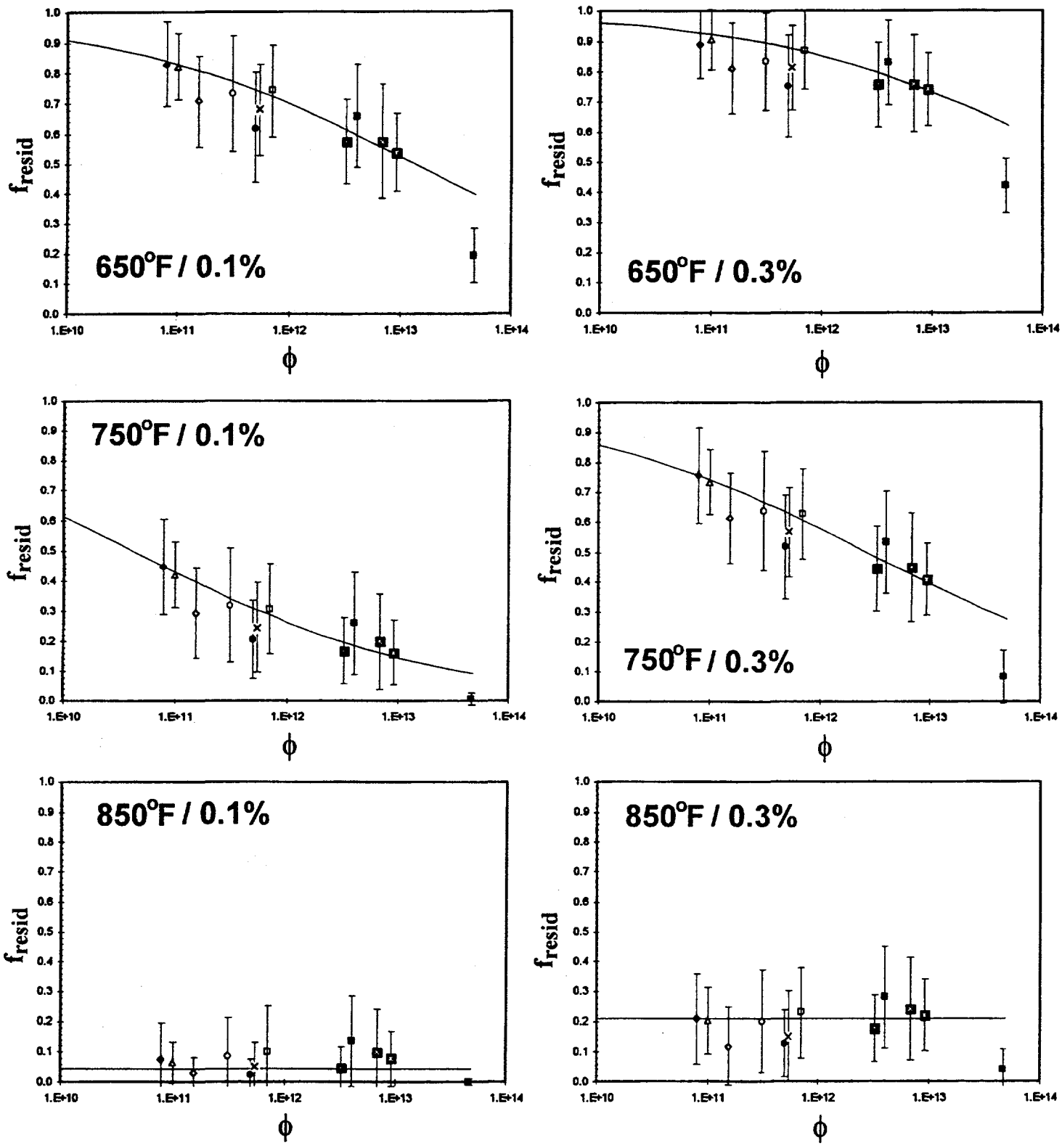

Figure 5-7 Normalized Residual Fractional Recovery vs. Flux and T_s, *tanh* Model, Westinghouse Surveillance Hardness (△, X, ◊, ◆), UCSB Hardness (■, □, ●, ○), and Shift Data (, ,)

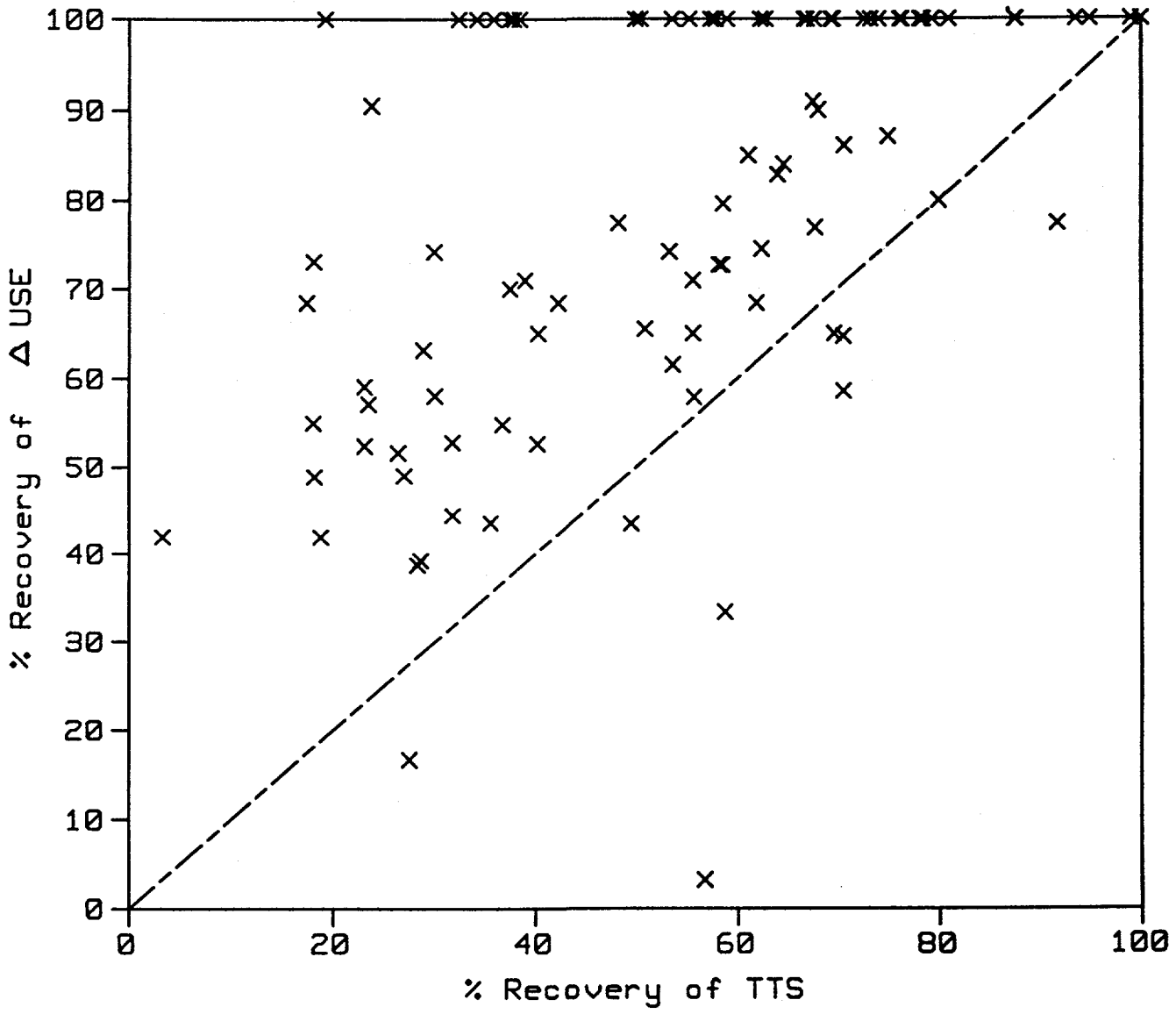

Figure 5-8 Percent Recovery Due to Annealing of TTS vs. USE

6 CONCLUSIONS

Correlation models for predicting both USE and TT embrittlement recovery due to annealing have been developed.

For predicting recovery in USE, the standard error of the calibrated data about the model line (Eq. 4-2) is 5.1 ft-lb, which is no greater than the expected experimental error. The model is presented in a form that predicts the USE after irradiation and subsequent annealing; it can be converted algebraically to predict the fraction of the drop in USE or other measure of recovery. The model may predict over-recovery of USE due to annealing, as was evident in the data.

The transition temperature at 30 ft-lb can be predicted after irradiation and annealing by a *tanh* model (Eqs. 4-6 through 4-10) with a standard error of 17.2°F, comparable to the uncertainty in unirradiated TTS within well-characterized welds. The model has several physical features built in, including a limit on effective Cu based on solubility considerations and nonlinear effects of annealing temperature. The flux effect is tentative, having been calibrated to a mix of hardness and Charpy data, but it is consistent with the large hardness data base with a range in flux spanning more than two orders of magnitude. The flux effect, like the Cu effect, varies with annealing temperature because of the different responses of the various hardening features.

The *tanh* model represents a significant improvement over previous model formulations. The model is consistent with an extensive hardness data base as well as physically-motivated models reflecting current understanding of both embrittlement and annealing mechanisms. The model also provides some important insights lacking in previous treatments, suggesting that flux effects and secondary composition variables can be neglected at high annealing temperatures. While requiring additional confirmation, this is a conclusion of enormous importance. The *tanh* model also promotes greater flexibility in annealing applications. For example, the non-linear changes in recovery with annealing temperature and time suggest that annealing temperatures slightly lower that 850°F, and/or times shorter than 168 hr may be worth considering, if they provide some significant practical engineering benefit. The results can help guide future research studies aimed at refining the predictions and optimizing annealing treatments, considering the effects of both recovery and re-irradiation embrittlement.

Though they are consistent with the current understanding of embrittlement and annealing, both the upper shelf and transition temperature recovery models should be treated as curve-fits with substantial physical insight built in, rather than as fundamental physical models. Thus, care should be taken to avoid extreme extrapolation beyond the ranges presented in Section 5.4. The clumping and patterns in the available data, as discussed in Section 2.5, should be considered during applications. The fact that all the Charpy data are from short-term test reactor irradiations should be considered; the resulting flux effects have been estimated for the shift model (but not for the upper shelf model) using hardness data.

The results suggest a need for additional experimentation and confirmation in certain areas. To the extent possible, weaknesses of the Charpy data were addressed by using the surrogate hardness data during the model development. The lack of the Cu-Ni compositions most critical to actual plants that may use annealing is a serious drawback to the available data base that should be addressed by additional experiments. Additional Charpy data, irradiated at power reactor fluxes and over the critical range of Cu and Ni compositions for U.S. plants, would provide valuable confirmation.

7 REFERENCES

Eason, E. D., and E. E. Nelson, "Correlations Between Grain Boundary Composition and IASCC Susceptibility in Austenitic Stainless Steel," EPRI Report TR-103508, April 1994.

Eason, E. D., J. E. Wright, and E. E. Nelson, "Improved Irradiation Embrittlement and Annealing Correlations," 21st Water Reactor Safety Information Meeting, Bethesda, MD, October 1993.

Fabry, A., "The BR3 Pressure Vessel Anneal: Lessons and Perspective," *Reactor Pressure Vessel Thermal Annealing Workshop*, Albuquerque, New Mexico, February 17-18, 1994.

Fisher, S. B. and J. T. Buswell, "A Model for PWR Pressure Vessel Embrittlement," *International Journal of Pressure Vessels and Piping, Volume 27*, 1987, p. 91.

Hawthorne, J. R., "Compendium of Irradiation-Anneal Data for RPV Steels and Welds from MEA and NRL Weldments," MEA-2541, September 1994.

Lietz, C., Klausnitser, E., and Hoffman, G., "Annealing Experiments on Irradiated NiCrMo Weld Metal," *Effects of Radiation on Materials: 17th Conference, ASTM STP 1175*, (A. Kumar, et. al., eds.), American Society for Testing and Materials, 1994, p. 352.

Macdonald, B., "Post-Irradiation Annealing Recovery of Commercial Pressure Vessel Steels," *Effects of Radiation on Materials: Twelfth International Symposium. ASTM STP 870*, F. A. Garner and J. S. Perrin, Eds., American Society for Testing and Materials, Philadelphia, 1985. pp. 972-978.

Mader, E. V., G. E. Lucas and G. R. Odette, "The Effects of Metallurgical and Irradiation Variables on the Kinetics of Post-Irradiation Annealing of Pressure Vessel Steels," The Effects of Radiation on Materials: 16th International Symposium, ASTM STP 1125, (R. Stoller, A. Kumar and J. Packan, eds.), American Society for Testing and Materials, 1992, p. 151.

Mager, T. R. and R. G. Lott, "Feasibility of a Methodology for Thermal Annealing an Embrittled Reactor Vessel," EPRI Report NP-6113-M, Electric Power Research Insitute, February 1989.

Odette, G. R. and G. E. Lucas, "An Experimental Investigation of Kinetic Aspects of Neutron Irradiation Embrittlement of Light Water Reactor Pressure Vessel Steels," EPRI Report NP 6114, Electric Power Research Institute, 1989.

Odette, G. R., P. M. Lombrozo and R. A. Wullaert, "The Relationship Between Irradiation Hardening and Embrittlement of Pressure Vessel Steels," *Effects of Radiation on Materials: 12th International Symposium, ASTM STP 870*, (F. A. Garner and J. S. Perrin, eds.), American Society for Testing and Materials, 1985, p. 840.

Odette, G. R. and G. E. Lucas, "Irradiation Embrittlement of Reactor Pressure Vessel Steels: Mechanisms, Models and Data Correlations," *Radiation Embrittlement of Nuclear Reactor Pressure Vessel Steels: An International Review - Volume II*, ASTM STP 909, (L. E. Steele, ed.), American Society for Testing and Materials, 1986, p. 206.

Odette, G. R., et. al., "The Effect of Flux on Irradiation Hardening of Pressure Vessel Steels," *Effects of Radiation on Materials: 17th Conference, ASTM STP 1175*, (A. Kumar, et. al., eds.), American Society for Testing and Materials, 1994, p. 373.

Odette, G. R., "Microstructural Evolution in Irradiated Pressure Vessel Steels," Microstructure of Irradiated Materials, MRS Symposium Series, MRS, 1995

Odette, G. R., "Modeling the Irradiation Embrittlement of Reactor Pressure Vessel Steels," Irradiation Effects in Pressure Vessel Steels, International Atomic Energy Agency Technical Report Series, (M. Davies, ed.), IAEA, Vienna, Austria, 1995

Potapovs, U., G. W. Knighton and A. S. Denton, "Critique of In-Place Annealing of SM-1A Nuclear Reactor Vessel," *American Society of Mechanical Engineers*, Paper 67-WA/ER-3, November 1967; also, *Nuclear Engineering and Design*, Volume 8, 1968, pp. 39-57.

Powers, A. E., "Post-Irradiation and Co-Irradiation Annealing of Iron and Steel," Knolls Atomic Power Lab Report, KAPL 3440, Sept. 1968.

APPENDIX A

Annealing Charpy Data Base

Notes:

1. There are no blank entries in the annealing Charpy data base. An entry of "-999" indicates that no reliable value is available.
2. Pages 60-63 show columns 1-19 of the data base, and pages 64-67 show columns 20-32, indexed by "Final Record No."
3. The "Final Record No." is used for indexing, while the "Original Record No." is referenced by J. R. Hawthorne in the "Compendium of Irradiation-Anneal Data."
4. The "Primary Ref." is the reference where the data were originally acquired by Modeling and Computing Services.
5. The "TR-EDF Ref." is the reference cited in the TR-EDB.
6. The "Raw Data Ref." is the Charpy data reference cited by J. R. Hawthorne in the "Compendium of Irradiation-Anneal Data."
7. Reference citations for the data base are listed at the end of this Appendix, pages 68-69.

M&CS ANNEALING DATA BASE

Final Record No.	Original Record No.	Fluence (10^19)	Ti (F)	ti (h)	Ta (F)	ta (h)	TTu (F)	TTi (F)	dTTi (F)	TTia (F)	dTTa (F)	dTTres (F)	Trec (F)	USEu (ft-lb)	USEi (ft-lb)	dUSEi (ft-lb)	USEia (ft-lb)	dUSEa (ft-lb)	dUSEres (ft-lb)
1	1	3.30	500	1062	650	168	-15	310	325	105	205	120	0.631	76	36	40	56	20	20
2	2	0.84	550	912	650	168	3	178	175	127	50	124	0.289	61	42	19	54	12	7
3	3	0.84	550	912	700	168	3	178	175	147	31	144	0.175	61	42	19	55	13	6
4	4	0.84	550	912	750	2	3	178	175	108	70	104	0.402	61	42	19	52	10	10
5	5	0.84	550	912	750	24	3	178	175	104	74	101	0.423	61	42	19	55	13	7
6	6	0.84	550	912	750	168	3	178	175	70	108	67	0.619	61	42	19	55	13	7
7	7	0.84	550	912	800	55	3	178	175	61	117	58	0.670	61	42	19	67	25	-6
8	8	0.84	550	912	800	168	3	178	175	39	139	36	0.794	61	42	19	63	21	-1
9	9	0.84	550	912	850	2	3	178	175	81	97	77	0.557	61	42	19	53	11	8
10	10	0.84	550	912	850	168	3	178	175	25	153	22	0.876	61	42	19	64	22	-3
11	11	1.50	550	912	700	168	3	230	227	97	133	94	0.587	61	41	21	48	7	13
12	12	1.50	550	912	850	168	3	230	227	46	184	43	0.810	61	41	21	63	22	-1
13	13	0.84	550	912	650	168	-6	124	130	100	23	106	0.181	67	47	20	58	11	9
14	14	0.84	550	912	700	168	-6	124	130	75	49	81	0.375	67	47	20	61	14	6
15	15	0.84	550	912	750	2	-6	124	130	52	72	58	0.556	67	47	20	60	13	7
16	16	0.84	550	912	750	24	-6	124	130	72	52	77	0.403	67	47	20	60	13	7
17	17	0.84	550	912	750	168	-6	124	130	36	88	41	0.681	67	47	20	66	18	1
18	18	0.84	550	912	800	4	-6	124	130	25	99	31	0.764	67	47	20	68	21	-1
19	19	0.84	550	912	800	168	-6	124	130	34	90	40	0.694	67	47	20	70	23	-3
20	20	0.84	550	912	850	2	-6	124	130	45	79	50	0.611	67	47	20	64	17	3
21	21	0.84	550	912	850	168	-6	124	130	10	113	16	0.875	67	47	20	71	24	-4
22	22	1.50	550	912	700	168	-6	172	178	84	88	90	0.495	67	44	23	54	10	13
23	23	1.50	550	912	850	168	-6	172	178	-4	176	2	0.990	67	44	23	72	28	-5
24	24	0.84	550	912	650	168	-89	19	108	16	4	104	0.033	133	102	31	115	13	18
25	25	0.84	550	912	700	168	-89	19	108	-13	32	76	0.300	133	102	31	120	18	13
26	26	0.84	550	912	750	2	-89	19	108	-20	40	68	0.367	133	102	31	119	17	14
27	27	0.84	550	912	750	24	-89	19	108	-13	32	76	0.300	133	102	31	125	23	8
28	28	0.84	550	912	750	168	-89	19	108	-11	31	77	0.283	133	102	31	114	12	19
29	29	0.84	550	912	800	24	-89	19	108	-33	52	56	0.483	133	102	31	126	24	7
30	30	0.84	550	912	800	168	-89	19	108	-62	81	27	0.750	133	102	31	128	27	4
31	31	0.84	550	912	850	2	-89	19	108	-42	61	47	0.567	133	102	31	103	1	30
32	32	0.84	550	912	850	168	-89	19	108	-80	99	9	0.917	133	102	31	125	24	7
33	33	1.50	550	912	700	168	-89	79	167	19	59	108	0.355	133	94	39	111	17	22
34	34	1.50	550	912	850	168	-89	79	167	-53	131	36	0.785	133	94	39	133	39	0
35	35	2.40	550	741	650	168	-30	200	230	80	120	110	0.522	111	78	32	-999	-999	-999
36	36	2.40	550	741	750	24	-30	200	230	45	155	75	0.676	111	78	33	108	30	3
37	37	2.40	550	741	750	168	-30	200	230	20	180	50	0.783	111	78	33	115	37	-4
38	38	2.40	550	741	800	168	-30	200	230	10	190	40	0.824	111	78	32	-999	-999	-999
39	39	2.40	550	741	850	24	-30	200	230	0	200	30	0.870	111	78	32	-999	-999	-999
40	40	2.40	550	741	850	168	-30	200	230	-30	230	0	1.000	111	78	32	-999	-999	-999
41	41	0.88	550	249	750	168	-20	60	80	10	50	30	0.623	76	69	7	84	15	-8
42	42	0.88	550	249	850	168	-20	60	80	-15	75	-5	0.935	76	69	7	84	15	-8
43	43	2.40	550	800	750	24	60	175	115	95	80	35	0.696	103	103	0	-999	-999	-999
44	44	2.40	550	800	750	168	60	175	115	95	80	35	0.696	103	103	0	103	0	0
45	45	2.78	550	843	750	168	60	185	125	85	100	25	0.800	103	83	20	99	16	4
46	46	2.40	550	800	750	24	50	210	160	110	100	60	0.625	106	103	3	-999	-999	-999
47	47	2.40	550	800	750	168	50	210	160	85	125	35	0.782	106	103	3	106	3	0
48	48	2.78	550	843	750	168	50	185	135	85	100	35	0.741	106	82	24	111	29	0
49	49	2.55	550	761	750	168	45	155	110	45	110	0	1.000	108	85	23	-999	-999	-999
50	50	2.55	550	761	750	168	20	165	145	20	145	0	1.000	114	82	32	-999	-999	-999
51	51	2.55	550	761	750	168	0	290	290	120	170	120	0.586	111	62	49	101	39	10
52	52	2.55	550	761	750	168	0	320	320	120	200	120	0.624	107	56	51	94	38	13
53	53	2.55	550	761	750	168	20	345	325	135	210	115	0.646	106	56	50	98	42	8
54	54	2.60	550	800	750	168	35	190	155	100	90	65	0.582	106	84	22	100	16	6
55	55	2.78	550	843	750	168	35	190	155	85	105	50	0.678	106	80	26	100	20	6
56	56	2.60	550	800	750	168	35	180	145	95	85	60	0.585	106	84	22	100	16	6
57	57	2.78	550	843	750	168	35	170	135	95	75	60	0.556	106	75	31	97	22	9
58	58	2.60	550	800	750	168	25	220	195	95	125	70	0.640	112	77	35	106	29	6
59	59	2.78	550	843	750	168	25	230	205	120	110	95	0.536	101	75	26	91	16	10
60	60	1.44	550	447	750	168	-10	205	215	-999	-999	-999	-999.000	58	38	20	58	20	0
61	61	1.44	550	447	850	168	-10	205	215	55	150	65	0.696	58	38	20	64	26	-6

M&CS ANNEALING DATA BASE

Final Record No.	Original Record No.	Fluence (10^19)	Ti (F)	ti (h)	Ta (F)	ta (h)	TTu (F)	TTi (F)	dTTi (F)	TTia (F)	dTTa (F)	dTTres (F)	Trec (F)	USEu (ft-lb)	USEi (ft-lb)	dUSEi (ft-lb)	USEia (ft-lb)	dUSEa (ft-lb)	dUSEres (ft-lb)
62	62	1.44	550	447	750	168	-80	80	160	-5	85	75	0.533	115	84	31	107	23	8
63	63	1.44	550	447	850	168	-80	80	160	-20	100	59	0.628	115	84	31	122	38	-7
64	64	1.44	550	447	750	168	-35	55	90	-30	85	5	0.949	95	78	17	105	27	-10
65	65	1.44	550	447	850	168	-35	55	90	-30	85	5	0.949	95	78	17	109	31	-14
66	66	1.44	550	447	750	168	5	150	145	70	80	65	0.553	62	44	18	63	19	-1
67	67	1.44	550	447	850	168	5	150	145	45	105	40	0.727	62	44	18	76	32	-14
68	68	0.24	430	-999	572	172	10	125	115	105	20	95	0.175	83	-999	-999	-999	-999	-999
69	69	0.24	430	-999	700	48	10	125	115	60	65	50	0.567	83	-999	-999	-999	-999	-999
70	70	0.48	430	-999	572	172	-45	70	115	0	70	40	0.606	128	-999	-999	-999	-999	-999
71	71	0.48	430	-999	572	172	-45	70	115	0	70	40	0.606	128	-999	-999	-999	-999	-999
72	72	1.26	240	500	585	168	-80	215	295	-55	270	25	0.916	130	-999	-999	-999	-999	-999
73	73	1.26	240	500	700	48	-80	235	315	-80	235	0	1.000	130	-999	-999	-999	-999	-999
74	74	2.31	430	1472	585	168	-80	255	335	5	250	85	0.747	130	-999	-999	-999	-999	-999
75	75	2.73	430	1736	585	168	-80	310	390	5	305	85	0.783	130	-999	-999	-999	-999	-999
76	76	0.12	430	-999	572	172	-80	-50	30	-60	10	20	0.331	130	-999	-999	-999	-999	-999
77	77	0.70	430	48	572	172	-80	115	195	-50	165	30	0.848	130	90	40	-999	-999	-999
78	78	1.31	430	917	572	172	-80	180	260	-30	210	50	0.809	130	-999	-999	-999	-999	-999
79	79	2.51	430	1743	572	172	-80	230	310	20	210	100	0.678	130	70	60	-999	-999	-999
80	80	2.51	430	1743	572	172	-80	230	310	20	210	100	0.678	130	70	60	-999	-999	-999
81	81	3.10	550	959	650	168	-25	85	110	20	65	45	0.590	104	98	6	104	6	0
82	82	3.20	550	959	650	168	-25	195	220	120	75	145	0.342	104	82	22	104	22	0
83	83	3.20	550	959	650	168	-20	180	200	115	65	135	0.324	105	80	25	105	25	0
84	84	2.80	550	959	650	168	-15	225	240	180	45	195	0.188	105	74	31	87	13	18
85	85	2.80	550	959	750	168	-15	225	240	105	120	120	0.500	105	74	31	105	31	0
86	86a	3.20	550	959	650	168	-15	240	255	180	60	195	0.235	105	77	28	93	16	12
87	87	3.20	550	959	800	168	-15	240	255	70	170	85	0.667	105	77	28	105	28	-0
88	88	3.30	550	959	650	168	20	150	130	60	90	40	0.694	78	69	9	78	9	0
89	89	2.80	550	959	700	168	15	140	125	55	85	40	0.677	81	66	15	81	15	0
90	90	3.40	550	959	650	168	15	135	120	90	45	75	0.375	81	68	13	81	13	0
91	91	3.40	550	959	750	168	15	135	120	15	120	0	1.000	81	68	13	81	13	0
92	92	3.40	550	959	650	168	15	210	195	165	45	150	0.231	82	60	22	73	13	9
93	93	3.40	550	959	750	168	15	210	195	135	75	120	0.385	82	60	22	82	22	0
94	94	3.30	550	959	650	168	15	220	205	181	40	166	0.193	84	63	21	84	21	0
95	95	3.30	550	959	750	168	15	220	205	110	110	95	0.536	84	63	21	84	21	0
96	96	2.44	550	851	650	168	60	245	185	-999	-999	-999	-999.000	60	40	20	48	8	12
97	97	2.44	550	851	700	168	60	245	185	-999	-999	-999	-999.000	60	40	20	60	20	-0
98	98	2.44	550	851	650	168	20	150	130	-999	-999	-999	-999.000	75	55	20	67	12	8
99	99	2.44	550	851	700	168	20	-999	-999	-999	-999	-999	-999.000	75	55	20	69	14	6
100	100	5.90	550	2456	650	168	-5	205	210	155	50	160	0.238	115	94	21	113	19	2
101	101	1.58	490	1023	600	24	15	215	200	160	55	145	0.275	87	51	36	57	6	30
102	102	3.27	540	2085	750	24	15	180	165	100	80	85	0.485	87	55	32	-999	-999	-999
103	103	3.27	540	2085	750	72	15	180	165	80	100	65	0.606	87	55	32	-999	-999	-999
104	104	3.27	540	2085	800	24	15	180	165	80	100	65	0.606	87	55	32	-999	-999	-999
105	105	3.27	640	2085	800	24	15	125	110	55	70	40	0.639	87	58	29	-999	-999	-999
106	106	1.13	500	1183	650	168	30	210	180	120	90	90	0.500	82	66	16	82	16	0
107	107	1.24	550	1183	650	168	30	170	140	120	50	90	0.359	82	69	13	82	13	0
108	109	1.85	700	1180	850	168	30	60	30	30	30	0	1.000	72	63	9	-999	-999	-999
109	110	3.50	550	2253	750	168	30	185	155	70	115	40	0.743	72	63	9	-999	-999	-999
110	111	1.74	550	646	750	168	10	85	75	10	75	0	1.000	127	105	21	-999	-999	-999
111	112	2.00	500	799	650	168	-80	65	145	0	65	80	0.448	137	112	25	-999	-999	-999
112	113	3.05	550	537	650	168	-80	60	140	-999	-999	-999	-999.000	137	119	18	137	18	0
113	114	3.05	550	537	700	168	-80	60	140	-999	-999	-999	-999.000	137	119	18	139	20	-2
114	115	2.30	440	799	650	168	-80	220	300	0	220	80	0.733	137	104	33	-999	-999	-999
115	116	2.00	500	799	650	168	-75	-25	50	-45	20	30	0.397	145	136	9	-999	-999	-999
116	117	2.30	440	799	650	168	-75	110	185	-30	140	45	0.755	145	119	25	-999	-999	-999
117	119	0.76	550	244	750	168	0	125	125	-999	-999	-999	-999.000	72	56	16	72	16	0
118	120	1.60	550	500	650	168	-10	190	200	-999	-999	-999	-999.000	79	57	22	79	22	-0
119	121	0.67	550	244	750	168	-15	110	125	-999	-999	-999	-999.000	82	66	16	92	26	-10
120	122	0.90	550	244	750	168	15	195	180	-999	-999	-999	-999.000	79	59	20	79	20	0
121	123	2.32	550	997	650	168	-60	50	110	30	20	90	0.182	155	110	45	132	22	23
122	124	2.32	550	997	650	168	10	215	205	135	80	125	0.390	139	108	31	130	22	9

M&CS ANNEALING DATA BASE

Final Record No.	Original Record No.	Fluence (10^19)	Ti (F)	ti (h)	Ta (F)	ta (h)	TTu (F)	TTi (F)	dTTi (F)	TTia (F)	dTTa (F)	dTTres (F)	Trec (F)	USEu (ft-lb)	USEi (ft-lb)	dUSEi (ft-lb)	USEia (ft-lb)	dUSEa (ft-lb)	dUSEres (ft-lb)
123	125	2.32	550	997	650	336	10	215	205	135	80	125	0.391	139	108	31	-999	-999	-999
124	126	1.30	550	442	650	168	-25	180	205	115	65	140	0.317	117	81	36	97	16	20
125	127	1.30	550	442	650	336	-25	180	205	115	65	140	0.317	117	81	36	100	19	17
126	128	1.30	550	442	750	168	-25	180	205	35	145	60	0.707	117	81	36	112	31	5
127	129	1.30	550	442	650	168	10	205	195	160	45	150	0.231	82	61	21	72	11	10
128	130	1.30	550	442	650	336	10	205	195	160	45	150	0.231	82	61	21	72	11	10
129	131	1.30	550	442	750	168	10	205	195	70	135	60	0.694	78	61	17	79	18	-1
130	132	2.44	550	782	750	168	-20	215	235	80	135	100	0.574	69	42	27	69	27	0
131	133	2.68	550	537	650	168	-20	-999	-999	-999	20	-999	-999.000	69	53	16	56	3	13
132	134	2.68	550	537	700	168	-20	-999	-999	-999	85	-999	-999.000	69	53	16	66	13	3
133	135	3.13	550	1190	700	168	-20	235	255	105	130	125	0.509	69	40	29	59	19	10
134	136	3.13	550	1190	750	168	-20	235	255	55	180	75	0.706	69	40	29	57	17	12
135	137	1.80	550	1300	650	168	-5	140	145	85	55	90	0.379	115	93	22	115	22	0
136	138	3.20	550	1300	650	168	10	175	165	145	30	135	0.182	110	84	26	103	19	7
137	139	3.00	550	1300	650	168	-30	285	315	200	85	230	0.270	107	56	51	81	25	26
138	140	5.30	550	2456	650	168	-30	320	350	220	100	250	0.286	107	56	51	76	20	31
139	141	3.00	550	1300	650	168	-35	60	95	35	25	70	0.264	129	98	31	114	16	15
140	143	3.13	550	1200	650	168	-25	125	150	60	65	85	0.432	120	102	18	-999	-999	-999
141	144	3.13	550	1200	750	168	-25	125	150	-5	130	20	0.864	120	102	18	-999	-999	-999
142	145	0.42	550	110	750	168	5	80	75	5	75	0	1.000	79	76	3	-999	-999	-999
143	146	0.42	550	110	750	168	30	135	105	80	55	50	0.524	77	67	10	-999	-999	-999
144	147	0.95	550	244	750	168	30	200	170	80	120	50	0.706	77	60	17	71	11	6
145	149	0.85	550	244	750	168	15	185	170	125	60	110	0.353	74	60	14	-999	-999	-999
146	150	0.36	550	110	650	168	0	80	80	30	50	30	0.630	72	66	6	-999	-999	-999
147	151	0.32	550	110	650	168	-15	55	70	35	20	50	0.285	82	78	4	-999	-999	-999
148	152	0.39	550	110	650	168	15	145	130	70	75	55	0.579	79	68	11	79	11	0
149	153	1.96	550	710	650	168	-40	-0	40	-20	20	20	0.505	161	152	9	161	9	-0
150	154	2.64	550	909	650	168	20	145	125	70	75	50	0.600	137	116	21	-999	-999	-999
151	155	3.80	550	1315	650	168	20	55	35	55	0	35	0.011	104	107	-3	118	11	0
152	156	5.00	550	2298	650	168	20	75	55	75	0	55	0.004	104	111	-7	115	4	0
153	157	3.50	550	1315	650	168	0	45	45	45	0	45	-0.009	119	130	-11	130	0	0
154	158	4.70	550	2298	650	168	0	85	85	60	25	60	0.294	119	130	-11	130	0	0
155	159	4.20	550	1315	650	168	-30	5	35	-30	35	0	1.000	157	155	2	180	25	0
156	160	4.30	550	2298	650	168	-30	20	50	-30	50	0	1.000	157	155	2	-999	-999	-999
157	161	0.95	450	500	650	72	130	440	310	230	210	100	0.677	-999	-999	-999	-999	-999	-999
158	162	1.22	450	500	650	648	130	440	310	200	240	70	0.774	-999	-999	-999	-999	-999	-999
159	163	1.51	450	500	650	1944	130	450	320	210	240	80	0.749	-999	-999	-999	-999	-999	-999
160	164	1.59	450	500	625	216	130	460	330	260	200	130	0.607	-999	-999	-999	-999	-999	-999
161	165	1.59	450	500	625	1944	130	460	330	210	250	80	0.757	-999	-999	-999	-999	-999	-999
162	166	1.73	450	500	650	216	130	450	320	200	250	70	0.781	-999	-999	-999	-999	-999	-999
163	167	1.83	450	500	625	72	130	465	335	290	175	160	0.522	-999	-999	-999	-999	-999	-999
164	168	1.98	450	500	625	648	130	465	335	220	245	90	0.731	-999	-999	-999	-999	-999	-999
165	169	0.85	450	500	650	216	35	340	305	125	215	90	0.705	-999	-999	-999	-999	-999	-999
166	170	0.95	450	500	650	1944	35	340	305	125	215	90	0.705	-999	-999	-999	-999	-999	-999
167	171	0.98	450	500	625	72	35	315	280	180	138	145	0.483	-999	-999	-999	-999	-999	-999
168	172	1.20	450	500	625	648	35	315	280	145	170	110	0.605	-999	-999	-999	-999	-999	-999
169	173	1.78	450	500	650	72	35	365	330	155	210	120	0.636	-999	-999	-999	-999	-999	-999
170	174	2.15	450	500	650	648	35	365	330	140	225	105	0.682	-999	-999	-999	-999	-999	-999
171	175	2.49	450	500	625	216	35	365	330	190	175	155	0.529	-999	-999	-999	-999	-999	-999
172	176	2.89	450	500	625	1944	35	365	330	165	200	130	0.605	-999	-999	-999	-999	-999	-999
173	177	1.13	500	1184	650	168	40	210	170	120	90	80	0.529	82	67	15	-999	-999	-999
174	188	1.20	550	440	750	168	10	220	210	60	150	50	0.762	78	56	22	80	24	0
175	191	1.30	550	441	750	168	10	235	225	70	165	60	0.733	78	58	20	80	22	0
176	193	1.20	550	440	750	168	-25	190	215	-999	-999	-999	-999.000	117	78	39	-999	-999	-999
177	195	1.30	550	441	750	168	-25	-999	-999	35	-999	60	-999.000	117	74	43	110	36	7
178	196	2.77	500	985	650	168	-5	-999	-999	135	-999	140	-999.000	89	-999	-999	83	-999	6
179	197	2.77	500	985	650	168	-10	-999	-999	170	-999	180	-999.000	69	-999	-999	60	-999	9
180	198	2.77	500	985	650	168	-45	-999	-999	90	-999	135	-999.000	72	-999	-999	63	-999	9
181	202	2.60	550	800	850	168	-999	-999	155	-999	90	65	0.581	106	84	22	-999	-999	-999
182	204	2.60	550	800	850	168	-999	-999	145	-999	90	55	0.621	106	84	22	-999	-999	-999
183	206	2.40	550	741	750	336	-30	200	230	20	180	50	0.783	111	78	33	-999	-999	-999

M&CS ANNEALING DATA BASE

Final Record No.	Original Record No.	Fluence (10^19)	Ti (F)	ti (h)	Ta (F)	ta (h)	TTu (F)	TTi (F)	dTTi (F)	TTia (F)	dTTa (F)	dTTres (F)	Trec (F)	USEu (ft-lb)	USEi (ft-lb)	dUSEi (ft-lb)	USEia (ft-lb)	dUSEa (ft-lb)	dUSEres (ft-lb)
184	222	1.06	550	318	850	168	5	140	135	40	100	35	0.741	62	50	12	-999	-999	-999
185	108	7.10	585	9700	800	168	30	180	165	65	115	50	0.697	78	57	20	70	13	8
186	178	7.00	487	7650	640	168	10	-999	-999	210	-999	200	-999.000	76	-999	-999	53	-999	23
187	179	9.00	487	7650	750	168	10	-999	-999	120	-999	110	-999.000	76	-999	-999	64	-999	12
188	180	9.00	487	7650	850	168	10	-999	-999	10	-999	0	-999.000	76	-999	-999	76	-999	0

Final Record No.	Cu	Ni	P	S	Si	Cr	Mn	Mo	Heat ID	Material Type	Primary Ref.	TR-EDB Ref.	Raw Data Ref.
1	0.310	0.640	0.016	0.016	0.555	0.070	1.36	0.45	W1	Linde 80 Weld	MEA-2218	MEA-2218	MEA-2218
2	0.409	0.591	0.006	0.013	0.510	0.044	1.36	0.45	E19	Linde 80 Weld	NP-2712	NP-2712	
3	0.409	0.591	0.006	0.013	0.510	0.044	1.36	0.45	E19	Linde 80 Weld	NP-2712	NP-2712	
4	0.409	0.591	0.006	0.013	0.510	0.044	1.36	0.45	E19	Linde 80 Weld	NP-2712	NP-2712	
5	0.409	0.591	0.006	0.013	0.510	0.044	1.36	0.45	E19	Linde 80 Weld	NP-2712	NP-2712	
6	0.409	0.591	0.006	0.013	0.510	0.044	1.36	0.45	E19	Linde 80 Weld	NP-2712	NP-2712	
7	0.409	0.591	0.006	0.013	0.510	0.044	1.36	0.45	E19	Linde 80 Weld	NP-2712	NP-2712	
8	0.409	0.591	0.006	0.013	0.510	0.044	1.36	0.45	E19	Linde 80 Weld	NP-2712	NP-2712	
9	0.409	0.591	0.006	0.013	0.510	0.044	1.36	0.45	E19	Linde 80 Weld	NP-2712	NP-2712	
10	0.409	0.591	0.006	0.013	0.510	0.044	1.36	0.45	E19	Linde 80 Weld	NP-2712	NP-2712	
11	0.409	0.591	0.006	0.013	0.510	0.044	1.36	0.45	E19	Linde 80 Weld	NP-2712	NP-2712	
12	0.409	0.591	0.006	0.013	0.510	0.044	1.36	0.45	E19	Linde 80 Weld	NP-2712	NP-2712	
13	0.223	0.594	0.008	0.013	0.507	0.044	1.38	0.45	E23	Linde 80 Weld	NP-2712	NP-2712	
14	0.223	0.594	0.008	0.013	0.507	0.044	1.38	0.45	E23	Linde 80 Weld	NP-2712	NP-2712	
15	0.223	0.594	0.008	0.013	0.507	0.044	1.38	0.45	E23	Linde 80 Weld	NP-2712	NP-2712	
16	0.223	0.594	0.008	0.013	0.507	0.044	1.38	0.45	E23	Linde 80 Weld	NP-2712	NP-2712	
17	0.223	0.594	0.008	0.013	0.507	0.044	1.38	0.45	E23	Linde 80 Weld	NP-2712	NP-2712	
18	0.223	0.594	0.008	0.013	0.507	0.044	1.38	0.45	E23	Linde 80 Weld	NP-2712	NP-2712	
19	0.223	0.594	0.008	0.013	0.507	0.044	1.38	0.45	E23	Linde 80 Weld	NP-2712	NP-2712	
20	0.223	0.594	0.008	0.013	0.507	0.044	1.38	0.45	E23	Linde 80 Weld	NP-2712	NP-2712	
21	0.223	0.594	0.008	0.013	0.507	0.044	1.38	0.45	E23	Linde 80 Weld	NP-2712	NP-2712	
22	0.223	0.594	0.008	0.013	0.507	0.044	1.38	0.45	E23	Linde 80 Weld	NP-2712	NP-2712	
23	0.223	0.594	0.008	0.013	0.507	0.044	1.38	0.45	E23	Linde 80 Weld	NP-2712	NP-2712	
24	0.364	0.591	0.005	0.009	0.170	0.039	1.29	0.44	E24	Linde 0091 Weld	NP-2712	NP-2712	
25	0.364	0.591	0.005	0.009	0.170	0.039	1.29	0.44	E24	Linde 0091 Weld	NP-2712	NP-2712	
26	0.364	0.591	0.005	0.009	0.170	0.039	1.29	0.44	E24	Linde 0091 Weld	NP-2712	NP-2712	
27	0.364	0.591	0.005	0.009	0.170	0.039	1.29	0.44	E24	Linde 0091 Weld	NP-2712	NP-2712	
28	0.364	0.591	0.005	0.009	0.170	0.039	1.29	0.44	E24	Linde 0091 Weld	NP-2712	NP-2712	
29	0.364	0.591	0.005	0.009	0.170	0.039	1.29	0.44	E24	Linde 0091 Weld	NP-2712	NP-2712	
30	0.364	0.591	0.005	0.009	0.170	0.039	1.29	0.44	E24	Linde 0091 Weld	NP-2712	NP-2712	
31	0.364	0.591	0.005	0.009	0.170	0.039	1.29	0.44	E24	Linde 0091 Weld	NP-2712	NP-2712	
32	0.364	0.591	0.005	0.009	0.170	0.039	1.29	0.44	E24	Linde 0091 Weld	NP-2712	NP-2712	
33	0.364	0.591	0.005	0.009	0.170	0.039	1.29	0.44	E24	Linde 0091 Weld	NP-2712	NP-2712	
34	0.364	0.591	0.005	0.009	0.170	0.039	1.29	0.44	E24	Linde 0091 Weld	NP-2712	NP-2712	
35	0.200	0.630	0.017	0.008	0.190	0.190	1.40	0.54	D2819_(TA)	A533-B Plate	NRC-3229	NRC-3228/V1	NUREG/CR-3229
36	0.200	0.630	0.017	0.008	0.190	0.190	1.40	0.54	D2819_(TA)	A533-B Plate	NRC-3229		NUREG/CR-3229
37	0.200	0.630	0.017	0.008	0.190	0.190	1.40	0.54	D2819_(TA)	A533-B Plate	NRC-3229	NRC-3228/V1	NUREG/CR-3229
38	0.200	0.630	0.017	0.008	0.190	0.190	1.40	0.54	D2819_(TA)	A533-B Plate	NRC-3229	NRC-3228/V1	NUREG/CR-3229
39	0.200	0.630	0.017	0.008	0.190	0.190	1.40	0.54	D2819_(TA)	A533-B Plate	NRC-3229	NRC-3228/V1	NUREG/CR-3229
40	0.200	0.630	0.017	0.008	0.190	0.190	1.40	0.54	D2819_(TA)	A533-B Plate	NRC-3229	NRC-3228/V1	NUREG/CR-3229
41	0.150	0.790	0.015	0.018	0.210	0.370	0.71	0.67	GEB	20NiMoCr26 Forging	NRC-5201	NRC-3228/V1	NUREG/CR-5201
42	0.150	0.790	0.015	0.018	0.210	0.370	0.71	0.67	GEB	20NiMoCr26 Forging	NRC-5201	NRC-3228/V1	NUREG/CR-5201
43	0.160	0.270	0.002	0.014	0.210	0.003	1.30	0.53	5C	A302-B Plate (1/2 in.)	NRC-2948	NRC-2948	NUREG/CR-2948
44	0.160	0.270	0.002	0.014	0.210	0.003	1.30	0.53	5C	A302-B Plate (1/2 in.)	NRC-2948	NRC-3228/V1	NUREG/CR-2948
45	0.160	0.270	0.002	0.014	0.210	0.003	1.30	0.53	5C	A302-B Plate (1/2 in.)	NRC-2948	NRC-3228/V1	NUREG/CR-5388
46	0.160	0.680	0.002	0.014	0.210	0.003	1.30	0.53	5D	A533-B Plate (1/2 in.)	NRC-2948	NRC-2948	NUREG/CR-2948
47	0.160	0.680	0.002	0.014	0.210	0.003	1.30	0.53	5D	A533-B Plate (1/2 in.)	NRC-2948	NRC-3228/V1	NUREG/CR-2948
48	0.160	0.680	0.002	0.014	0.210	0.003	1.30	0.53	5D	A533-B Plate (1/2 in.)	NRC-2948	NRC-3228/V1	NUREG/CR-5388
49	0.002	0.700	0.015	0.018	0.200	0.003	1.31	0.51	67B	A533-B Plate (1/2 in.)	NRC-5388	NRC-5388	NUREG/CR-5388
50	0.002	0.700	0.025	0.018	0.200	0.003	1.31	0.51	67C	A533-B Plate (1/2 in.)	NRC-5388	NRC-5388	NUREG/CR-5388
51	0.300	0.700	0.003	0.017	0.220	0.003	1.31	0.52	68A	A533-B Plate (1/2 in.)	NRC-5388	NRC-5388	NUREG/CR-5388
52	0.300	0.700	0.016	0.017	0.220	0.003	1.31	0.52	68B	A533-B Plate (1/2 in.)	NRC-5388	NRC-5388	NUREG/CR-5388
53	0.300	0.700	0.028	0.017	0.220	0.003	1.31	0.52	68C	A533-B Plate (1/2 in.)	NRC-5388	NRC-5388	NUREG/CR-5388
54	0.280	0.050	0.002	0.013	0.220	0.003	1.29	0.53	6A	A302-B Plate (1/2 in.)	NRC-5388,3229	NRC-3228/V1	NUREG/CR-2948
55	0.280	0.050	0.002	0.013	0.220	0.003	1.29	0.53	6A	A302-B Plate (1/2 in.)	NRC-5388,3229	NRC-3228/V1	NUREG/CR-5388
56	0.280	0.270	0.002	0.013	0.220	0.003	1.29	0.53	6B	A302-B Plate (1/2 in.)	NRC-5388,3229	NRC-3228/V1	NUREG/CR-2948
57	0.280	0.270	0.002	0.013	0.220	0.003	1.29	0.53	6B	A302-B Plate (1/2 in.)	NRC-5388,3229	NRC-3228/V1	NUREG/CR-5388
58	0.280	0.690	0.002	0.013	0.220	0.003	1.29	0.53	6C	A533-B Plate (1/2 in.)	NRC-5388,3229	NRC-3228/V1	NUREG/CR-2948
59	0.280	0.690	0.002	0.013	0.220	0.003	1.29	0.53	6C	A533-B Plate (1/2 in.)	NRC-5388,3229	NRC-3228/V1	NUREG/CR-5388
60	0.395	0.615	0.014	0.016	0.750	0.115	1.32	0.46	W8A	Linde 80 Weld	NRC-5469	NRC-5469	NUREG/CR-5469
61	0.395	0.615	0.014	0.016	0.750	0.115	1.32	0.46	W8A	Linde 80 Weld	NRC-5469	NRC-5469	NUREG/CR-5469

Final Record No.	Cu	Ni	P	S	Si	Cr	Mn	Mo	Heat ID	Material Type	Primary Ref.	TR-EDB Ref.	Raw Data Ref.
62	0.390	0.705	0.010	0.008	0.230	0.105	1.24	0.50	W9A	Linde 0091 Weld	NRC-5469	NRC-5469	NUREG/CR-5469
63	0.390	0.705	0.010	0.008	0.230	0.105	1.24	0.50	W9A	Linde 0091 Weld	NRC-5469	NRC-5469	NUREG/CR-5469
64	0.160	0.650	0.013	0.018	0.490	0.100	1.38	0.44	WW4	Linde 124 Weld	NRC-5469	NRC-5469	NUREG/CR-5469
65	0.160	0.650	0.013	0.018	0.490	0.100	1.38	0.44	WW4	Linde 124 Weld	NRC-5469	NRC-5469	NUREG/CR-5469
66	0.350	0.100	0.013	0.008	0.600	0.120	1.56	0.54	WW7	Linde 80 Weld	NRC-5469	NRC-5469	NUREG/CR-5469
67	0.350	0.100	0.013	0.008	0.600	0.120	1.56	0.54	WW7	Linde 80 Weld	NRC-5469	NRC-5469	NUREG/CR-5469
68	0.260	0.280	0.012	0.036	0.220	0.120	0.80	0.03	A212-B	A212-B	NRL-6721		NRL-6721
69	0.260	0.280	0.012	0.036	0.220	0.120	0.80	0.03	A212-B	A212-B	NRL-6721		NRL-6721
70	-999.000	1.720	0.011	0.030	0.250	0.140	0.75	0.10	NRLD54	A350-LF1 (MOD) Forging	NRL-6721		NRL-6721
71	-999.000	1.720	0.011	0.030	0.250	0.140	0.75	0.10	NRLD54	A350-LF1 (MOD) Forging	NRL-6721		NRL-6721
72	-999.000	1.720	0.011	0.030	0.250	0.140	0.75	0.10	SM1A-Fdup	A350-LF1 (MOD) Forging	NRL-6721		NRL-6721
73	-999.000	1.720	0.011	0.030	0.250	0.140	0.75	0.10	SM1A-Fdup	A350-LF1 (MOD) Forging	NRL-6721		NRL-6721
74	-999.000	1.720	0.011	0.030	0.250	0.140	0.75	0.10	SM1A-Fdup	A350-LF1 (MOD) Forging	NRL-6721		NRL-6721, NRL-7121
75	-999.000	1.720	0.011	0.030	0.250	0.140	0.75	0.10	SM1A-Fdup	A350-LF1 (MOD) Forging	NRL-6721		NRL-6721, NRL-7121
76	-999.000	1.720	0.011	0.030	0.250	0.140	0.75	0.10	SM1A-Fdup	A350-LF1 (MOD) Forging	NRL-6721		Raw data not available
77	-999.000	1.720	0.011	0.030	0.250	0.140	0.75	0.10	SM1A-Fdup	A350-LF1 (MOD) Forging	NRL-6721		NRL-6721
78	-999.000	1.720	0.011	0.030	0.250	0.140	0.75	0.10	SM1A-Fdup	A350-LF1 (MOD) Forging	NRL-6721		NRL-6721
79	-999.000	1.720	0.011	0.030	0.250	0.140	0.75	0.10	SM1A-Fdup	A350-LF1 (MOD) Forging	NRL-6721		NRL-6721
80	-999.000	1.720	0.011	0.030	0.250	0.140	0.75	0.10	SM1A-Fdup	A350-LF1 (MOD) Forging	NRL-6721		NRL-6721
81	0.150	-999.000	0.002	0.017	0.260	-999.000	1.38	0.50	V61	A302-B Plate (1/2 in.)	NRL-8264	NRL-8264	NRL-8264
82	0.150	-999.000	0.014	0.017	0.260	-999.000	1.28	0.49	V63	A302-B Plate (1/2 in.)	NRL-8264	NRL-8264	NRL-8264
83	0.160	-999.000	0.024	0.017	0.260	-999.000	1.36	0.50	V65	A302-B Plate (1/2 in.)	NRL-8264	NRL-8264	NRL-8264
84	0.290	-999.000	0.024	0.017	0.260	-999.000	1.37	0.50	V67	A302-B Plate (1/2 in.)	NRL-8264	NRL-8264	NRL-8264
85	0.290	-999.000	0.024	0.017	0.260	-999.000	1.37	0.50	V67	A302-B Plate (1/2 in.)	NRL-8264	NRL-8264	NRL-8264
86	0.290	-999.000	0.024	0.017	0.260	-999.000	1.37	0.50	V67	A302-B Plate (1/2 in.)	NRL-8264	NRL-8264	NRL-8264
87	0.290	-999.000	0.024	0.017	0.260	-999.000	1.37	0.50	V67	A302-B Plate (1/2 in.)	NRL-8264	NRL-8264	NRL-8264
88	0.045	-999.000	0.016	0.029	0.250	-999.000	1.23	0.49	V71	A302-B Plate (1/2 in.)	NRL-8264	NRL-8264	NRL-8264
89	0.160	-999.000	0.016	0.029	0.250	-999.000	1.23	0.49	V73	A302-B Plate (1/2 in.)	NRL-8264	NRL-8264	NRL-8264
90	0.160	-999.000	0.016	0.029	0.250	-999.000	1.23	0.49	V73	A302-B Plate (1/2 in.)	NRL-8264	NRL-8264	NRL-8264
91	0.160	-999.000	0.016	0.029	0.250	-999.000	1.23	0.49	V73	A302-B Plate (1/2 in.)	NRL-8264	NRL-8264	NRL-8264
92	0.300	-999.000	0.016	0.029	0.250	-999.000	1.23	0.49	V75	A302-B Plate (1/2 in.)	NRL-8264	NRL-8264	NRL-8264
93	0.300	-999.000	0.016	0.029	0.250	-999.000	1.23	0.49	V75	A302-B Plate (1/2 in.)	NRL-8264	NRL-8264	NRL-8264
94	0.300	-999.000	0.024	0.029	0.250	-999.000	1.23	0.49	V77	A302-B Plate (1/2 in.)	NRL-8264	NRL-8264	NRL-8264
95	0.300	-999.000	0.024	0.029	0.250	-999.000	1.23	0.49	V77	A302-B Plate (1/2 in.)	NRL-8264	NRL-8264	NRL-8264
96	0.240	0.520	0.012	0.024	0.280	-999.000	1.30	0.40	1T	A533-B Plate	NRL-8287	NRL-8287	NRL P.R. (Mar77), NRL M.R. 3512
97	0.240	0.520	0.012	0.024	0.280	-999.000	1.30	0.40	1T	A533-B Plate	NRL-8287	NRL-8287	NRL P.R. (Mar77), NRL M.R. 3512
98	0.008	0.050	0.021	0.022	0.210	0.020	1.30	0.53	40C	A302-B Plate	NRL-8287	NRL-8287	NRL P.R. (Mar77), NRL M.R. 3512
99	0.008	0.050	0.021	0.022	0.210	0.020	1.30	0.53	40C	A302-B Plate	NRL-8287	NRL-8287	NRL P.R. (Mar77), NRL M.R. 3512
100	0.170	0.560	0.009	0.015	0.210	0.100	1.29	0.57	CEP1	A533-B Plate	NRL-8287	NRL-8287	ASTM STP 570
101	0.220	0.220	0.015	0.021	0.220	0.120	1.35	0.52	D36	A302-B Plate	NRL-8287,ASTM DS 54	NRL-8287	NRL M.R. 1448
102	0.220	0.220	0.015	0.021	0.220	0.120	1.35	0.52	D36	A302-B Plate	NRL-8287,ASTM DS 54	NRL-8287	ASTM DS 54
103	0.220	0.220	0.015	0.021	0.220	0.120	1.35	0.52	D36	A302-B Plate	NRL-8287,ASTM DS 54	NRL-8287	ASTM DS 54
104	0.220	0.220	0.015	0.021	0.220	0.120	1.35	0.52	D36	A302-B Plate	NRL-8287,ASTM DS 54	NRL-8287	ASTM DS 54
105	0.220	0.220	0.015	0.021	0.220	0.120	1.35	0.52	D36	A302-B Plate	NRL-8287,ASTM DS 54	NRL-8287	NUREG/CR-0486
106	0.220	0.220	0.015	0.021	0.220	0.120	1.35	0.52	F23	A302-B Plate	NRL-8287	NRL-8287	NRL-6616, ASME Paper No. 67-WA/ER-1
107	0.220	0.220	0.015	0.021	0.220	0.120	1.35	0.52	F23	A302-B Plate	NRL-8287	NRL-8287	NRL M.R. 1753
108	0.220	0.220	0.015	0.021	0.220	0.120	1.35	0.52	F26	A302-B Plate	NRL-8287	NRL-8287	NRL M.R. 1572
109	0.220	0.220	0.015	0.021	0.220	0.120	1.35	0.52	F26	A302-B Plate	NRL-8287	NRL-8287	NRL M.R. 1593
110	0.150	0.260	0.006	0.011	0.210	0.110	1.37	0.63	MBU	A302-B Plate	NRL-8287,6620	NRL-8287	NRL-6620
111	0.130	0.580	0.008	0.008	0.190	0.060	1.22	0.50	N27	A533-B Plate	NRL-8287,7917	NRL-8287	NRL-7917, NRL-8357
112	0.130	0.580	0.008	0.008	0.190	0.060	1.22	0.50	N27	A533-B Plate	NRL-8287	NRL-8287	NRL P.R. (Mar77), NRL M.R. 3512, NRL-8357
113	0.130	0.580	0.008	0.008	0.190	0.060	1.22	0.50	N27	A533-B Plate	NRL-8287	NRL-8287	NRL P.R. (Mar77), NRL M.R. 3512, NRL-8357
114	0.130	0.580	0.008	0.008	0.190	0.060	1.22	0.50	N27	A533-B Plate	NRL-8287,7917	NRL-8287	NRL-7917, NRL-8357
115	0.030	0.560	0.008	0.007	0.200	0.060	1.21	0.50	N29	A533-B Plate	NRL-8287,7917	NRL-8287	NRL-7917, NRL-7121
116	0.030	0.560	0.008	0.007	0.200	0.060	1.21	0.50	N29	A533-B Plate	NRL-8287,7917	NRL-8287	NRL-7917, NRL-7121
117	0.160	0.580	-999.000	-999.000	-999.000	0.080	1.51	0.37	N4	Linde 80 Weld	NRL-8287,8357	NRL-8287	NRL-8357
118	0.160	0.580	-999.000	-999.000	-999.000	0.090	1.49	0.39	N6	Linde 80 Weld	NRL-8287,8357	NRL-8287	NRL-8357
119	0.270	0.560	-999.000	-999.000	-999.000	0.060	1.42	0.36	N7	Linde 80 Weld	NRL-8287,8357	NRL-8287	NRL-8357
120	0.320	0.680	-999.000	-999.000	-999.000	0.070	1.51	0.39	N8	Linde 80 Weld	NRL-8287,8357	NRL-8287	NRL-8357
121	0.260	0.180	0.010	0.010	0.180	0.080	1.17	0.51	Q96	Weld	NRL-8287	NRL-8287	NRL files (?)
122	0.220	0.580	0.006	0.010	0.230	0.120	1.44	0.52	Q98	A533-B Plate	NRL-8287	NRL-8287	NRL files (?)

Final Record No.	Cu	Ni	P	S	Si	Cr	Mn	Mo	Heat ID	Material Type	Primary Ref.	TR-EDB Ref.	Raw Data Ref.
123	0.220	0.580	0.006	0.010	0.230	0.120	1.44	0.52	Q98	A533-B Plate	NRL-8287	NRL-8287	NRL files (?)
124	0.350	0.620	0.013	0.011	0.140	0.030	1.56	0.53	V84	Linde 1092 Weld	NRL-8287,ASTM STP 683	ASTM STP	ASTM STP 683
125	0.350	0.620	0.013	0.011	0.140	0.030	1.56	0.53	V84	Linde 1092 Weld	NRL-8287,ASTM STP 683	ASTM STP	ASTM STP 683
126	0.350	0.620	0.013	0.011	0.140	0.030	1.56	0.53	V84	Linde 1092 Weld	NRL-8287,ASTM STP 683	ASTM STP	ASTM STP 683
127	0.350	0.690	0.016	0.013	0.550	-999.000	1.60	0.40	V86	Linde 80 Weld	NRL-8287,ASTM STP 683	ASTM STP	ASTM STP 683
128	0.350	0.690	0.016	0.013	0.550	-999.000	1.60	0.40	V86	Linde 80 Weld	NRL-8287,ASTM STP 683	ASTM STP	ASTM STP 683
129	0.350	0.690	0.016	0.013	0.550	-999.000	1.60	0.40	V86	Linde 80 Weld	NRL-8287,ASTM STP 683	ASTM STP	ASTM STP 683
130	0.350	0.570	0.020	0.013	0.680	-999.000	1.45	0.39	W_(W1)	A533-B Weld	NRL-8287,8357	NRL-8287	NRL-8171
131	0.350	0.570	0.020	0.013	0.680	-999.000	1.45	0.39	W_(W1)	Weld	NRL-8287,8357	NRL-8287	NRL P.R. (Mar77), NRL M.R. 3512
132	0.350	0.570	0.020	0.013	0.680	-999.000	1.45	0.39	W_(W1)	A533-B Weld	NRL-8287,8357	NRL-8287	NRL P.R. (Mar77), NRL M.R. 3512
133	0.350	0.570	0.020	0.013	0.680	-999.000	1.45	0.39	W_(W1)	A533-B Weld	NRL-8287,8357	NRL-8287	No reference available
134	0.350	0.570	0.020	0.013	0.680	-999.000	1.45	0.39	W_(W1)	A533-B Weld	NRL-8287,8357	NRL-8287	No reference available
135	0.170	0.560	0.009	0.015	0.210	0.100	1.29	0.57	CEP1	A533-B Plate	NRL-CE	ASTM STP	ASTM STP 570
136	0.240	0.620	0.008	0.011	0.230	0.110	1.40	0.59	CEP2	A533-B Plate	NRL-CE	ASTM STP	NRL-8136
137	0.360	0.780	0.015	0.012	0.220	0.070	1.38	0.55	CEW1	A533-B Weld	NRL-CE	ASTM STP	ASTM STP 570
138	0.360	0.780	0.015	0.012	0.220	0.070	1.38	0.55	CEW1	A533-B Weld	NRL-CE	ASTM STP	ASTM STP 570
139	0.200	0.040	0.016	0.013	0.170	0.050	1.11	0.53	CEW2	A533-B Weld	NRL-CE	ASTM STP	ASTM STP 570
140	0.055	0.970	0.022	0.012	0.440	0.070	1.33	0.54	AW	Weld	NRL-8357,8287	NRL-8287	NRL-8287, files
141	0.055	0.970	0.022	0.012	0.440	0.070	1.33	0.54	AW	Weld	NRL-8357,8287	NRL-8287	NRL-8287, files
142	0.190	0.560	-999.000	-999.000	-999.000	0.080	1.43	0.36	N1	Linde 80 Weld	NRL-8357,8287	NRL-8287	NRL-8357
143	0.290	0.650	-999.000	-999.000	-999.000	0.080	1.56	0.39	N2	Linde 80 Weld	NRL-8357,8287	NRL-8287	NRL-8357
144	0.290	0.650	-999.000	-999.000	-999.000	0.080	1.56	0.39	N2	Linde 80 Weld	NRL-8357,8287	NRL-8287	NRL-8357
145	0.300	0.680	-999.000	-999.000	-999.000	0.080	1.53	0.40	N3	Linde 80 Weld	NRL-8357,8287	NRL-8287	NRL-8357
146	0.160	0.580	-999.000	-999.000	-999.000	0.080	1.51	0.37	N4	Linde 80 Weld	NRL-8357,8287	NRL-8287	NRL-8357
147	0.270	0.560	-999.000	-999.000	-999.000	0.060	1.42	0.36	N7	Linde 80 Weld	NRL-8357,8287	NRL-8287	NRL-8357
148	0.320	0.680	-999.000	-999.000	-999.000	0.070	1.51	0.39	N8	Linde 80 Weld	NRL-8357,8287	NRL-8287	NRL-8357
149	0.090	0.710	0.005	0.008	0.270	0.390	0.68	0.59	Q41	A508-2 Forging	NRL-8287,Memo 2531	NRL-8287	NRL M.R. 2531
150	0.130	0.820	0.007	0.009	0.310	0.380	0.69	0.62	Q71	A508-2 Forging	NRL-8287,Memo 2531	NRL-8287	NRL M.R. 2531
151	0.090	0.580	0.009	0.017	0.220	-999.000	1.29	0.57	CEP3	A533-B Plate	NRL-CE,8136		ASTM STP 570
152	0.090	0.580	0.009	0.017	0.220	-999.000	1.29	0.57	CEP3	A533-B Plate	NRL-CE,8136		ASTM STP 570
153	0.090	0.660	0.011	0.018	0.280	-999.000	1.38	0.52	CEP4	A533-B Plate	NRL-CE,8136		NRL-8136
154	0.090	0.660	0.011	0.018	0.280	-999.000	1.38	0.52	CEP4	A533-B Plate	NRL-CE,8136		NRL-8136
155	0.070	0.120	0.010	0.010	0.250	0.040	1.15	0.59	CEW3	Linde 0091 Weld	NRL-CE,8136		ASTM STP 570
156	0.070	0.120	0.010	0.010	0.250	0.040	1.15	0.59	CEW3	Linde 0091 Weld	NRL-CE,8136		ASTM STP 570
157	0.140	0.080	0.023	0.031	0.470	0.080	1.53	0.47	S	A302-B Plate	WAPD-1095	WAPD-1095	
158	0.140	0.080	0.023	0.031	0.470	0.080	1.53	0.47	S	A302-B Plate	WAPD-1095	WAPD-1095	
159	0.140	0.080	0.023	0.031	0.470	0.080	1.53	0.47	S	A302-B Plate	WAPD-1095	WAPD-1095	
160	0.140	0.080	0.023	0.031	0.470	0.080	1.53	0.47	S	A302-B Plate	WAPD-1095	WAPD-1095	
161	0.140	0.080	0.023	0.031	0.470	0.080	1.53	0.47	S	A302-B Plate	WAPD-1095	WAPD-1095	
162	0.140	0.080	0.023	0.031	0.470	0.080	1.53	0.47	S	A302-B Plate	WAPD-1095	WAPD-1095	
163	0.140	0.080	0.023	0.031	0.470	0.080	1.53	0.47	S	A302-B Plate	WAPD-1095	WAPD-1095	
164	0.140	0.080	0.023	0.031	0.470	0.080	1.53	0.47	S	A302-B Plate	WAPD-1095	WAPD-1095	
165	0.220	0.230	0.021	0.027	0.220	0.140	1.34	0.50	U	A302-B Plate	WAPD-1095	WAPD-1095	
166	0.220	0.230	0.021	0.027	0.220	0.140	1.34	0.50	U	A302-B Plate	WAPD-1095	WAPD-1095	
167	0.220	0.230	0.021	0.027	0.220	0.140	1.34	0.50	U	A302-B Plate	WAPD-1095	WAPD-1095	
168	0.220	0.230	0.021	0.027	0.220	0.140	1.34	0.50	U	A302-B Plate	WAPD-1095	WAPD-1095	
169	0.220	0.230	0.021	0.027	0.220	0.140	1.34	0.50	U	A302-B Plate	WAPD-1095	WAPD-1095	
170	0.220	0.230	0.021	0.027	0.220	0.140	1.34	0.50	U	A302-B Plate	WAPD-1095	WAPD-1095	
171	0.220	0.230	0.021	0.027	0.220	0.140	1.34	0.50	U	A302-B Plate	WAPD-1095	WAPD-1095	
172	0.220	0.230	0.021	0.027	0.220	0.140	1.34	0.50	U	A302-B Plate	WAPD-1095	WAPD-1095	
173	0.220	0.220	0.015	0.021	0.220	0.120	1.35	0.52	ASTM	A302-B Plate	NRL-6616, files		NRL-6616
174	0.350	0.690	0.016	0.013	0.550	-999.000	1.60	0.40	V86		(ASTM STP 683, files)	ASTM STP 683/278	ASTM STP 725
175	0.350	0.690	0.016	0.013	0.550	-999.000	1.60	0.40	V86		(ASTM STP 683, files)	ASTM STP 725/63	ASTM STP 725
176	0.350	0.620	0.013	0.011	0.140	0.030	1.56	0.53	V84		(ASTM STP 683, files)	ASTM STP 725/63	ASTM STP 725
177	0.350	0.620	0.013	0.011	0.140	0.030	1.56	0.53	V84		(ASTM STP 683, files)	ASTM STP 725/63	ASTM STP 725
178	0.200	0.540	0.008	0.016	0.220	-999.000	1.30	0.55	PlatePA		(MEA-2218)	MEA-2218	MEA-2218
179	0.210	0.630	0.014	0.013	0.410	0.150	1.69	0.40	WeldWD		(MEA-2218)	MEA-2218	MEA-2218
180	0.200	0.490	0.013	0.013	0.560	0.080	1.41	0.38	WeldWE		(MEA-2218)	MEA-2218	MEA-2218
181	0.280	0.050	0.002	0.013	0.220	0.003	1.29	0.53	PME06A		(NRC-2948)	NUREG/CR-2948	NUREG/CR-2948
182	0.280	0.270	0.002	0.013	0.220	0.003	1.29	0.53	PME06B		(NRC-2948)	NUREG/CR-2948	NUREG/CR-2948
183	0.200	0.630	0.017	0.008	0.190	0.190	1.40	0.54	D2819(TA)		(NRC-3229)	NUREG/CR-3228/V1/81	NUREG/CR-3229

M&CS ANN

Final Record No.	Cu	Ni	P	S	Si	Cr	Mn	Mo	Heat ID	Material Type	Primary Ref.	TR-EDB Ref.	Raw Data Ref.
184	0.350	0.100	0.013	0.008	0.600	0.120	1.56	0.54	WW7		(NRC-5469)	NUREG/CR-5469	NUREG/CR-5469
185	0.220	0.220	0.015	0.021	0.220	0.120	1.35	0.52	F23	A302-B Plate	NRL-8287	NRL-8287	Serpan, Watson, & Hawthorne article
186	0.180	0.180	0.020	0.025	0.220	0.080	1.16	0.50	YR-UP	A302-B Plate	NRL-6616	NRL-6616	NRL-6616
187	0.180	0.180	0.020	0.025	0.220	0.080	1.16	0.50	YR-UP	A302-B Plate	NRL-6616	NRL-6616	NRL-6616
188	0.180	0.180	0.020	0.025	0.220	0.080	1.16	0.50	YR-UP	A302-B Plate	NRL-6616	NRL-6616	NRL-6616

DATA BASE REFERENCES

ASTM Papers:

Lott, R. et. al., "Annealing and Reirradiation Response of Irradiated Pressure Vessel Steels," Westinghouse, *ASTM STP 909*, pp. 242-259, 1986.

Hawthorne, J. R., J. J. Koziol and R. C. Groeschel, "Evaluation of Commercial Production A533-B Plates and Weld Deposits Tailored for Improved Radiation Embrittlement Resistance," *Properties of Reactor Structural Alloys After Neutron or Particle Irradiation, ASTM STP 570*, American Society for Testing and Materials, 1975, pp. 83-102.

Sprague, J. A, and D. Kramer, eds., "Effects of Radiation on Structural Materials," *Proceedings of the Ninth International Symposium, ASTM STP 683*, American Society for Testing and Materials, 1979.

Hawthorne, J. R., H. E. Watson and F. J. Loss, "Experimental Investigation of Multicycle Irradiation and Annealing Effects on Notch Ductility of A533-B Weld Deposits," *Effects of Radiation on Materials: Tenth Conference, ASTM STP 725*, (David Kramer, H. R. Brager and J. S. Perrin, eds.), American Society for Testing and Materials, 1971, pp. 63-75.

Hawthorne, J. R., "Radiation Effects Information Generated on the ASTM Reference Correlation-Monitor Steels," *ASTM Data Series Publication DS 54*, American Society for Testing and Materials.

In-House Reports:

Hawthorne, J. R., and A. L. Hiser, "Irradiation and Irradiation-Anneal-Reirradiation Studies of RPV Steels and Welds in Support of the BR-3 Reactor," MEA-2218, November 1988.

Hall, J., and D. Seman, "The Effect of Post-Irradiation Annealing and Re-Irradiation on the Fracture Properties of A302B Pressure Vessel Steel," WAPD-TM-1095, July 1973.

Journal Articles:

Serpan, C. Z., H. E. Watson and J. R. Hawthorne, "Interaction of Neutron and Thermal Environmental Factors in the Embrittlement of Selected Structural Alloys for Advanced Reactor Applications," Nuclear Engineering and Design II, North-Holland Publishing Company, Amsterdam, 1970, pp. 368-380.

Symposium Articles:

Kampmann, R. et. al., "SANS Analysis of Reactor Vessel Materials in Neutron Irradiated, Annealed and Re-Irradiated Conditions," Proceedings of the Fifth International Symposium on Environmental Degradation of Materials in Nuclear Reactors - Water Reactors, (D. Cubicciotti, E. P. Simonen and R. Gold, eds.), ANS, 1992, p. 679.

Government Reports:

Serpan, C. Z. et. al., "Yankee Reactor Pressure-Vessel Surveillance: Notch Ductility Performance of Vessel Steel and Maximum Service Fluence Determined from Exposure During Cores II, III, and IV," NRL Report 6616, Sept. 1967.

Potapovs, U. et. al., "Notch Ductility Properties of SM-1A Reactor Pressure Vessel Following the In-Place Annealing Operation," NRL Report 6721, May 1968.

Hawthorne, J. R., and F. J. Loss, "The Effects of Coupling Nuclear Radiation with Static and Cyclic Service Stresses and of Periodic Proof Testing on Pressure Vessel Material Behavior," NRL Report 6620, August, 1967.

Hawthorne, J. R., "Further Observations on A533-B Steel Plate Tailored for Improved Radiation Embrittlement Resistance," NRL Report 7917, September 1975.

Hawthorne, J. R., "Demonstration of Improved Radiation Embrittlement Resistance of A533-B Steel Through Control of Selected Residual Elements," NRL Report 7121, May 1970.

Hawthorne, J. R., "Exploratory Investigations of Low Charpy-V Upper Shelf Energy Steels With Irradiation," NRL Report 8171, December 1977.

Hawthorne, J. R., J. J. Koziol and S. T. Byrne, "Evaluation of Commercial Production A533-B Steel Plates and Weld Deposits with Extra-Low Copper Content for Radiation Resistance," NRL Report 8136, October 1977.

Hawthorne, J. R., "Influence of Phosphorus and Copper on Postirradiation Upper-shelf Performance of Steel," Report of NRL Progress, U. S. Naval Research Laboratory, March, 1977, pp. 25-27.

Loss, F. J., Ed., "Structural Integrity of Water Reactor Pressure Boundary Components, Progress Report Ending 28 February 1977," NRL Memorandum Report 3512, NRL NUREG 3, May 1977, p. 20.

Steele, L. E., J. R. Hawthorne and H. E. Watson, "Irradiation Effects on Structural Materials, Quarterly Progress Report (1 May - 31 July 1963)," NRL Memorandum Report 1448, U. S. Naval Research Laboratory, August 1963.

Hawthorne, J. R. et. al., "Irradiation Effects on Reactor Structural Materials, Quarterly Progress Report (1 November 1966 - 31 January 1967)," NRL Memorandum Report 1753, U. S. Naval Research Laboratory, February 1967.

Steele, L. E., J. R. Hawthorne and C. Z. Serpan, "Irradiation Effects on Reactor Structural Materials, Quarterly Progress Report (1 August - 31 October 1964)," NRL Memorandum Report 1572, U. S. Naval Research Laboratory, November 1964.

Steele, L. E. et. al., "Irradiation Effects on Reactor Structural Materials, Quarterly Progress Report (1 November 1964 - 31 January 1965)," NRL Memorandum Report 1593, U. S. Naval Research Laboratory, February 1965.

Steele, L. E., ed., "Irradiation Effects on Reactor Structural Materials, Quarterly Progress Report, (1 August - 31 October 1972)," NRL Memorandum Report 2531, U. S. Naval Research Laboratory, November 1972.